The mitigation of underwater cumulative noise for impact piling by operational strategies

European Wind Energy Master - Offshore Engineering

BY
KATRIEN DE JONG

To obtain the degrees of

Master of Science in Offshore Engineering
At Delft University of Technology

Master of Science in Technology - Wind Energy
At Norwegian University of Science and Technology

To be defended publicly on June 26 2025

Student number:	4660943	TU Delft	
Thesis committee:	Dr. Ir. L. Savio	NTNU	Responsible professor
	Dr. Ir. A. Tsouvalos	TU Delft	Chairman
	Dr. Ir. Y. Peng	TU Delft	University supervisor
	Ir. S. de Bode	HES	Company supervisor
	Ir. H. Ottens	HES	Company supervisor

TU Delft ENGINEERING SOLUTIONS NTNU

Preface

This thesis was written in partial fulfillment of the European Wind Energy Master (EWEM) program, a joint degree between Delft University of Technology (TU Delft) and the Norwegian University of Science and Technology (NTNU). The project was carried out in collaboration with Heerema Engineering Solutions (HES) between January and June 2025.

I would like to thank Sam de Bode from HES for his involvement throughout the project. From the initial conversations to the final weeks, Sam provided helpful direction, asked critical questions, and helped shape the scope of this thesis. His support in structuring the research and connecting me with the right people has been greatly appreciated. I also want to thank Harald Ottens for his sharp technical input, especially when defining realistic scenarios for noise mitigation. His ability to challenge assumptions strengthened the overall quality of the work. Furthermore, I would like to thank Toon van der Linden for sharing his geotechnical expertise and for his guidance in learning to work with DYNPAC.

I would also like to thank Yaxi Peng, who helped me understand both the complexity of soil and acoustics, as well as the fundamentals behind the computational SILENCE model. Her clear explanations and patience made it much easier to work with such a complex tool. I am also grateful to Apostolos Tsouvalas for his academic guidance and expertise in underwater acoustics. His deep knowledge in offshore acoustics and noise control provided a strong academic foundation for my research, and his feedback challenged me to refine my methodology and ensure scientific rigour in my work. Finally, I would like to thank Luca Savio for his kind and supportive guidance from a distance. Despite not being physically present, his friendly and approachable nature made working with him a pleasure.

Beyond my supervisors, I would also like to express my appreciation to everyone at Heerema Engineering Solutions for creating such a welcoming and supportive environment. The discussions, feedback, and laughs have enriched my experience and made this journey even more enjoyable.

This thesis marks the completion of an exciting and challenging period, and I am grateful for the people who have supported me along the way. I hope this research contributes to the ongoing efforts in offshore wind development and noise mitigation, and I look forward to seeing how the field evolves in the coming years.

Katrien de Jong
Delft, June 2025

Abstract

The large-scale deployment of offshore wind farms is critical to achieving global renewable energy targets. However, the installation of monopile foundations through impact pile driving generates significant underwater noise, posing risks to marine ecosystems. While noise mitigation measures, such as air-bubble curtains and pulse elongation systems, have been developed to reduce peak sound levels (Lpeak) and sound exposure levels (SEL), less is understood about their effects on cumulative noise exposure (cumSEL) - a key metric in regulatory frameworks like that of the United States.

This study investigates the influence of operational parameters, including the target blow count and impulse elongation, on cumulative underwater noise levels during offshore pile driving. Using the SILENCE model, a semi-analytical approach is applied to simulate noise propagation in realistic offshore conditions. The research evaluates the combined effectiveness of mitigation strategies such as pulse elongation and air-bubble curtains, as well as the effect of frequency weighting on sound levels for specific species.

The results show that varying the target blow count has negligible influence on cumulative underwater noise, while impulse elongation (PULSE) achieves modest broadband reductions and more substantial reductions when *species-specific*[1] frequency weighting is applied. The combination of PULSE with a Double Big Bubble Curtain (DBBC) offers the most effective mitigation across all marine mammal hearing groups.

This study provides insights into the complex interactions between operational parameters and noise mitigation strategies, supporting the development of effective solutions to comply with cumulative noise regulations. The findings aim to contribute to more sustainable offshore wind farm construction while minimizing impacts on marine ecosystems.

[1] "Species-specific" refers here to the hearing sensitivity curves prescribed for different marine-mammal groups (low-, mid-, and high-frequency cetaceans and pinnipeds) in current regulatory guidance.

Executive summary

Nations worldwide are accelerating the transition to renewable energy sources to reduce greenhouse gas emissions and meet ambitious climate targets. Offshore wind energy plays a crucial role in this transition, offering large-scale, low-carbon electricity generation. However, the construction of offshore wind farms presents environmental challenges, particularly regarding underwater noise pollution caused by impact pile driving. This method, commonly used to install steel monopiles as foundations for offshore wind turbines, generates significant acoustic energy that propagates through water and seabed sediments. The resulting noise can disrupt marine ecosystems, affecting species that rely on sound for navigation, communication, and survival. To mitigate these impacts, governments have introduced regulations that limit underwater noise levels and mandate the use of noise abatement measures during installation.

A key challenge in regulating underwater noise is the shift from measuring individual sound events to assessing cumulative noise exposure over extended periods. Many countries enforce limits based on peak sound pressure level (L_{peak}) and sound exposure level (SEL), which quantify the intensity of single noise events. However, in the United States, cumulative Sound Exposure Level (cumSEL) over a 24-hour period serves as a primary regulatory criterion. This cumulative approach complicates compliance for offshore wind developers, as it requires precise management of pile driving schedules and noise mitigation strategies to ensure that cumulative thresholds are not exceeded.

While noise mitigation technologies such as air-bubble curtains and pulse elongation systems are widely used, the effectiveness of these measures in reducing cumulative noise levels is not yet fully understood. One of the primary knowledge gaps is the impact of pile driving operational parameters, such as hammer strike energy and blow rate, on cumulative underwater noise. Lowering hammer energy per blow, for example, may reduce instantaneous noise levels but increase the total number of blows required, potentially leading to higher cumulative exposure. Similarly, modifying the blow rate or combining different mitigation strategies could influence cumulative noise levels in ways that are not yet systematically quantified.

This study investigates the relationship between operational pile driving parameters and cumulative underwater noise exposure. The objective is to assess how variations in hammer strike energy and blow rate affect cumulative Sound Exposure Level (cumSEL) and to evaluate the effectiveness of noise mitigation strategies, such as pulse elongation and air-bubble curtains, in reducing cumulative noise. The research seeks to provide insights that contribute to regulatory compliance and improve noise management practices for offshore wind turbine installation.

To achieve this, a computational modeling approach is employed, utilizing two key simulation tools: DYNPAC and SILENCE. DYNPAC is a pile driving simulation model used to calculate the energy input required to achieve a specified penetration depth, while SILENCE is a semi-analytical noise prediction model that simulates underwater noise generation and propagation. The SILENCE model consists of a sound generation module, which captures the interaction between the pile, water, and soil, and a sound propagation module, which traces the transmission of noise to greater distances.

Using these models, multiple pile driving scenarios are analyzed to explore how different operational strategies influence cumulative noise exposure. The first set of simulations examines the effect of varying the target blow count, with scenarios comparing 20, 25, and 30 blows per 25 cm of pile penetration. The second set of simulations investigates the impact of spreading hammer energy over a longer duration using PULSE. In the third set, an integrated analysis is conducted to assess the combined effects of impulse elongation and air-bubble curtains, determining whether their individual noise reductions can be linearly added or whether interaction effects influence their combined effectiveness. Finally, the influence of frequency weighting on the cumulative sound emissions is studied.

The results show that varying the target blow count has a negligible effect on cumulative noise emissions. Although lower blow counts result in higher hammer energy per strike and elevated peak levels, the total acoustic energy released over the full installation remains nearly constant. Consequently, differences in cumulative Sound Exposure Level (cumSEL) between blow count scenarios are less than 0.1 dB, confirming that blow count optimisation alone is not an effective noise mitigation strategy when total energy input remains unchanged.

A 50% elongation of the impact duration (PULSE) yields only a modest broadband reduction in cumulative SEL (-1.18 dB). This limited effect arises because pulse shaping lowers the force per strike but simultaneously increases both the number and total energy of blows, partly negating the acoustic benefit and highlighting a drivability-mitigation trade-off. When frequency weighting is applied, however, the same pulse shaping proves more effective: weighted cumSEL decreases by more than 11 dB for mid- and high-frequency cetaceans, as spectral energy is shifted away from their most sensitive hearing bands.

The most effective reduction in cumulative underwater noise is achieved through the combined application of PULSE and a Double Big Bubble Curtain (DBBC). These methods operate through complementary mechanisms: PULSE reshapes the impact force and redistributes energy across frequencies, while the DBBC attenuates mid- and high-frequency sound via acoustic scattering and impedance mismatch. Their combined effect results in broadband and frequency-weighted cumSEL reductions across all marine mammal hearing groups. Yet, the incremental benefit of PULSE over DBBC alone is limited to approximately 0.6 dB, indicating diminishing returns when multiple strategies are stacked.

Overall, the study demonstrates that operational parameters influence underwater noise through distinct mechanisms. The DBBC provides the most robust, broadband attenuation, whereas 50% PULSE mainly benefits those hearing groups that are most sensitive to mid- and high-frequency sound. The apparent effectiveness of any mitigation method depends on the noise metric used: a change that brings only a small improvement in unweighted cumSEL can produce much larger reductions when species-specific, frequency-weighted metrics are applied.

Because all main simulations were conducted for a specific sand profile, the results and conclusions are most relevant to sandy seabeds with similar acoustic properties. Strongly layered or non-sandy soils – such as clay, silt, or mixed deposits – can alter both drivability and sound propagation; therefore, the present findings should be viewed as case-specific rather than universal, and future work should test a wider range of soil conditions.

Contents

Preface i

Abstract ii

Executive summary iii

1 Introduction 1
- 1.1 Relevancy . . . 1
- 1.2 Research Gap . . . 2
- 1.3 Objective and Scope . . . 2
- 1.4 Approach and Methodology . . . 3

2 Research Background and Motivation 5
- 2.1 Understanding Acoustic Principles . . . 5
  - 2.1.1 Sound Waves . . . 5
  - 2.1.2 Acoustic Impedance . . . 6
  - 2.1.3 Sound Intensity and the Decibel Scale . . . 6
  - 2.1.4 Sound Pressure Level . . . 6
  - 2.1.5 Zero-to-peak Sound Pressure Level . . . 6
  - 2.1.6 Sound Exposure Level . . . 7
  - 2.1.7 Cumulative Sound Exposure Level (cumSEL) . . . 7
  - 2.1.8 Power and sound exposure spectral density level . . . 7
- 2.2 Legal requirements for the protection of the marine environment against pile-driving 8
  - 2.2.1 Regulatory Framework for Underwater Noise . . . 9
  - 2.2.2 Marine Animal Sensitivity to Noise . . . 9
  - 2.2.3 Limitations in the regulations . . . 11
- 2.3 Underwater noise generation from impact pile-driving . . . 12
  - 2.3.1 Interaction between piles, soil and water . . . 13
  - 2.3.2 Site-specific influencing factors . . . 16
- 2.4 Underwater noise mitigation for impact pile driving . . . 17
  - 2.4.1 Air-Bubble Curtains . . . 17
  - 2.4.2 Pulse prolongation by adaptation of hydraulic hammers . . . 20

3 State of the art in noise prognosis 24
- 3.1 Existing computational models . . . 24
  - 3.1.1 First-Generation Models . . . 24
  - 3.1.2 Second-Generation Models . . . 25
  - 3.1.3 State-of-the-Art Acoustic Models . . . 26
- 3.2 SILENCE model . . . 27
  - 3.2.1 Description of the model . . . 28
  - 3.2.2 Governing equations . . . 29

3.2.3 Sound Generation Module . . . 30
3.2.4 Sound Propagation Module . . . 31
3.2.5 Implementation of Air-Bubble Curtains . . . 33
3.3 Computational methods for drivability . . . 34
3.3.1 State-of-the-art overview . . . 34
3.3.2 Position of DYNPAC . . . 35

4 Modeling configuration and approach 36
4.1 Configuration and validation of the acoustic model . . . 36
4.1.1 Model Setup and Input Parameters . . . 36
4.1.2 Model Assumptions and Limitations . . . 42
4.1.3 Validation of the model . . . 43
4.2 Scenario definition . . . 44
4.2.1 Overview of scenarios . . . 45
4.2.2 Frequency weighting . . . 48

5 Numerical study on cumulative underwater noise 49
5.1 The effect of target blow count variation . . . 49
5.1.1 Drivability analysis . . . 49
5.1.2 Single strike sound levels . . . 51
5.1.3 Cumulative sound exposure . . . 53
5.1.4 Spectral distribution . . . 54
5.2 Impact of impulse elongation . . . 55
5.2.1 Drivability analysis . . . 56
5.2.2 Single strike sound levels . . . 58
5.2.3 Cumulative sound exposure . . . 59
5.2.4 Spectral distribution . . . 60
5.3 Combined impact of PULSE and a Double Big Bubble Curtain (DBBC) . . . 62
5.3.1 Single strike and cumulative sound levels . . . 62
5.3.2 Spectral distribution . . . 63
5.4 Frequency-weighted noise impact . . . 65
5.5 Sensitivity to clay-sand stratigraphy . . . 68
5.5.1 Drivability analysis . . . 68
5.5.2 Single strike and cumulative sound levels . . . 70
5.5.3 Spectral distribution . . . 72
5.5.4 Frequency-weighted noise impact . . . 73

6 Discussion, Conclusions, and Recommendations 75
6.1 Discussion and Conclusions . . . 75
6.1.1 Operational Parameter Influence on Cumulative Sound Exposure Level (cumSEL) . . . 75
6.1.2 Impact of Acoustic Metrics on Perceived Effectiveness . . . 77
6.2 Limitations of the study . . . 77
6.2.1 DYNPAC model limitations . . . 78
6.2.2 SILENCE model limitations . . . 79
6.2.3 Study-wide limitations . . . 80
6.3 Recommendations . . . 80
6.3.1 Academic perspective . . . 80
6.3.2 Industry perspective . . . 81
6.3.3 Regulatory perspective . . . 82

A Sensitivity study for the influence of the penetration depth on noise levels **89**
A.1 SEL and L_{peak} values over the penetration depth at 750 m from the monopile . . 89
A.2 SEL and L_{peak} values over the penetration depth in the frequency domain 90

B Effect of operational parameters on the drivability **91**
B.1 Drivability results for target blow count variation 91
B.2 Drivability results for impulse elongation 93

C Noise levels per hammer energy level **94**
C.1 Noise levels for varying target blow counts 94
C.1.1 Without additional mitigation measures 94
C.1.2 In combination with a DBBC 94
C.2 Noise levels for impulse elongation 95
C.2.1 Without additional mitigation measures 95
C.2.2 In combination with a DBBC 95

D Frequency-weighted noise impact **96**
D.1 Weighted cumulative noise (PULSE) 96
D.2 Weighted cumulative noise (PULSE+DBBC) 99

E Clay-sand case **102**
E.1 Input parameters 102
E.2 Drivability results for impulse elongation 103
E.3 Noise levels for impulse elongation 104
E.4 Weighted cumulative noise (PULSE) 104

Abbreviations

Abbreviation	Definition
BBC	Big Bubble Curtain
BOEM	Bureau of Ocean Energy Management
BSH	Federal Maritime and Hydrographic Agency
CPT	Cone Penetration Test
cumSEL	Cumulative Sound Exposure Level
DBBC	Double Big Bubble Curtains
dB	Decibel
EPA	Environmental Protection Agency
ESA	Endangered Species Act
FEM	Finite Element Model
GWEC	Global Wind Energy Council
HSD-system	Hydro-Sound-Damper System
L_{peak}	Peak Sound Level
MNRU	Modulated Noise Reference Unit
MSFD	Marine Strategy Framework Directive
NMS	Noise Mitigation System
NMFS	National Marine Fisheries Service
NOAA	National Oceanic and Atmospheric Administration
OWF	Offshore Wind Farm
Pa	Pascal
PE	Parabolic Equation
PML	Perfectly Matched Layer
P_{rms}	Root Mean Squared Sound Pressure
P_{ref}	Reference Pressure
PTS	Permanent Threshold Shift
PULSE	Piling Under Limited Stress Equipment
SEL	Sound Exposure Level
SILENCE	Semi-analytical computational noise prediction model
SPL	Sound Pressure Level
TBBC	Triple Big Bubble Curtain
TTS	Temporary Threshold Shift

1 | Introduction

1.1 Relevancy

The transition from fossil fuels to renewable energy sources is being driven by the urgent need to address climate change and reduce greenhouse gas emissions. In 2022, renewable energy accounted for 23% of the total energy consumption within the EU, marking a 1.1% increase compared to the previous year [1]. However, to achieve the 2030 target of 42.5% renewables, significant expansion is required. Wind and solar energy are currently the primary contributors to this growth. The Global Wind Energy Council (GWEC) reported that 2023 was a landmark year for the wind energy sector, with a record-breaking 117 GW of new capacity installed - a 50% increase from 2022 [2].

The pursuit of stronger wind resources and the aim to minimize visual impact prompted the construction of the first offshore wind farm, Vindeby, in Danish waters in 1991. The success of the turbines, which generated more power than their onshore counterparts due to higher wind speeds at sea, marked the beginning of large-scale offshore wind development [3].
The large-scale deployment of offshore wind farms requires the installation of stable foundations, often achieved through impact pile driving, a process in which large steel monopiles, sometimes exceeding 10 meters in diameter, are driven into the seabed using hydraulic hammers. This method, used in about 75% of offshore wind turbine installations, generates significant underwater noise, posing risks to marine ecosystems [4]. Many marine species rely on sound for critical behaviors like communication and navigation, and excessive noise can disrupt these activities, leading to stress, behavioral changes, and even physical harm [5, 6].

To address these impacts, several countries enforce noise mitigation measures targeting metrics such as Sound Exposure Level (SEL) and peak sound pressure level (L_{peak}) [7]. The SEL quantifies the total acoustic energy of a single sound event, standardized to a one-second duration, allowing comparison of events with different durations. The L_{peak} represents the maximum instantaneous sound pressure level reached during a noise event. Since both SEL and L_{peak} are linked to short, well-defined time intervals, they can be measured in real time, enabling immediate adjustments to construction activities if limits are approached or exceeded. In contrast, certain countries, including Denmark, Poland, and the United States, place a stronger emphasis on cumulative Sound Exposure Level (cumSEL) over a set time period, often 24 hours [8]. Unlike SEL and L_{peak}, the cumSEL requires continuous tracking and projection of noise exposure over time, making real-time adjustments more challenging. Biologically, this metric is relevant because many hearing-related effects (such as irreversible hearing damage and long-term behavioural disruption) scale with the total acoustic energy received rather than with a single peak or short-duration pulse; studies on harbour porpoises and seals show that cumulative doses above species-specific thresholds correlate strongly with sustained stress responses and irreversible hearing loss [6, 9]. Consequently, regulators that emphasize cumSEL aim to protect marine fauna from the additive impact of thousands of hammer blows rather than just the loudest individual hits.

For this study, the focus will be on the regulatory framework of the United States, as its emphasis on cumulative thresholds provides a well-defined and structured case for analysis. By narrowing the scope to one country's regulatory system, the study aims to provide a focused exploration of how these noise limits influence offshore wind installation procedures, with broader insights that may be applicable to other nations with similar approaches, such as Denmark [10].

1.2 Research Gap

Regulatory context. Offshore piling noise is typically assessed using three metrics:

1. The peak sound pressure level L_{peak} for acute injury risk;
2. The single-strike sound exposure level (SEL), the integral of acoustic energy over one blow; and
3. The cumulative SEL (cumSEL), obtained by summing SEL over all blows within a chosen time window.

Each metric captures a different biological endpoint, yet none is entirely satisfactory. L_{peak} ignores the total dose; SEL ignores the accumulation of blows; cumSEL cannot be tracked in real time because it requires post-integration of the full strike series. These shortcomings complicate operational decision making, especially when regulators set limits on more than one metric or apply species-specific frequency weighting.

Existing mitigation. External measures such as single or double bubble curtains attenuate broadband sound, but are known to be less effective for low-frequency noise [11]. Operational measures, e.g. pulse elongation or deliberate variation of hammer energy and blow rate, offer additional control but change installation logistics.

Unresolved interactions. Lower per-blow energy decreases SEL but necessitates more blows; a slower blow rate redistributes strike energy in time but leaves cumSEL uncertain. Although practitioners acknowledge these trade-offs, quantitative relationships between hammer settings, all three regulatory metrics, and associated ecological risks remain poorly documented.

Research gap. Robust guidance is lacking on how specific operational adjustments influence L_{peak}, SEL, and cumSEL, and whether those influences persist under alternative soil stratigraphies or when combined with external mitigation (e.g. bubble curtains).

These unresolved questions highlight a critical research gap. The interactions between operational parameters and cumulative noise are not yet fully established, complicating efforts to predict and manage underwater noise levels during offshore wind turbine installation. This study aims to address these knowledge gaps by investigating how changes in hammer energy, blow rate, and mitigation systems affect cumulative noise exposure. By providing insight into these relationships, the research seeks to support the development of more effective noise mitigation strategies and facilitate compliance with cumulative noise regulations.

1.3 Objective and Scope

This study investigates the operational parameters influencing cumulative noise levels during offshore pile driving and explores strategies to minimize these impacts. Specifically, it examines how variations in strike energy, blow rate, and mitigation systems, such as pulse prolongation equipment and air-bubble curtains, affect cumulative sound exposure thresholds.

The primary research question is:

How do operational parameters affect the cumulative Sound Exposure Level (cumSEL) during offshore pile driving?

To answer this research question, the following subquestions are formulated:

1. Does variation in the target blow count (number of blows per 25 cm of pile penetration) influence the cumulative Sound Exposure Level?
2. Is impulse elongation effective in reducing the cumulative Sound Exposure Level?
3. What is the effect of impulse elongation in combination with an air-bubble curtain on the cumulative Sound Exposure Level?
4. What is the effect of frequency weighting on the cumulative Sound Exposure Level?

1.4 Approach and Methodology

Noise can be evaluated using different modeling approaches, including empirical, semi-analytical, and numerical models, as discussed in Chapter 3. For this study, the SILENCE model, a semi-analytical computational tool, is utilized for its combination of computational efficiency and high accuracy. This makes it a viable alternative to more time-consuming methods, such as Finite Element Methods (FEM) [12].

To answer the subquestions, a scenario-based approach is employed to explore how variations in operational parameters affect the cumulative Sound Exposure Level (cumSEL) during offshore pile driving. The analysis focuses on the impact of blow rate, pulse prolongation, and the use of an air-bubble curtain.

The first subquestion, "Does variation in the target blow count (number of blows per 25 cm of pile penetration) influence the cumulative Sound Exposure Level?", is addressed by designing three distinct scenarios. These scenarios represent different blow rates for every 25 cm of pile penetration: 20 blows (Scenario A), 25 blows (Scenario B - the industry standard), and 30 blows (Scenario C). For each scenario, the hammer energy is optimized using the DYNPAC program, a computational model which calculates the required energy input to achieve the target blow count and penetration depth. The Sound Exposure Level (SEL) for each energy level is then determined using the SILENCE model. The cumulative SEL (cumSEL) is calculated by summing the products of SEL and the total number of blows for each scenario.

The second subquestion, "Is impulse elongation effective in reducing the cumulative Sound Exposure Level?", is approached by adjusting the hammer's energy profile within the SILENCE model. Pulse prolongation can be achieved using an add-on component installed between the impact hammer and the monopile. This component modifies the impact pulse by spreading the energy input over an extended time frame. As a result, the hammer's peak energy is reduced, which can potentially lower sound pressure levels. This adjustment allows for a comparison of cumulative SEL under different pulse prolongation strategies.

The third subquestion, "What is the effect of impulse elongation in combination with an air-bubble curtain on the cumulative Sound Exposure Level?", is investigated with the SILENCE model, which allows direct specification of bubble-curtain parameters [13]. Air-bubble curtains are modeled as a spatial mitigation measure that attenuates underwater sound propagation. Their effectiveness is quantified by simulating the additional transmission loss for each pulse

elongation scenario, after which the combined impact on cumulative SEL is evaluated to explore potential synergies between temporal and spatial mitigation strategies.

Finally, the fourth subquestion, "What is the effect of frequency weighting on the cumulative Sound Exposure Level?", is addressed by applying species-specific frequency weighting to the cumSEL values obtained in the previous sub-questions, thereby converting a purely physical quantity into a biologically meaningful metric. The analysis evaluates whether the spectral changes introduced by PULSE and the DBBC reduce acoustic exposure in the frequency bands most relevant to each hearing group, allowing comparison of both overall noise reduction and species-specific mitigation effectiveness.

This thesis is structured in seven chapters, each building on the previous one to provide a comprehensive numerical investigation of the research question. After introducing underwater-noise generation, regulatory frameworks and mitigation techniques, the text describes the computational methodology and model configuration, presents the cumulative-noise simulations, and concludes with key findings and recommendations.

- **Chapter 1:** Introduces the study and presents the problem statement, research gap, objectives, and overall methodology.
- **Chapter 2:** Provides the acoustic background, explaining sound-wave propagation, acoustic impedance, and cumulative sound exposure levels. It also summarises underwater noise regulations, describes how impact piling generates sound, and reviews the relevant noise-abatement systems (air-bubble curtains and pulse-prolongation devices) together with their physical mechanisms and limitations.
- **Chapter 3:** Surveys computational tools for pile-driving noise prediction. First- and second-generation acoustic models are compared, the semi-analytical SILENCE model is introduced in detail, and the drivability model DYNPAC is discussed as the source of depth-dependent hammer energy and blow counts.
- **Chapter 4:** Describes the model configuration – geometry, material, soil, and environmental inputs to SILENCE – and defines the scenarios used to evaluate the influence of operational parameters on underwater noise.
- **Chapter 5:** Presents the simulation results, supported by figures and tables that illustrate drivability trends, single-strike SEL, and cumulative SEL for all scenarios, in both the time- and frequency domain.
- **Chapter 6:** Summarises the principal findings, discusses limitations, and offers recommendations for future research and industry practice.

This structure provides a logical progression from foundational knowledge to scenario-based analysis, forming a robust framework for addressing the research objectives.

2 | Research Background and Motivation

Governments have introduced regulations to limit underwater noise and protect marine life, often based on specific acoustic metrics [7]. This chapter introduces these acoustic principles, forming the basis for the regulatory discussion in Section 2.2. In Section 2.3, the generation and propagation of sound are discussed.

2.1 Understanding Acoustic Principles

As a type of vibration, sound moves through media like seawater or sediment in the form of acoustic waves [14]. During offshore construction activities, vibrating structures, such as monopiles, act as primary sources of underwater sound.

2.1.1 Sound Waves

Sound waves are mechanical waves that propagate through a medium such as water [15]. These waves are characterized by their frequency, amplitude, and wavelength, as shown in Figure 2.1. When sound waves travel, they create alternating regions of compression and rarefaction, which transfer energy through the medium without transferring matter [16].
The speed of sound in water is determined by the medium's properties, including density and temperature. The general formula for the speed of sound in a medium is given by:

$$c = \sqrt{\frac{B}{\rho}} \tag{2.1}$$

where c is the speed of sound (m/s), B is the bulk modulus of the medium (Pa), and ρ is the density of the medium (kg/m^3). For seawater, this speed is typically around 1500 m/s, though it varies with temperature, salinity, and depth [16].

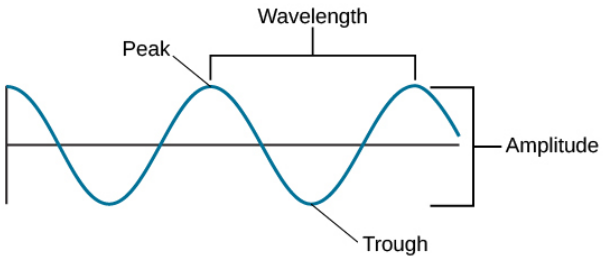

Figure 2.1: A simple sound wave

2.1.2 Acoustic Impedance

When sound waves pass between different media, such as water and seabed sediments, they may be reflected or transmitted depending on the mismatch in acoustic impedance [15]. Acoustic impedance, Z, quantifies the resistance a medium offers to the passage of sound waves and is defined by:

$$Z = \rho c \tag{2.2}$$

where ρ is the density of the medium (kg/m^3), and c is the speed of sound in that medium (m/s). Impedance is measured in Rayls (Pa $\cdot$ s/m^3). The degree to which sound is transmitted or reflected at the interface between two media depends on the impedance mismatch:

$$R = \left(\frac{Z_2 - Z_1}{Z_2 + Z_1} \right) \tag{2.3}$$

where Z_1 and Z_2 are the acoustic impedances of the two media (Pa $\cdot$ s/m), and R is the reflection coefficient.

2.1.3 Sound Intensity and the Decibel Scale

The decibel (dB) is a logarithmic unit widely used in underwater acoustics to express the relative difference between two values, such as sound intensity or pressure [17]. This logarithmic representation makes it easier to handle extremely large or small quantities by transforming multiplicative relationships into additive ones, thus simplifying calculations and visual interpretation. The decibel scale is defined mathematically as:

$$\text{Level} = 10 \log_{10} \left(\frac{I}{I_{\text{ref}}} \right) \tag{2.4}$$

where I is the intensity of the sound (W/m^2), and I_{ref} is the intensity of a reference sound.

2.1.4 Sound Pressure Level

Sound pressure, p, is the variation in pressure due to the passage of sound waves through a medium. It is typically measured in Pascals (Pa). However, due to the wide range of sound pressures encountered, especially underwater, the decibel (dB) scale is used to express sound pressure levels (SPL) logarithmically [14]. The SPL is given by:

$$\text{SPL} = 10 \log_{10} \left(\frac{1}{T} \int_0^T \frac{p(t)^2}{p_0^2} \, dt \right) \quad [\text{dB re } 1\ \mu\text{Pa}^2] \tag{2.5}$$

where $p(t)$ is the time-variant sound pressure (Pa), p_0 is the reference sound pressure (for underwater sound, $p_0 = 1\,\mu$Pa), and T is the averaging time (s). The logarithmic scale allows the representation of the vast range of sound pressures in a manageable format.

2.1.5 Zero-to-peak Sound Pressure Level

The zero-to-peak sound pressure level, $L_{\text{p,pk}}$, represents the highest instantaneous pressure during a sound event. It is particularly relevant for impulsive sounds like those generated during impact pile driving. Peak sound pressure is given by:

$$L_{p,pk} = 20 \log_{10} \left(\frac{|p_{\text{peak}}|}{p_0} \right) \quad [\text{dB re } 1\ \mu\text{Pa}] \tag{2.6}$$

where p_{peak} is the peak sound pressure (Pa).

p_{peak} does not account for the duration of the sound wave but is crucial for evaluating the immediate impact of high-intensity, short-duration noise sources. In Figure 2.2 an example of a zero-to-peak level and a peak-to-peak level is shown.

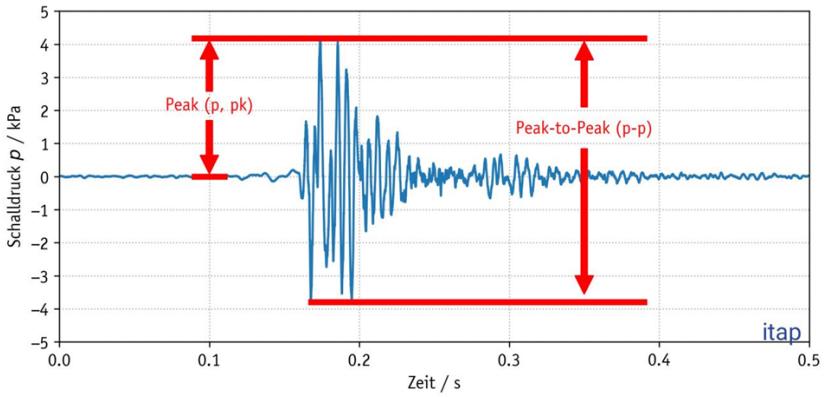

Figure 2.2: Typical measured time signal of the underwater noise during pile-driving in a distance of several 100 m [14].

2.1.6 Sound Exposure Level

The Sound Exposure Level (SEL resp. $L_{E,\text{p}}$) measures sound energy by taking both the received sound pressure and the exposure duration into account.

$$L_{E,\text{p}} = 10 \log_{10} \left(\frac{1}{p_0^2 T_0} \int_{T_1}^{T_2} p^2(t)\, dt \right) \text{ [dB re 1 } \mu Pa^2\text{]} \tag{2.7}$$

where T_1 and T_2 define the time window over which the integration is performed, and T_0 is a reference time of 1 second, used to normalize the SEL measurement.

$L_{E,p}$ can be calculated for either an individual sound event (commonly referred to as single-pulse or single-strike SEL, denoted as SEL_{SS}, in the context of pile driving) or over an extended period to determine the cumulative sound exposure (cumSEL).

2.1.7 Cumulative Sound Exposure Level (cumSEL)

For sound sources that occur repeatedly, such as multiple pile strikes, the cumulative sound exposure level (cumSEL resp. $L_{E,\text{cum}}$) is used to assess the total energy experienced over multiple events. It is calculated as:

$$L_{E,\text{cum}} = 10 \log_{10} \left(\sum_{i=24h}^{N} 10^{\text{SEL}_{\text{SS}}/10} \cdot N_i \right) \text{ [dB re 1 } \mu Pa^2\text{]} \tag{2.8}$$

This metric is essential for understanding the long-term exposure effects on marine life.

2.1.8 Power and sound exposure spectral density level

Power spectral density (PSD) describes the distribution of a signal's power across frequencies. It is calculated by dividing the mean squared pressure for each frequency band by its bandwidth. To express PSD in decibels, it is converted to Power Spectral Density Levels (PSDL). Similarly, the Sound Exposure Spectral Density Level (ESDL) quantifies sound exposure per unit bandwidth. The reference values for these metrics are:

- **PSDL:** $1\,\mu\text{Pa}^2/\text{Hz}$
- **ESDL:** $1\,\mu\text{Pa}^2 \cdot \text{s/Hz}$

Both PSDL and ESDL can be calculated over different frequency ranges (e.g., 1 Hz bands) and time periods (e.g., hourly, daily, monthly).

2.2 Legal requirements for the protection of the marine environment against pile-driving

Various countries have developed distinct regulatory frameworks to address underwater noise, reflecting differences in national approaches to marine protection. European nations, including the Netherlands, Germany, and Belgium, have established fixed threshold values for sound exposure levels (SEL) and peak sound pressure levels ($L_{p,pk}$). In contrast, the United States uses a species-specific approach, with regulations tailored to the sensitivities of different marine species.

In Europe, countries like the Netherlands regulate underwater noise by setting specific sound exposure limits at defined distances, such as the 750-meter threshold used to protect species like harbour porpoises. Germany and Belgium follow similar frameworks, applying consistent noise limits across various species. Table 2.1 provides a comparative overview of the noise limits established by several European countries.

Country	**dB limit**	**Explanation**
Netherlands	L_E : 164	Sound exposure level threshold at 750m.
Germany	L_E : 160, $L_{p,pk}$: 190	Sound exposure level and zero-to-peak pressure thresholds at 750m.
UK (Ireland)	-	Often using species-specific weighting functions.
Denmark	-	Using species-specific weighted sound exposure levels over 24 hours.
Belgium	$L_{p,pk}$: 185	A zero-to-peak pressure threshold at 750m.

Table 2.1: Noise limits for offshore wind farm (OWF) construction in countries with extensive OWF activity, as outlined by national regulations. The regulation is under different bodies: The Netherlands under the Ministry of Economic Affairs and Climate via the Water Act, Germany through the Federal Maritime and Hydrographic Agency (BSH), Belgium via the Belgian MSFD, Denmark by the Danish Environmental Protection Agency (EPA), and the UK following the Marine Strategy Framework Directive (MSFD). Each country aligns its regulations with the Marine Strategy Framework Directive (MSFD) [18, 19, 20, 21].

In some countries, like the United States, regulations regarding underwater noise are established using both peak sound pressure level (L_{pk}) and 24-hour cumulative sound exposure level (cumSEL) thresholds, which vary by species depending on their auditory sensitivity [6, 22]. This species-specific regulatory framework ensures that noise limits are tailored to the hearing abilities of different marine species. However, this approach requires offshore wind developers to manage compliance with multiple thresholds, depending on the species present in the project area, which can increase the complexity of planning and operations [23].

Furthermore, advancements in noise abatement technologies, including alternative foundation designs and construction methods, are being developed to reduce the impact of noise from offshore wind farm installations. These technologies, such as bubble curtains and vibratory pile driving, provide opportunities to further minimize the environmental effects of noise on marine ecosystems and could support greater consistency in meeting regulatory requirements [22, 23].

2.2.1 Regulatory Framework for Underwater Noise

To safeguard marine ecosystems, regulatory bodies worldwide have established thresholds for underwater sound exposure. This framework typically involves setting noise limits, developing mitigation guidelines based on scientific research and stakeholder input, and enforcing these standards through comprehensive environmental assessments.

Key Aspects of the Regulatory Process

- **Regulatory Authorities:** Typically, one or more governmental agencies are responsible for implementing and enforcing underwater noise regulations. These agencies set species- or ecosystem-specific noise thresholds and review environmental impact assessments (EIAs). They also issue permits that allow projects to have limited, controlled noise impacts during construction and operation.
- **Rule Development:** Noise thresholds and mitigation guidelines are developed based on scientific research and stakeholder input. The established thresholds focus on the cumulative exposure of sound (cumSEL) to ensure that adverse impacts on marine life are minimized.
- **Enforcement and Oversight:** During both the planning and construction phases, projects are required to implement noise mitigation measures. Authorities monitor compliance with these measures through rigorous pre- and post-construction surveys that assess species distribution, abundance, and overall environmental impact.

General Guidelines and Recommendations

Many guidelines require:

a) Detailed pre-construction assessments to map marine species presence and abundance.

b) Continuous monitoring during and after construction to ensure cumulative sound exposure does not exceed established thresholds.

c) The use of appropriate noise mitigation systems (e.g., bubble curtains, hydro-acoustic dampers) to reduce excessive noise emissions.

2.2.2 Marine Animal Sensitivity to Noise

The effects of underwater noise on marine animals vary significantly, as different species have differing sensitivities to sound based on factors such as intensity, frequency, and duration. These variations are often linked to the animal's specific hearing range and biological characteristics [6, 24].

For instance, low-frequency noise can interfere with communication and navigation in certain marine mammals, such as baleen whales, which rely heavily on low-frequency vocalizations. Conversely, high-intensity sounds, like those produced by impact piling, can cause direct physical harm, including hearing damage and behavioral disturbances in species sensitive to these frequencies, such as dolphins and porpoises [25, 26]. Understanding the diverse sensitivities of marine animals to different noise frequencies and levels is essential for developing effective mitigation measures and regulations [8].

Hearing groups and Frequency Sensitivity

Recent research, using both direct behavioral and electrophysiological data, as well as predictions based on factors like inner ear structure, behavior, and vocalizations, shows that different marine mammal species have varying hearing capabilities. These differences exist in both absolute hearing sensitivity and the range of frequencies they can hear [25, 24, 6, 26]. As a result, marine mammal species are categorized into hearing groups to account for their differing sensitivities and vulnerabilities to noise-related hearing loss. These groups and their respective hearing ranges are shown in Table 2.2.

Hearing Group	**Generalized Hearing Range**
UNDERWATER	
Low-frequency (LF) cetaceans (baleen whales)	7 Hz to 35 kHz
Mid-frequency (MF) cetaceans (dolphins, toothed whales, beaked whales, bottlenose whales)	150 Hz to 160 kHz
High-frequency (HF) cetaceans (true porpoises, Kogia, river dolphins, cephalorhynchid, *Lagenorhynchus cruciger & L. australis*)	275 Hz to 160 kHz
Phocid pinnipeds (PW) (true seals)	50 Hz to 86 kHz
Otariid pinnipeds (OW) (sea lions and fur seals)	60 Hz to 39 kHz

Table 2.2: Marine mammal hearing groups [27].

Weighting factors

The ability to detect sounds varies within an animal's hearing range. Auditory weighting functions are used to represent how well an animal can detect sounds at different frequencies, though they do not necessarily indicate how the animal perceives or responds to those sounds behaviorally. To account for heightened sensitivity at certain frequencies, sounds are often weighted accordingly [8]. The weighting factor is calculated by Equation 2.9.

$$W(f) = C + 10\log_{10}\left(\frac{(f/f_1)^{2a}}{[1+(f/f_1)^{2a}]\,[1+(f/f_2)^{2b}]}\right) \text{ dB} \tag{2.9}$$

Species group	**a**	**b**	**f1 (Hz)**	**f2 (Hz)**	**C (dB)**
LF cetaceans (baleen whales)	1	2	200	19,000	0.13
MF cetaceans (larger odontocetes and most dolphins)	1.6	2	8,800	110,000	1.3
HF cetaceans (high-frequency specialists, incl. porpoises)	1.8	2	12,000	140,000	1.36
Phocid seals (true seals)	2	2	940	45,000	0.64
Otariid seals (sea lions and fur seals)	1	2	1,900	30,000	0.75

Table 2.3: Auditory time and frequency weighting parameters for different hearing groups of marine mammals [27]

Acoustic Thresholds

Some regulatory frameworks around the world establish acoustic thresholds in terms of both Cumulative Sound Exposure Level (cumSEL) and peak sound pressure level (L_{peak}) measured

over specified time periods. For example, in the United States, these thresholds are defined based on the 24-hour cumSEL and L_{peak} values [28]. For regulatory purposes, noise exposure is typically categorized into two types of harassment based on its impact on marine mammals:

- **Level A harassment**: Refers to physical injuries, including **Permanent Threshold Shift (PTS)**, which is a lasting reduction in hearing sensitivity due to intense or prolonged noise exposure. Other forms of auditory or physical injury may also fall under this category.
- **Level B harassment**: Involves behavioral disturbances caused by noise, such as disruptions in migration, communication, or feeding patterns. This category can also include **Temporary Threshold Shift (TTS)**, a transient reduction in hearing sensitivity that typically recovers after the noise exposure ends.

To manage these impacts, regulatory agencies like the National Marine Fisheries Service (NMFS) have established onset thresholds for PTS and TTS, which vary depending on the hearing group of the species in question. Table 2.4 below outlines the onset thresholds for TTS and PTS in various marine mammal hearing groups exposed to impulsive noise.

Marine mammal hearing group	TTS $L_{E,p,24h}$ (weighted)	TTS $L_{p,0-pk,flat}$ (unweighted)	PTS $L_{E,p,24h}$ (weighted)	PTS $L_{p,0-pk,flat}$ (unweighted)
Low-Frequency (LF) Cetaceans	168	213	183	219
Mid-Frequency (MF) Cetaceans	170	224	185	230
High-Frequency (HF) Cetaceans	140	196	155	202
Phocid Pinnipeds (PW) (Underwater)	170	212	185	218
Otariid Pinnipeds (OW) (Underwater)	188	226	203	232

Table 2.4: TTS- and PTS-onset thresholds for marine mammals exposed to impulsive noise: SEL thresholds in dB re 1 μPa^2s under water; and peak SPL thresholds in dB re 1 μPa under water [27]

.

2.2.3 Limitations in the regulations

The cumulative sound exposure metric employed by NMFS has notable limitations and introduces complexities.

1. Recovery Assumptions Between Exposures: NMFS assumes no recovery between intermittent, repeated exposures for cumulative SEL calculations. However, studies on both terrestrial and marine mammals suggest that intermittent exposure may reduce the risk of hearing damage, indicating that the assumption of no recovery may not fully capture real-world conditions [29].
2. Challenges in Quantifying Recovery: The potential for recovery from hearing loss (with PTS leading to incomplete recovery and TTS to full recovery) complicates predictions of cumulative effects. Currently, recovery in wild marine mammals is difficult to quantify accurately, and models of recovery (e.g., based on bottlenose dolphins) may not be generalizable to other species.
3. Lack of Modeling Guidance: NMFS does not provide specific guidelines for exposure modeling, leaving it to the action proponent to determine the best approach. This can be challenging for proponents with limited modeling capabilities or resources.

4. Ongoing Development: NMFS plans to convene a working group to explore more realistic accumulation periods, particularly for stationary sources, indicating that current guidance may still evolve [29].

Therefore, it is essential to investigate the optimal operational approach for installing offshore wind turbines in a way that minimizes cumulative sound exposure for marine life.

2.3 Underwater noise generation from impact pile-driving

Monopiles can be installed into the seabed through two primary methods: using hydraulic impact hammers and large vibratory devices. In impact piling, a hammer applies repeated short bursts of force to the top of the pile, driving it into the seabed. Alternatively, vibratory installation involves applying a continuous, quasi-periodic force at the pile head, which gradually pushes the pile into the ground [30]. Both techniques produce noise in the water, while also generating elastic waves that spread through the seabed. The way these waves behave depends on factors such as the installation method, the size of the pile, and local site characteristics [31]. These factors play a critical role in assessing noise pollution and understanding the complexities of sound propagation over long distances [32].
Studying noise generated by pile driving requires examining a system made up of three interconnected domains - seawater, seabed, and the pile - whose interactions determine the sound generation mechanism, see Figure 2.3.

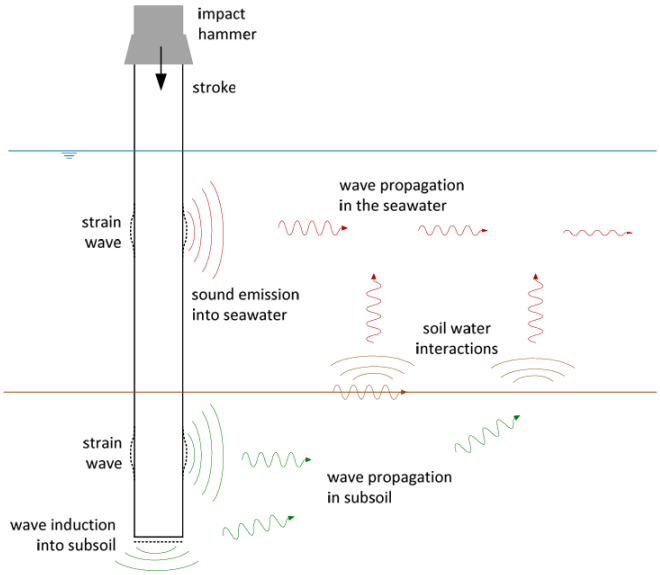

Figure 2.3: Interrelations of strain wave, hydrosound and ground vibration [33]

Given that impact piling is the predominant technique used for monopile installation [4], this report will focus specifically on this method. Impact piling is particularly suitable for the installation of larger monopiles, as vibratory hammers are often limited in their ability to achieve the required penetration depths and soil resistances for these larger structures. The high energy output and efficiency of impact hammers make them the preferred choice for ensuring monopiles are securely embedded in the seabed, especially in challenging soil conditions.

2.3.1 Interaction between piles, soil and water

This section explores the fundamental interactions between the pile, water, and soil during impact piling. It examines the propagation of compressional waves, the formation of Mach cones, and the generation of Scholte waves at the seabed-water interface, which act as an additional noise source. Additionally, the behavior of shear waves within the seabed is discussed.

Pile dynamics

An impact on an offshore monopile induces a force F and a particle velocity v at the top of the foundation (Pile 1 in Figure 2.4) [33]. This results in a compression wave propagating along the pile in the axial direction (pile 2 to 4 in Figure 2.4) with a speed c_p, which is a function of the modulus of elasticity E and the mass density ρ of the pile:

$$c_p = \sqrt{\frac{E}{\rho}} \tag{2.10}$$

Based on Poisson's contraction, the compression wave causes an associated radial expansion of the pile, increasing the radius. The compressional wave travels downwards to the pile's bottom and pushes it into the ground (pile 5 in Figure 2.4). Assuming the material properties specified in 2.10, as well as the pile's cross-sectional shape and area (A), remain constant, the wave will continue its movement towards the pile toe. Conversely, if the dynamic stiffness changes - characterized by the mechanical impedance of the pile (Z_{pile}) - a portion of the wave will be reflected, traveling back towards the pile head. The pile impedance is obtained by the following equation:

$$Z_{\text{pile}} = A \cdot \rho \cdot c_p \tag{2.11}$$

Depending on the resistance encountered, a tension or compression wave is reflected at the pile toe. For the initial blows, low resistance can be assumed, resulting in tension waves traveling to the top of the pile (pile 6 to 8 in Figure 2.4), causing a reduction in the radius. The extent to which wave components are reflected or transmitted depends on the change in impedance. A larger difference in pile impedance leads to increased reflection of the wave and a decrease in the amount of strain wave energy that is transmitted [34].

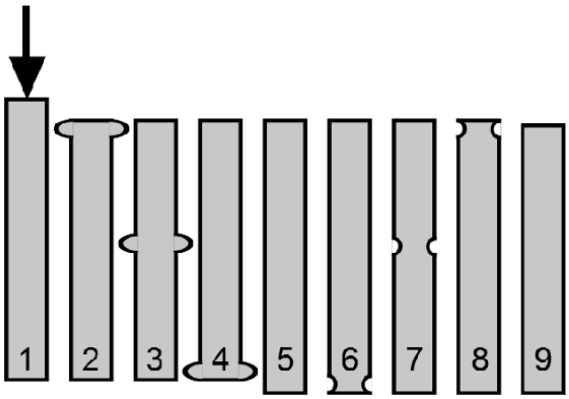

Figure 2.4: Simplified wave propagation in a monopile [33].

Energy transfer

Energy transfer from the pile to the surrounding water during impact piling occurs through two main mechanisms: a **primary noise source** and a **secondary noise source**. The primary source consists of Mach cones, which form due to the vibrations of the pile throughout the entire water column. These Mach cones travel at a speed of 1500 m/s, equivalent to the speed of sound in water, and encompass energy across the frequency spectrum. The secondary source involves Scholte waves, which occur only at the interface between the seabed and the water. Scholte waves are characterized by their low frequency and propagate at speeds lower than the shear wave velocity in the soil [31].

Primary noise source

The radial expansion during the compression phase of the impact generates an underwater pressure field (Figure 2.5 a). Due to the wave speed in water c_w, this field propagates downwards, forming a conical wave. The study by Reinhall and Dahl [34] revealed that the pressure field around the pile is characterized by Mach cones, which consist of coherent wave fronts that form alternating zones of compression and rarefaction in the seawater. These Mach cones are generated by supersonic compressional stress waves, which propagate from the pile head to the pile toe immediately following the hammer impact. Upon reflection of these stress waves from the pile toe, reverse Mach cones were also formed. The angles of the cones can be calculated based on the phase speeds of compressional waves in the pile, water, and seabed, denoted by c_p, c_w, and c_s, respectively.

The angle φ of the Mach cone is defined as:

$$\sin \varphi_w = \frac{c_w}{c_p} \tag{2.12}$$

The upward traveling tension wave and decreasing radius produce a pressure wave in the water, similar to the compression phase, but with an uprising cone shape (Figure 2.5 b). The angle of the refracted compression wave can be calculated similarly to that of the preceding cone:

$$\sin \varphi_s = \frac{c_s}{c_p} \tag{2.13}$$

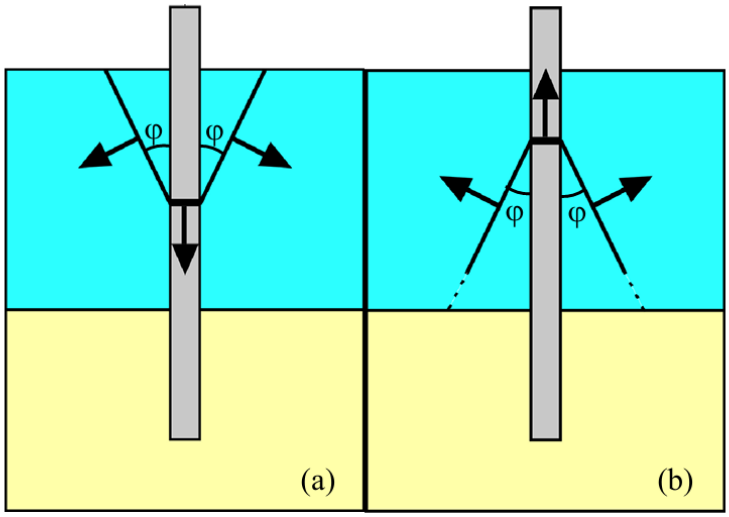

Figure 2.5: Mach cone generation due to compression and tension in a monopile [33].

As the compressional waves initiated at the pile head propagate downward, they reach the pile toe. Upon arrival, a portion of the wave energy is reflected due to the impedance mismatch

between the steel pile and the underlying soil. This reflection results in upward-travelling tension waves, which propagate back along the pile shaft. Similar to the initial downward wave, these returning tension waves induce radial motion in the pile wall, generating a second set of upward-propagating Mach cones. These cones appear in both the soil and the water layers and can be described using the same angular relationships as the downward-propagating cones.

In addition to these compression waves, the interaction between the pile and the surrounding soil produces shear waves [35]. Shear waves are categorized into two types: vertical shear waves and horizontal shear waves. According to Tsouvalas [31], the emitted shear waves predominantly exhibit vertical polarization, attributed to the significant difference in velocity between shear waves in the soil and structural waves in the monopile.

Secondary noise source

The secondary noise source arises from the waves at the interface between the seabed and the water. These interface waves are classified as either Scholte waves, which propagate along the boundary between a solid and a fluid, or Stoneley waves, which travel along a solid-solid interface [36]. Unlike body waves, which radiate spherically, interface waves propagate cylindrically, causing them to decay more slowly over distance [36]. Scholte waves traveling along the soil-water boundary play a significant role in causing pressure fluctuations in the water column near the seabed, although this effect diminishes with increasing distance from the seabed [31]. The different wave types are schematically shown in Figure 2.6.

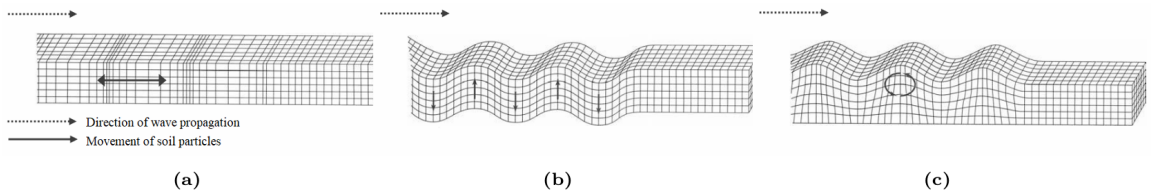

Figure 2.6: Different wave types: (a) compression wave, (b) shear wave, and (c) interface wave.

Technical and structural influencing factors

This section discusses key technical and structural parameters influencing underwater noise during monopile (MP) installation.

- **Pile diameter**
  This thesis focuses on monopile (MP) foundations. According to Bellmann et al. [14], the pile diameter plays a critical role in determining noise levels during MP installation. Figure 2.7 illustrates the relationship between pile diameter and the resulting Sound Exposure Level (SEL) and peak sound pressure level ($L_{p,\mathrm{pk}}$), showing a clear increase in noise levels with larger pile diameters. As the pile diameter grows, both the hammer size and the energy per blow must also increase to overcome the greater soil resistance associated with larger MPs [37].

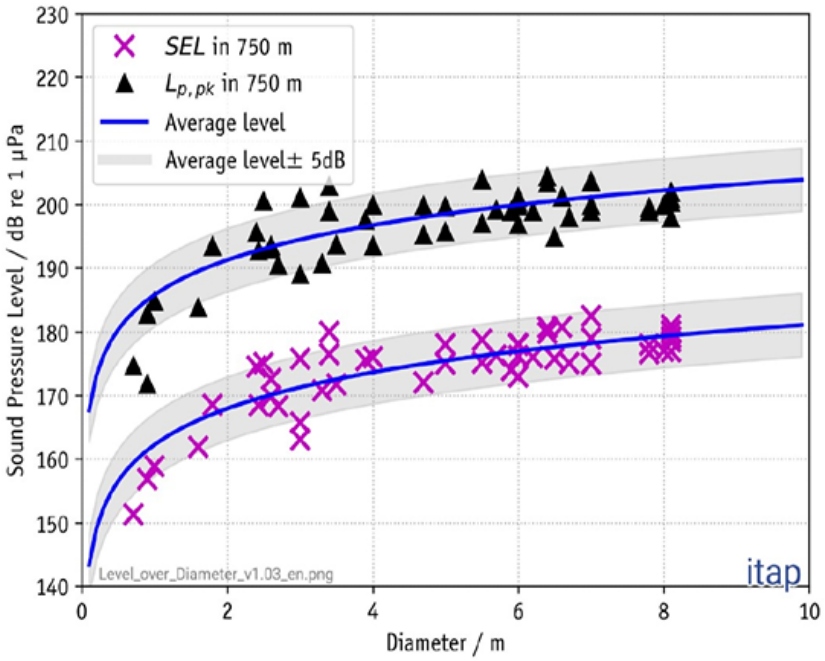

Figure 2.7: SEL and $L_{p,\mathrm{pk}}$ against the pile diameter [14].

For MPs with diameters exceeding 6 meters, the peak frequency in the noise spectrum shifts from approximately 160 Hz to 100 Hz [14]. This shift cannot be directly linked to the pile diameter or hammer size alone. Instead, it is likely that blow energy, pile diameter, and hammer size are interrelated and collectively influence the observed changes [14].

- **Impact hammer, blow-energy, and pile-driving process**
  The key parameters defining an (impulse) impact hammer include (i) the drop mass, (ii) the required acceleration-which determines the applied power-and (iii) the design of the anvil, which facilitates the transfer of force from the hammer to the pile head. The hydraulic control system, often managed through power packs, is critical for lifting and accelerating the drop mass. The resulting force is the product of the drop mass and acceleration. The anvil plays a pivotal role in transmitting the blow energy into the pile head and must be tailored to the specific requirements of the project, including the pile diameter and the design of the pile head [14].

2.3.2 Site-specific influencing factors

This section discusses key site-specific parameters influencing underwater noise during monopile (MP) installation.

- **Soil resistance**
  Soil resistance plays a significant role in pile-driving noise levels due to its influence on the required blow energy during monopile installation. Higher soil resistance necessitates greater blow energy to penetrate the seabed, which in turn correlates with increased noise levels generated during piling. While site-specific factors, such as soil composition and stratification, vary widely, the general relationship between blow energy and noise levels underscores the impact of soil resistance on underwater noise emissions during foundation installation [14].

- **Soil coupling**
  Soil coupling affects pile-driving noise by transferring part of the hammer's energy into the

soil, which is then reflected back into the water column. Its contribution to far-field noise levels is relatively small compared to direct pile noise. However, it influences near-pile noise mitigation systems by introducing noise pathways through the soil [14]. The extent of its impact depends on soil type and stratification, making it an important factor in noise abatement planning.

- **Water depth**
  Water depth influences pile-driving noise in shallow waters through two mechanisms: the reduction of noise emission into the water and the effect on sound propagation. Below a specific cut-off frequency, continuous noise input and propagation are constrained, with shallower water resulting in higher cut-off frequencies. For sandy soils, this cut-off frequency in water depths of around 25 m is typically below 50 Hz [14]. Frequencies near or below the cut-off frequency are less efficiently coupled into the water and experience stronger attenuation with distance.

  In offshore wind farms located in water depths of 20-40 m, the cut-off frequency is generally lower than the dominant frequencies in the unmitigated pile-driving noise spectrum (63-250 Hz) [14]. Measurements indicate that water depth within this range does not significantly impact overall noise levels for impulsive pile driving. However, in very shallow waters (e.g., 4.5 m), noise emission is constrained at lower frequencies, with sound coupling into the water occurring only above approximately 160 Hz for sandy soils [14].

- **Bathymetry**
  Bathymetry can significantly influence sound propagation over long distances. However, for shorter ranges, typically up to a few kilometers, the sea is often approximated as a flat surface for sound prediction [38]. Schecklman et al. [39] note that average water depth is the primary factor affecting long-range sound propagation, while variations in bathymetry generally result in localized effects.

2.4 Underwater noise mitigation for impact pile driving

To ensure compliance with legal noise limits during the installation of offshore monopile foundations, innovative technologies are continually being developed to minimize noise emissions. Several noise abatement systems are currently available on the market, including the hydro-sound damper (HSD), noise mitigation screen (IHC-NMS), AdBm system, cofferdam, big bubble curtain (BBC), and pulse prolongation by adaptation of hydraulic hammers.

The focus of this research is to minimize the cumulative noise by the optimization of the blow rate, the spreading of the hammer energy over time, and the use of a Bubble Curtain. This section delves into the fundamentals, advantages and limitations of the air-bubble curtain and pulse prolongation by adaptation of hydraulic hammers, done by systems such as IQIP's PULSE and Menck's MNRU.

2.4.1 Air-Bubble Curtains

Bubble curtains are a commonly used technique to mitigate underwater noise generated during offshore pile driving. They can be implemented as a single big bubble curtain (BBC), a double big bubble curtain (DBBC), a triple big bubble curtain (TBBC) or in combination with a close-range system (CRS) positioned directly around the pile [40]. In Figure 2.8a and 2.8b, an aerial view of the application of a double Big Double Curtain and the schematic concept are shown shown.

(a) Aerial view of an applicated double Big Bubble Curtain configuration [41].

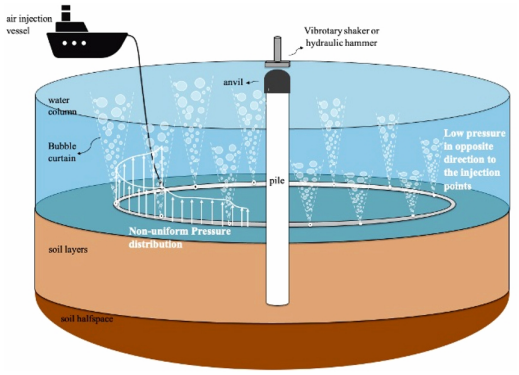

(b) Schematic depiction of the non-uniform pressure distribution in the hose [42].

Figure 2.8: (a) Aerial view of a double Big Bubble Curtain and (b) schematic depiction of pressure distribution in the hose.

Noise Reduction Mechanism

The primary mechanism of air-bubble curtains involves generating a rising wall of air bubbles that serves as a barrier to attenuate underwater noise. These bubbles are produced by injecting air into the water through perforated holes or nozzles in air supply hoses positioned on the seabed, see Figure 2.9a. The hoses are arranged to encircle the entire monopile at a specific radial distance. The curtain disrupts sound wave propagation through several key mechanisms, which are detailed in this section.

To start, the bubble layer's unique acoustic properties differ significantly from those of the surrounding water. This discrepancy leads to an impedance mismatch, causing sound waves to be partially reflected and scattered at the interface [43]. As a result, less noise travels further into the water column. The reflection effect is particularly useful across a wide range of frequencies, making the method versatile for various noise profiles.

The bubbles themselves play a dual role in noise attenuation. First, they scatter incoming sound waves in multiple directions, dispersing the energy and thereby lowering the overall sound intensity. Second, when the frequency of the noise approaches the resonance frequency of the bubbles, they absorb energy more effectively. The resonating bubbles convert the sound energy into thermal energy, which then dissipates, leading to additional noise reduction, especially at higher frequencies [13].

The efficiency of the curtain is also shaped by the characteristics of the bubbles, such as their size and spatial distribution. By adjusting these parameters, the system can be tuned to target specific noise frequencies, maximizing its effectiveness. Larger bubbles are more effective at lower frequencies, while smaller bubbles are better suited for high-frequency noise [43].

Additionally, air-bubble curtains help mitigate noise originating from the seabed, including waves like Mach cones generated during pile driving. These ground waves, when re-entering the water, contribute significantly to the overall noise levels [34]. The bubble barrier interrupts this transmission pathway, reducing the impact of soil-generated waves. Optimizing the curtain's configuration can further enhance its performance in intercepting these secondary noise sources.

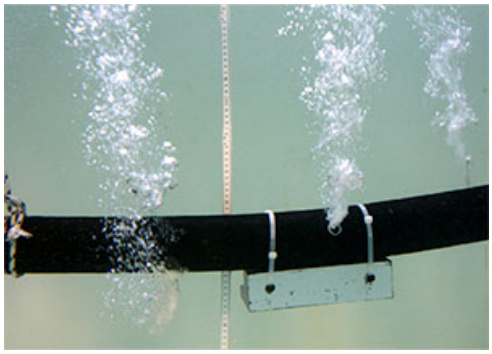

(a) Close-up view of a bubble curtain in operation. The bubble streams are exiting the hose through the nozzles [44].

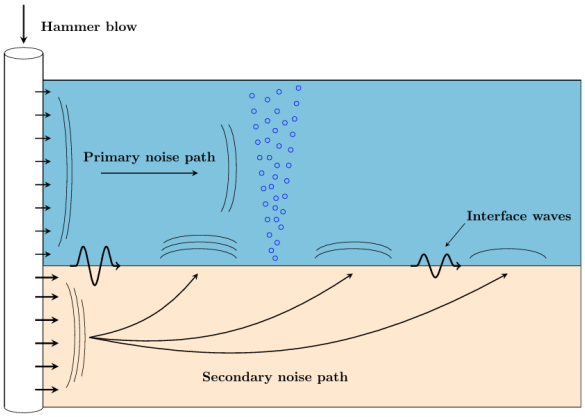

(b) Schematic overview of underwater noise emissions due to offshore pile driving in combination with a bubble curtain [45].

Figure 2.9: (a) Close-up view of the bubble curtain's operation and (b) schematic overview of noise emissions mitigated by the bubble curtain.

Advantages & Limitations

Air-bubble curtains offer several key advantages, making them a widely used choice for underwater noise mitigation during offshore pile driving.

Advantages:

- **Ease of Deployment and Operational Efficiency:** The deployment of air-bubble curtains involves placing perforated hoses on the seabed, which are connected to compressors on a support vessel [43]. These hoses can be pre-laid before piling begins and retrieved afterward, minimizing disruption to the project timeline. Once installed, the system can operate continuously, providing sustained noise mitigation throughout the pile-driving process [43].
- **Significant Noise Attenuation:** Air-bubble curtains are proven to be a powerful method for reducing underwater noise levels, effectively targeting both Sound Exposure Level (SEL) and peak pressure levels (L_{peak}). Studies, such as those by Koschinski et al. [46], highlight that employing a single bubble curtain (BBC) can achieve a reduction in SEL by up to 15 dB at a 750-meter range from the source. Utilizing a double bubble curtain (DBBC) can further enhance this effect, reaching noise reductions of up to 18 dB. Nevertheless, the effectiveness of these noise reductions can vary significantly, depending on site-specific factors like seabed composition, soil characteristics, water depth and environmental conditions [13, 42, 32].
- **Adaptability to Site Conditions:** One of the main advantages of air-bubble curtains is their flexibility in adapting to different operational environments. The system's design can be tailored to meet site-specific requirements, such as depth and seabed characteristics. However, for water depths greater than 50 m, the effectiveness of the system becomes uncertain. Adjustments can be made to the size of the curtain, the air injection rate, and the nozzle configuration, allowing the system to be optimized for maximum noise reduction in a variety of scenarios [42].

Limitations:

- **Susceptibility to Ocean Currents:** One challenge is the influence of ocean currents. Strong currents can disperse the rising bubbles, reducing the effectiveness of the noise barrier. This issue becomes more significant at greater depths, where stronger currents are often encountered, leading to a decrease in noise attenuation performance [46].
- **Uneven pressure:** To ensure even pressure distribution along the hose, the diameter of the nozzle openings should ideally increase as the distance from the feed points grows [46]. However, this approach is not practically feasible due to the complexity of manufacturing variable nozzle sizes, increased maintenance demands, and reduced operational flexibility.
- **Increased Air Demand at Greater Depths:** The compressibility of air requires a higher volume of air injection at greater depths. As the depth increases, additional compressors may be needed to maintain the required air volume, complicating the logistics and increasing operational costs [42].
- **Variability in Noise Reduction Efficiency:** The efficiency of noise reduction can vary significantly based on site conditions, such as the type of seabed and environmental factors. This variability makes it challenging to predict the exact level of noise attenuation, particularly in complex underwater environments with heterogeneous conditions.

2.4.2 Pulse prolongation by adaptation of hydraulic hammers

By adapting hydraulic hammers, the impact energy can be distributed over a longer time period, resulting in a potential reduction of the peak sound pressure level (L_{peak}). However, this approach may also influence the cumulative Sound Exposure Level (cumSEL), as the energy is released over an extended duration. Existing methods to achieve this are IQIP's PULSE and MENCK's MNRU, which operate on a similar principle: reducing the driving force while prolonging the time over which it acts on the pile. This section provides an in-depth explanation of the operating principles and functionalities of these systems.

PULSE system

PULSE is an innovative technique for mitigating underwater noise during offshore pile driving. It serves as an add-on component, installed between the impact hammer and the monopile.

Noise reduction mechanism

The PULSE system consists of an upper piston and a lower piston, separated by a fluid medium [47]. This fluid medium plays a critical role in the PULSE system by enabling adjustments to the impact characteristics, which are essential for its effective noise reduction performance. A schematic overview of the mechanism of PULSE is shown in Figure 2.10. Figure 2.10b shows the pistons without the fluid medium and Figure 2.10c shows the pistons with the fluid medium.

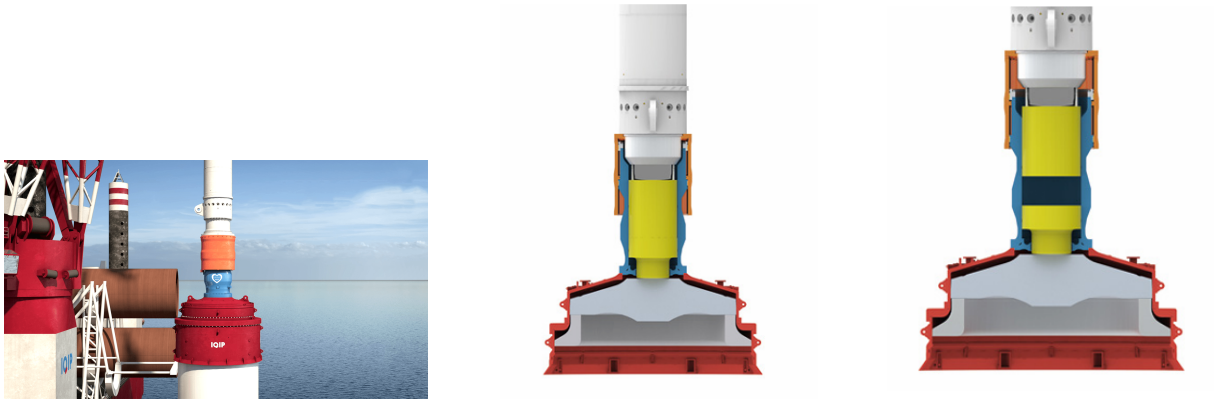

(a) Application of the PULSE system between the impact hammer and the monopile.

(b) PULSE without fluid medium between the pistons.

(c) PULSE with fluid medium between the pistons.

Figure 2.10: Schematic configurations of the PULSE system [48].

The PULSE system operates by modifying the transmission of impact energy during pile driving, leveraging a fluid medium. Its functionality can be explained through four key mechanisms:

When the hammer strikes the upper piston of the PULSE system, the force is transferred through the fluid medium to the lower piston, which is in contact with the monopile. The presence of the fluid medium extends the duration of the impulse, effectively distributing the applied force over a longer period. This principle, based on impulse and momentum, reduces the peak force transmitted to the monopile while maintaining the same overall impulse. The nearly incompressible nature of the fluid enables gradual energy transfer, providing a cushioning effect that mitigates the sudden intensity of the hammer's impact. The rate at which energy is transmitted can be regulated by adjusting the fluid properties, allowing for precise control over energy distribution [14].

The fluid medium also serves as a damping mechanism. By varying the fluid volume, the damping characteristics of the system can be modified. A larger fluid volume increases the damping effect, resulting in enhanced noise reduction, whereas a smaller volume reduces the damping capability. This adjustability allows the system to be tailored to specific operational requirements and environmental conditions, optimizing its performance for a range of scenarios.

In addition to transmitting energy, the fluid absorbs part of the impact energy and dissipates it as heat. This process reduces the amount of energy transferred to the monopile, thereby lowering the overall noise generated. However, this energy dissipation introduces losses, necessitating additional input energy to achieve the same driving efficiency as operations without the PULSE system.

By elongating the impulse duration and minimizing the peak force, the PULSE system reduces the radiated noise generated during pile driving [14].

Advantages

The manufacturer of PULSE, IQIP [47], claims several advantages of the system.

- **Energy efficiency and adaptability:** The design of the PULSE system allows for integration with other underwater noise mitigation measures. This adaptability makes the PULSE system versatile for varying project requirements and environmental conditions.

- **Secure and flexible installation:** The PULSE system is equipped with a liquid-filled chamber between the top and bottom pistons, which can be adjusted to match specific project needs. By draining the liquid, the system can function as a conventional Hydro-hammer, while a fully filled chamber represents the maximum noise-reduction mode.
- **Reduced noise levels in water and air:** During installation, the SEL is reduced by 6-10 dB and the L_{peak} by 5-12 dB [48].
- **Reduced installation fatigue:** Fatigue is reduced by up to 60%.

The claims regarding PULSE are based on information provided by its manufacturer, IQIP. However, the limited availability of independent scientific research on PULSE makes it difficult to substantiate these claims.

MNRU system

MNRU is a technique for mitigating underwater noise during offshore pile driving, developed by MENCK. It is an add-on component that is integrated between the hydraulic hammer and the monopile.

Noise reduction mechanism

The MNRU system operates on a similar principle to the PULSE system, aiming to reduce peak impact forces and extend the duration of impact energy transmission. The system achieves this by incorporating a number of metal blocks between the ram weight [46]. This configuration alters the energy transfer process, allowing the force to be distributed over a longer period, thereby reducing the peak sound pressure level (L_{peak}).

The MNRU system works by absorbing part of the kinetic energy from the hammer strike. When the hydraulic hammer delivers a blow to the upper part of the MNRU, the damping element deforms. This deformation increases the duration of the impact, effectively reducing the peak force transmitted to the monopile. Unlike fluid-based systems, the elastomer provides consistent damping properties that are less affected by temperature changes and fluid dynamics.

The compression and recovery of the elastomer act as a mechanical "buffer", dissipating energy in the form of internal strain. This dissipation reduces the sudden intensity of the hammer's impact while ensuring that sufficient force is applied to drive the monopile into the seabed. However, the deformability of the elastomer may vary depending on the applied force, requiring careful consideration during the system's design and operation [14].

The primary difference between MNRU and fluid-based systems like PULSE is the nature of the damping element. Instead of using a fluid medium to achieve damping, MNRU relies on a metal blocks.

Advantages

Several advantages of the MNRU are highlighted in Koschinski et al. [46].

- **Secure and flexible installation:** The MNRU can be simply added to existing standard hydraulic hammers without requiring major modifications [46].
- **Reduced noise levels in water and air:** During installation, the SEL is reduced by 9 dB and the L_{peak} by 11 dB for a 6.5 m monopile and a 3500 kJ hammer [46].
- **Reduced installation fatigue:** Damping the contact force between the anvil and pile reduces material fatigue of the pile [46].

Limitations for pulse prolongation (PULSE and MNRU)

- **No mitigation of ground-borne (low-frequency) noise:** Impulse elongation primarily reduces waterborne pressure peaks but does not address sound transmission via the soil (e.g., Mach or Rayleigh waves) [49].
- **Limited effectiveness for large diameter monopiles:** Since impulse elongation primarily attenuates high-frequency noise components, meaning its effectiveness diminishes with increasing pile and hammer size. For example, with an S-4000 hammer, the resulting SEL reduction is limited to approximately 4-6 dB, often insufficient to comply with stringent regulatory thresholds.
- **Higher energy consumption per blow:** The per-blow energy increases by 4%, potentially raising operational fuel costs and wear on equipment[50].
- **Increased mechanical load and logistical burden:** The PULSE module adds substantial weight and length to the hammer assembly (up to 108 t and 3.2 m), requiring heavier cranes and increasing offshore handling complexity [50, 51].
- **Lack of long-term independent validation:** Most performance claims originate from prototype tests or manufacturer reports. Peer-reviewed, long-term field studies are scarce [49, 50].
- **Reduced energy transfer efficiency:** Numerical models show that the efficiency drops from 97% to 84%, meaning less impact energy is transmitted to the pile. This can increase the total number of blows or require larger hammers [50].
- **Slowed down installation:** PULSE and the MNRU significantly elongate the duration of each impact, which, without system compensation, extends overall piling time [50].

3 | State of the art in noise prognosis

This chapter provides a comprehensive literature review of various models developed to predict underwater noise generated by pile driving. The models are categorized into first-generation (3.1.1), second-generation (3.1.2), and state-of-the-art models (3.1.3), following the classification by Tsouvalas [32]. The functioning of these models, along with their advantages and limitations, will be discussed, as well as the mathematical foundations underlying these models. The information is derived from the research conducted by Tsouvalas [32].

The accuracy of the models is subject to the complexity of the environment in which the noise propagates. While noise propagation in deep ocean settings is relatively well understood, shallow water environments pose significant challenges. This is primarily due to the complex interactions of sound waves with the seabed and water surface, involving phenomena such as reflections, refractions, and scattering. The seabed characteristics, in particular, introduce substantial uncertainty due to their heterogeneous and variable nature. This chapter discusses the evolution of acoustic models for underwater noise prediction, focusing on the first-generation models, recent advancements in second-generation models, and the current state of the art.

3.1 Existing computational models

3.1.1 First-Generation Models

First-generation models primarily employed numerical discretisation techniques to solve the underlying partial differential equations governing underwater acoustics. These models laid the groundwork for more detailed simulations but faced several limitations, particularly in capturing the interactions between the pile, water, and seabed.

One of the earliest detailed numerical models for predicting underwater noise from impact pile driving was developed by Reinhall and Dahl [34], as illustrated in Figure 3.1a. The model employed the Finite Element Method (FEM) to simulate sound generation mechanisms, while the parabolic equation (PE) method was used to describe sound propagation over longer distances. In both approaches, water and soil were represented as linear acoustic fluids, and the pile was modeled using structural elements.

To efficiently manage the computational domain in the FEM model, Perfectly Matched Layers (PMLs) were implemented, ensuring accurate truncation. The PE method simplified the wave equation under the assumption of predominantly forward wave propagation, optimizing it for long-distance modeling. A key outcome of the model by Reinhall and Dahl was the identification of Mach cones in the pressure field near the monopile, as shown in Figure 3.1b [34]. These cones result from supersonic compressional stress waves propagating from the monopile head to the toe and back following the hammer impact.

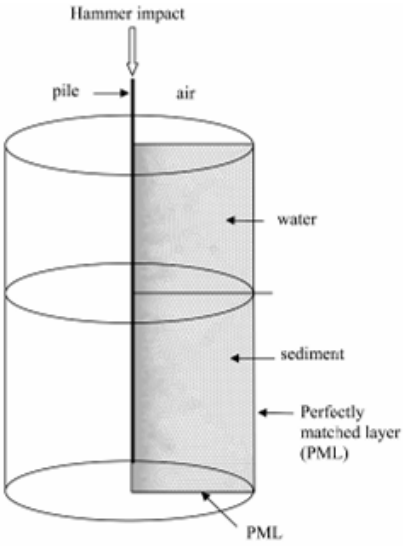

(a) Axisymmetric FE model of pile and water [34].

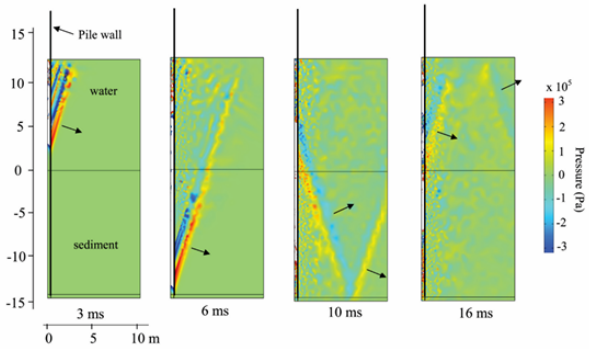

(b) Acoustic pressure surface plots showing acoustic radiation from the pile at 3, 6, 10, and 16 ms after impact. The wavefront propagation direction associated with Mach cones is indicated by the arrows [34].

An alternative approach was proposed by MacGillivray [52], who adopted a finite difference scheme for near-field acoustics, avoiding the inclusion of bending energy stored in the shell surface of the pile. For far-field sound propagation, various methods were used, including normal mode representations, wavenumber integration algorithms, energy flux-based methods and parabolic equation models.

Additionally, some models coupled the structural domain (modeled with FEM) with the exterior domain (soil), utilizing the Boundary Element Method [53, 54, 55]. These approaches focused on capturing the soil vibrations near the pile, providing insights into the local acoustic effects.

As an alternative modelling method, semi-analytical models provide a simplified yet efficient approach to noise prediction. One notable example is the analytical model by Hall [56], which considered a thin cylindrical shell immersed in a fluid. Another significant contribution was made by Tsouvalas and Metrikine [57], who employed shell theory to model the pile. In their model, the pile was represented using shell theory, the water as a linearized acoustic fluid, the seabed by using distributed springs and dashpots attached to the pile surface and the shell and water responses were expressed as modes, with a mode-matching technique used to solve the problem.

The primary advantage of semi-analytical models lies in their computational efficiency, making them suitable for a large number of simulations. However, they lack the detailed accuracy provided by numerical methods like FEM, especially in complex environments.

3.1.2 Second-Generation Models

The main limitation of the first-generation models, described in Section 3.1.1, is that the seabed is represented either as an acoustic medium or as spring-dashpot elements. This approach fails to capture all essential physics of the problem for two main reasons: (i) A significant portion of the energy during pile driving is released into the seabed while the pile is partially embedded in the soil [58], necessitating a detailed description of the seabed for accurate predictions. (ii) Addressing the coupled soil-fluid-pile interaction is crucial for accurately identifying the acoustic source amplitude.

To overcome the limitations of first-generation models, second-generation models incorporate an elastic description of the seabed. Notable contributions were made by Tsouvalas et al. [59],

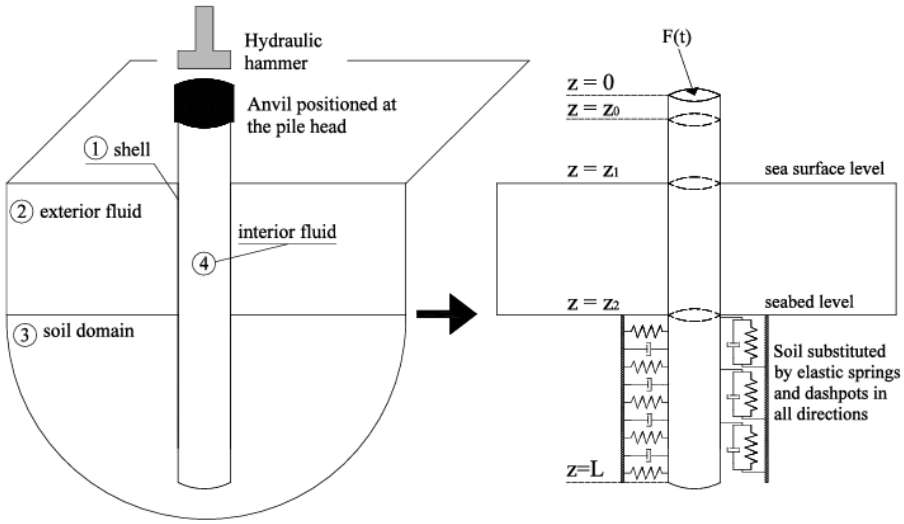

Figure 3.2: Semi-analytical model proposed by Tsouvalas and Metrikine [57].

whose work emphasized the importance of accounting for elastic waves within the seabed. Figure 3.3 illustrates the geometry of their model. Their findings demonstrated that during offshore pile installations, the seabed predominantly exhibits vertically polarized shear waves, induced by pulses traveling through the pile at supersonic speeds. Additionally, compressional waves, analogous to those in seawater, were identified within the seabed. Furthermore, Scholte waves, originating at the seabed-water interface, were observed to propagate at significantly lower speeds than compressional waves.

These findings, visualized in Figure 3.4, have been validated by subsequent studies and experiments, confirming the model's predictions [60, 35, 61, 62, 63].

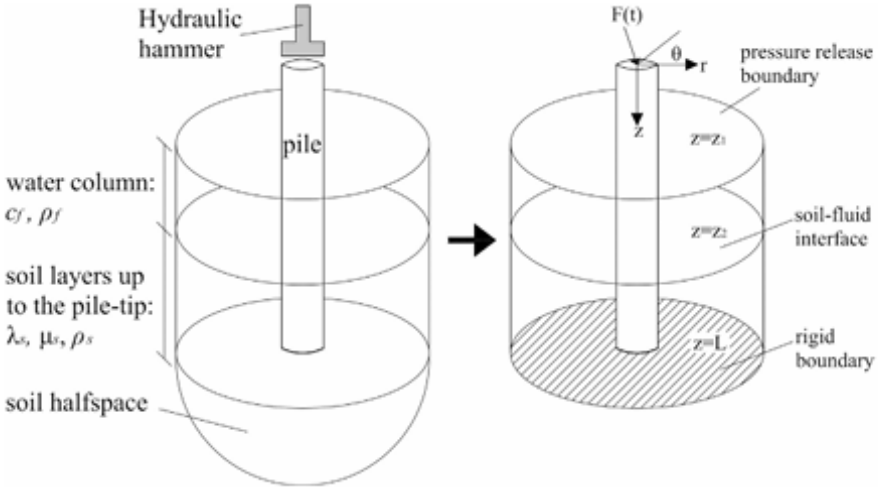

Figure 3.3: Geometry of the second generation model by Tsouvalas and Metrikine [59].

3.1.3 State-of-the-Art Acoustic Models

Acoustic models can be categorized based on the level of detail in representing the sound source and the domain of energy release. These models range from empirical approaches to highly detailed numerical simulations.

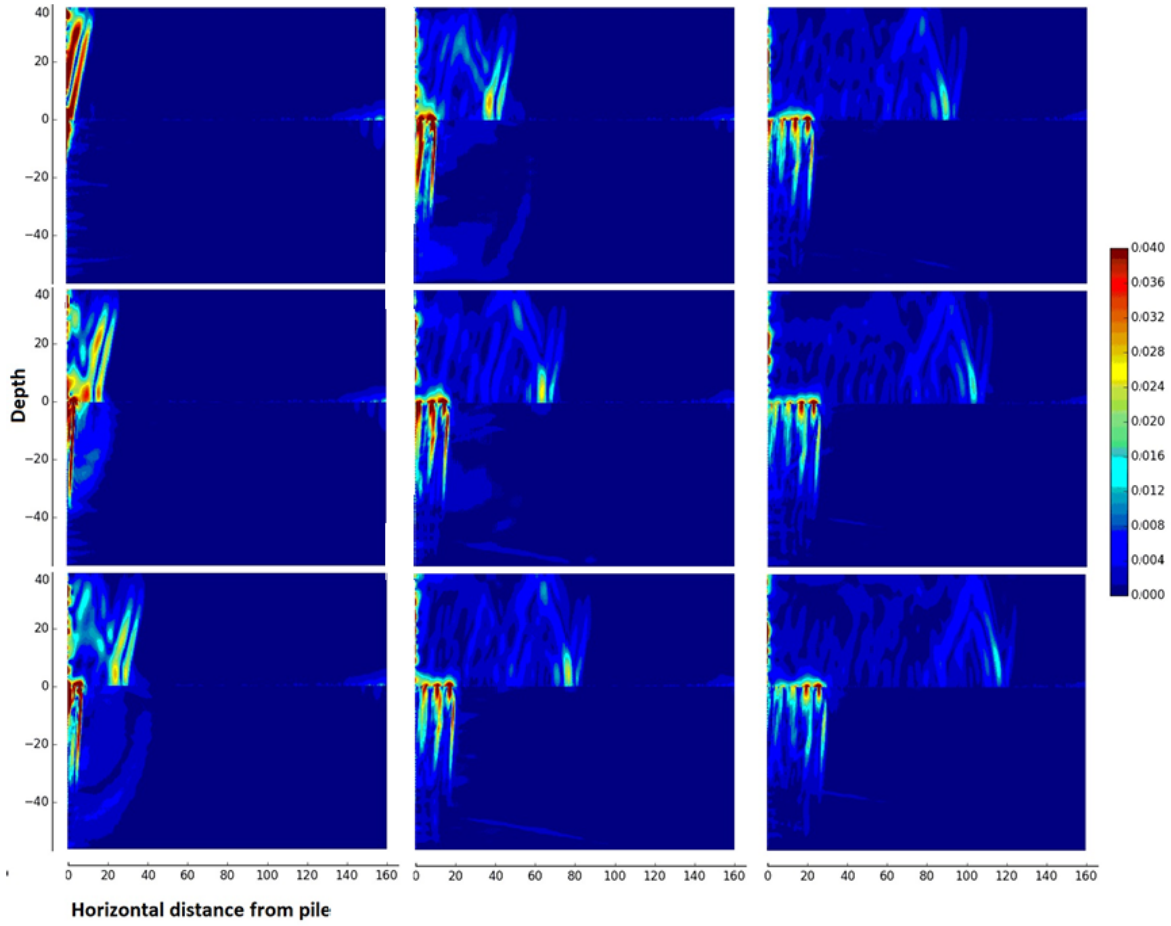

Figure 3.4: Evolution of the particle velocity norm in the seawater and the seabed for several moments in time after the hammer impact using the model by Tsouvalas and Metrikine [59].

Empirical models are based on the source-receiver distance and the characteristics of the acoustic environment. For greater distances, they rely on general transmission loss formulas. These models do not require detailed descriptions of the pile geometry or excitation characteristics. Instead, empirical or semi-empirical formulas are derived from energy attenuation laws and data collected from underwater noise measurements in various environments.

Semi-analytical approaches provide a more detailed representation. In these models, a close-range module is employed to simulate the wave field near the pile, while a far-range model is used for propagation over longer distances. The models are coupled through a boundary integral at the interface. Shell theories are applied to characterize the dynamics of the monopile. This model serves as the foundation for the SILENCE software, upon which this research is based. In Section 3.2, this model is discussed in detail.

Additionally, numerical models utilize finite element packages or finite difference schemes to simulate the acoustic field surrounding the pile. For longer distances, a sound propagation model is applied, as described in Section 3.1.1.

3.2 SILENCE model

This section delves into a state-of-the-art semi-analytical model developed by Tsouvalas et al. [31, 12], offering computational efficiency in predicting sound fields resulting from impact piling,

for both sound generation and sound propagation. This chapter describes the model and the governing equations of the fully coupled vibroacoustic system.

3.2.1 Description of the model

The total system consists of the monopile, hydraulic hammer, surrounding fluid and soil media, as shown in Figure 3.5. A cylindrical coordinate system (r, ϕ, z) is utilized for the fluid and soil domains, where z represents the downward vertical direction, and r indicates the radial distance from the pile. Since the model is assumed to be axisymmetric, the displacement along the ϕ-direction is considered to be zero [12]. Based on the assumption that the fluid and soil inside the pile have negligible influence on pile vibration and radiated energy [57], these regions are excluded from the model.

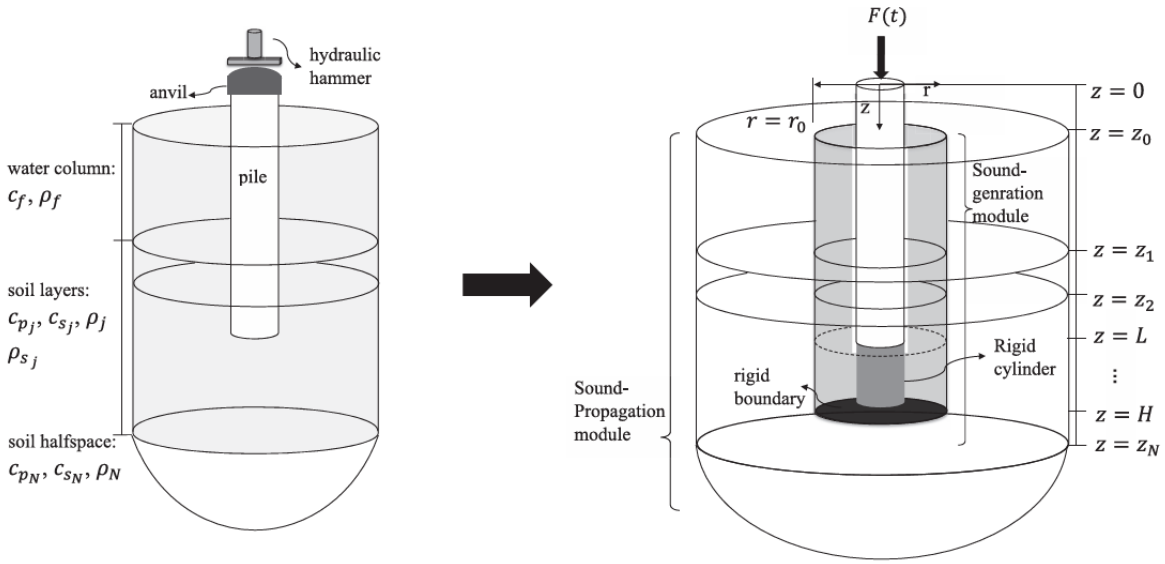

Figure 3.5: Schematic of the complete system (left) and the coupled model (right). r_0 represents the radial distance of the coupled cylindrical surface, z_0 denotes the sea surface level, and z_1 corresponds to the seabed level. z_j indicates the bottom level of the $(j-1)$th soil layer, L is the bottom level of the pile, and H represents the level of the rigid boundary within the sound generation module [12].

The complete model consists of two modules: a sound generation module and a sound propagation module. The sound generation module models the pile as a linear elastic thin shell, while the surrounding medium is represented as a horizontally stratified acousto-elastic waveguide [31, 59]. A rigid cylinder beneath the pile tip $(H - L)$ prevents radiation of elastic waves into deeper soil layers, simplifying computations without significantly affecting noise predictions in shallow layers near the seafloor.

The hydraulic hammer and anvil are not explicitly modeled but replaced by an external force applied at the pile top $(z = 0)$. This force is derived from measurement data or numerical models [35, 64]. The dynamic response of the pile is described using a linear high-order shell theory [65], chosen for its accuracy across various pile sizes and excitation frequencies without additional computational cost.

The pile occupies the domain $0 \leq z \leq L$, with material and geometrical parameters: modulus of elasticity (E), Poisson's ratio (ν), radius of the shell mid-surface (R), density (ρ), and shell thickness (t). The fluid is modeled as a three-dimensional inviscid compressible medium with wave speed (c_f) and density (ρ_f), occupying the domain $z_0 \leq z \leq z_1$ with $R \leq r \leq r_0$ for the sound generation module and $r \geq r_0$ for the sound propagation module.

The soil is represented as a three-dimensional elastic continuum in the domain $z \geq z_1$. Soil properties are defined by Lamé coefficients (λ_j, μ_j) and density (ρ_j) for each layer, where $j = 1, 2, \ldots, N$. Damping in the soil is introduced via complex Lamé coefficients $\tilde{\lambda}_j$ and $\tilde{\mu}_j$.

3.2.2 Governing equations

The physical quantities in the frequency domain, such as shell displacement, soil stresses, or fluid pressure, are defined as $g(t)$ and $\tilde{G}(\omega)$. To analyze these quantities, the following Fourier transform pair is used:

$$g(t) = \frac{1}{2\pi} \int_{-\infty}^{+\infty} \tilde{G}(\omega) e^{-i\omega t}\, d\omega \quad \text{and} \quad \tilde{G}(\omega) = \int_{-\infty}^{+\infty} g(t) e^{i\omega t}\, dt. \tag{3.1}$$

By performing the forward Fourier transform, the governing equations are derived in the frequency domain.

The dynamic response of the coupled system, comprising the shell structure and the acousto-elastic media, is governed by the following partial differential equations in the time domain:

$$\mathbf{L}\mathbf{u} + \mathbf{I}\ddot{\mathbf{u}} = -\big(H(z - z_1) - H(z - L)\big)\mathbf{t}_s + \big(H(z - z_0) - H(z - z_1)\big)\mathbf{p}_f + \mathbf{f}_e, \tag{3.2}$$

$$\nabla^2 p_f(r, z, t) - \frac{1}{c_f^2} \ddot{p}_f(r, z, t) = 0, \tag{3.3}$$

$$(\lambda_j + 2\mu_j)\nabla(\nabla \cdot \mathbf{u}_j) - \mu_j \nabla \times (\nabla \times \mathbf{u}_j) = \rho_j \ddot{\mathbf{u}}_j. \tag{3.4}$$

The variables are explained as follows:

- $\mathbf{u} = [u_z(z,t), u_r(z,t)]^\mathsf{T}$**:** The displacement vector of the mid-surface of the shell for $0 \leq z < L$.
- **L and I:** The stiffness and modified inertia matrices of the shell, respectively.
- $\mathbf{t_s}$**:** The boundary stress vector accounting for the soil's reaction surrounding the shell in the range $z_1 \leq z \leq L$.
- $\mathbf{p_f}$**:** The fluid pressure exerted at the outer surface of the shell between $z_0 \leq z \leq z_1$.
- $H(z - z_i)$**:** The Heaviside step functions used to define the spatial limits of the applied forces or boundaries.
- $\mathbf{f_e} = [f_z(z,t), f_r(z,t)]^\mathsf{T}$**:** The externally applied force vector acting on the shell's surface.
- $p_f(r, z, t)$**:** The pressure field of the fluid described in Equation 3.3.
- $\mathbf{u_j} = [w_j(r,z,t), u_j(r,z,t)]^\mathsf{T}$**:** The vertical ($w_j$) and radial ($u_j$) displacements of the j-th soil layer, as defined in Equation 3.4.

For the fluid-soil domain, the Helmholtz decomposition can be applied:

$$\mathbf{u}_f = \nabla\phi_f, \quad \mathbf{u}_j = \nabla\phi_j + \nabla \times \left(0, -\tfrac{\partial \psi_j}{\partial r}, 0\right). \tag{3.5}$$

Eventually, Eq. 3.5 can be substituted in Eq. 3.3 and Eq. 3.4, which yields the following equations.

$$\nabla^2 \phi_f(r, z, t) = \frac{1}{c_f^2} \frac{\partial^2 \phi_f}{\partial t^2}, \tag{3.6}$$

$$\nabla^2\phi_j(r,z,t) = \frac{1}{c_{pj}^2}\frac{\partial^2\phi_j}{\partial t^2}, \tag{3.7}$$

$$\nabla^2\psi_j(r,z,t) = \frac{1}{c_{sj}^2}\frac{\partial^2\psi_j}{\partial t^2}. \tag{3.8}$$

The variables are explained as follows:

- c_{pj}: speed of compressional waves in soil layer j.
- c_{sj}: speed of shear waves in soil layer j.

Boundary and interface conditions

With full contact at the soil-soil interface, both stress equilibrium and displacement continuity are enforced [12]. The resulting boundary and interface conditions are expressed as:

$$p_f(r,z_0,t) = 0, \quad r \geq R, \tag{3.9}$$

$$\sigma_{zz_1}(r,z_1,t) + p_f(r,z_1,t) = 0, \quad u_{zf}(r,z_1,t) = w_{s_1}(r,z_1,t), \quad \sigma_{zr_1}(r,z_1,t) = 0, \quad r \geq R, \tag{3.10}$$

$$w_j(r,z_j,t) = w_{j-1}(r,z_j,t), \quad u_j(r,z_j,t) = u_{j-1}(r,z_j,t), \quad 2 \leq j \leq N, \quad r \geq R, \tag{3.11}$$

$$\sigma_{zz_j}(r,z_j,t) = \sigma_{zz_{j-1}}(r,z_j,t), \quad \sigma_{zr_j}(r,z_j,t) = \sigma_{zr_{j-1}}(r,z_j,t), \quad 2 \leq j \leq N, \quad r \geq R. \tag{3.12}$$

Assuming no pile slip, a perfect contact condition is enforced at the pile-soil interface [12]. The kinematic conditions at the interface between the shell and the surrounding medium (r=R) are defined as:

$$u_r(z,t) = u_f(R,z,t), \quad z_0 \leq z \leq z_1, \quad u_r(z,t) = u_j(R,z,t) \quad \text{and} \quad u_z(z,t) = w_j(R,z,t),$$

3.2.3 Sound Generation Module

The sound generation module uses a 3D cylindrically symmetric vibroacoustic model [59] to capture dynamic interactions between the pile and surrounding media. By applying modal decomposition and a mode-matching technique, the coupled pile-water-soil system's response is determined in the frequency domain. Key response functions (pressure, velocity, displacement, stress) are provided as input for the sound propagation model [12]. Expressions for the fluid pressure are given as follows [59]:

$$\tilde{p}_f(r,z,\omega) = \sum_{p=1}^{\infty} C_p H_0^{(2)}(k_p r)\tilde{p}_{f,p}(z), \tag{3.14}$$

In this equation: $\tilde{p}_f(r,z,\omega)$ represents the complex pressure field in the fluid, expressed in Pascals (Pa). The coefficients C_p are dimensionless and determined by solving the forced response of the coupled system. The term $H_0^{(2)}(k_p r)$ is the Hankel function of the second kind, describing the radial behavior of the wave. The eigenfunction $\tilde{p}_{f,p}(z)$ accounts for the vertical pressure

distribution, also expressed in Pascals (Pa). Finally, k_p is the wavenumber for mode p, with units of m^{-1}, defining the spatial variation of the wave.

The linearity of the system and the independent solving of the shell and acousto-elastic waveguide eigenvalue problems make the sound generation module computationally efficient. Unlike finite element or finite-difference models, it requires only partial re-evaluation of simulations when input parameters such as forcing functions, soil conditions, or penetration depths are varied, enabling quicker analysis of multiple scenarios.

3.2.4 Sound Propagation Module

The sound propagation module receives its input from the sound generation module through a boundary integral formulation [12]. Green's tensors are derived for a fluid overlying a multilayered soil half-space, considering sources located both in the fluid and in the soil. These tensors are computed by placing a ring source in cylindrical coordinates at the boundary of the sound generation module. In the fluid, a pressure-type ring source is positioned at $[r_s, z_s]$, while in the soil, either a radial or vertical ring source is placed at $[r_s, z_s]$, generating pressure waves with a unit pressure amplitude at the source location. Figure 3.6 provides a schematic representation of these ring sources.

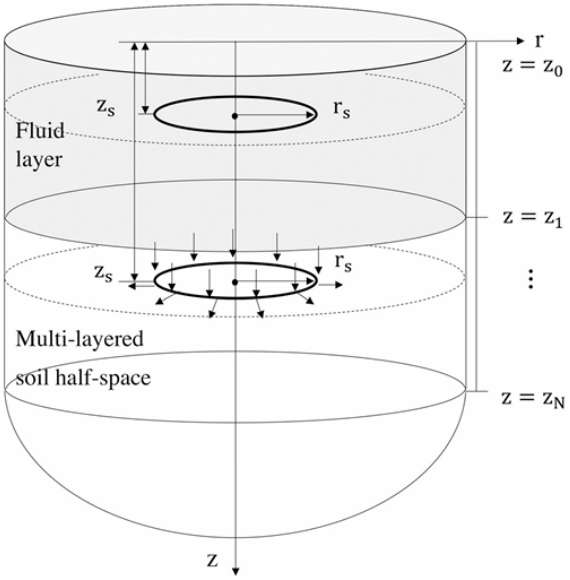

Figure 3.6: Ring source at $r = r_s$ in the configuration of acousto-elastic layered half-space [12].

Fluid source

To derive the Green's functions for an acoustic source, a pressure-type ring source is placed at $[r_s, z_s]$ in the fluid domain, generating pressure waves with a unit amplitude at the source location. The displacement potential satisfies:

$$\left[\nabla^2 + k_f^2\right] \phi_f^f(r, z; r_s, z_s, \omega) = \frac{1}{-\rho_0 \omega^2} \frac{\delta(r - r_s, z - z_s)}{2\pi r}, \quad r_s \geq R, \quad z_0 \leq z_s \leq z_1. \tag{3.15}$$

Applying the forward Hankel transform reduces the wave equations to depth-separated forms, as detailed in Bakr [66]. The resulting equations for fluid and soil displacement potentials in the Hankel domain are:

$$\left[\frac{d^2}{dz^2}+k_{z,f}^2\right]\phi_f^g(k_r,z;r_s,z_s,\omega)=\frac{1}{-\rho\omega^2}\delta(z-z_s)\frac{J_0(k_r r_s)}{2\pi}, \tag{3.16}$$

$$\left[\frac{d^2}{dz^2}+k_{z,p,j}^2\right]\phi_{j,f}^g(k_r,z;r_s,z_s,\omega)=0, \tag{3.17}$$

$$\left[\frac{d^2}{dz^2}+k_{z,s,j}^2\right]\psi_{j,f}^g(k_r,z;r_s,z_s,\omega)=0. \tag{3.18}$$

in which $k_{z,n}=\sqrt{k_n^2-k_r^2}$ is the vertical wavenumber in the domain n ($n=f,p_j,\text{or }s_j$). The boundary conditions are provided in Section 3.2.2.

The solutions for the displacement potentials consist of a particular solution added to the general solution of the homogeneous equation.

$$\phi_f^g(k_r,z;r_s,z_s,\omega)=\left(\frac{1}{-\rho\omega^2}\frac{e^{-ik_{z,f}|z-z_s|}}{4\pi ik_{z,f}}+A_1^g e^{ik_{z,f}z}+A_2^g e^{-ik_{z,f}z}\right)J_0(k_r r_s), \tag{3.19}$$

$$\phi_{j,f}^g(k_r,z;r_s,z_s,\omega)=\left(A_{4j-1}^g e^{ik_{z,p,j}z}+A_{4j}^g e^{-ik_{z,p,j}z}\right)J_0(k_r r_s), \tag{3.20}$$

$$\psi_{j,f}^g(k_r,z;r_s,z_s,\omega)=\left(A_{4j+1}^g e^{ik_{z,s,j}z}+A_{4j+2}^g e^{-ik_{z,s,j}z}\right)J_0(k_r r_s), \tag{3.21}$$

in which the coefficients A_g^i ($i=1,2,\ldots,4N+2$) are undetermined complex amplitudes [12].

By applying the inverse Hankel transform and utilizing the properties of Bessel functions [67], the Green's tensor for the acousto-elastic medium in the frequency domain is derived as:

$$\tilde{\Phi}_{\Xi,f}^g(r,z;r_s,z_s,\omega)=-\frac{1}{2}\int_{-\infty}^{+\infty}\left(\hat{\Phi}_{\Xi,f}^g(k_r,z;r_s,z_s,\omega)\right)H_0^{(2)}(k_r r)k_r\,dk_r, \tag{3.22}$$

where

$$\hat{\Phi}_{\Xi,f}^g=\begin{bmatrix}\hat{\phi}_{f,f}^g & \hat{\phi}_{j,f}^g & \hat{\psi}_{j,f}^g\end{bmatrix}^T$$

represents the solutions of the displacement potential functions in the Hankel domain, and $\tilde{\Phi}_{\Xi,f}^g$ denotes the corresponding potential functions in the frequency domain.

The pressure, displacements, and stresses in the acousto-elastic medium are expressed through Green's functions of displacement potentials, which are omitted here for brevity [68]. By substituting these expressions into the boundary and interface conditions outlined in Section 3.2.2, the final set of linear algebraic equations with the unknowns A_g^i is derived. This derivation, omitted here for brevity, is discussed in detail by Peng et al. [12]. Once the amplitude coefficients are determined for each k_r, the Green's tensor for a pressure-type ring source in the fluid domain is obtained.

Soil source

For a radial or vertical ring load applied in the soil, as illustrated in Fig. 3.6, the corresponding jump condition for stresses is imposed at the source level $z=z_s$. Since all soil layers are assumed to be free of body-force sources, the solutions for the potential functions are expressed as:

$$\hat{\phi}_{f,s,n}^g(k_r,z;r_s,z_s,\omega)=\left(A_1^g e^{ik_{z,f}z}+A_2^g e^{-ik_{z,f}z}\right)J_0(k_r r_s), \tag{3.23}$$

$$\hat{\phi}^{g}_{j,f,s,n}(k_r, z; r_s, z_s, \omega) = \left(A^{g}_{4j-1} e^{ik_{z,p,j}z} + A^{g}_{4j} e^{-ik_{z,p,j}z} \right) J_0(k_r r_s), \tag{3.24}$$

$$\hat{\psi}^{g}_{j,f,s,n}(k_r, z; r_s, z_s, \omega) = \left(A^{g}_{4j+1} e^{ik_{z,s,j}z} + A^{g}_{4j+2} e^{-ik_{z,s,j}z} \right) J_0(k_r r_s), \tag{3.25}$$

For the radial load case, the following set of interface conditions hold at $z = z_s$ in the Hankel domain:

$$\hat{\sigma}^{g+}_{zr,sn}(k_r, z_s, \omega) - \hat{\sigma}^{g-}_{zr,sn}(k_r, z_s, \omega) = \frac{J_0(k_r r_s)}{2\pi}, \tag{3.26}$$

$$\hat{\sigma}^{g+}_{zz,sn}(k_r, z_s, \omega) = \hat{\sigma}^{g-}_{zz,sn}(k_r, z_s, \omega), \tag{3.27}$$

$$\hat{u}^{g+}_{\alpha,sn}(k_r, z_s, \omega) = \hat{u}^{g-}_{\alpha,sn}(k_r, z_s, \omega), \quad \alpha = r, z. \tag{3.28}$$

Similarly, for the vertical load case, one obtains:

$$\hat{\sigma}^{g+}_{zz,sn}(k_r, z_s, \omega) - \hat{\sigma}^{g-}_{zz,sn}(k_r, z_s, \omega) = \frac{J_0(k_r r_s)}{2\pi}, \tag{3.29}$$

$$\hat{\sigma}^{g+}_{zr,sn}(k_r, z_s, \omega) = \hat{\sigma}^{g-}_{zr,sn}(k_r, z_s, \omega), \tag{3.30}$$

$$\hat{u}^{g+}_{\alpha,sn}(k_r, z_s, \omega) = \hat{u}^{g-}_{\alpha,sn}(k_r, z_s, \omega), \quad \alpha = r, z. \tag{3.31}$$

By combining Eqs. (3.26)–(3.31) with Eqs. (3.9)–(3.12), after transforming the latter into the Hankel domain, a linear algebraic system is constructed with unknowns A^i_g for $i = 1, 2, \ldots, 4N+6$. Once the displacement potentials are resolved in the Hankel domain, the Green's tensors for displacement and stress in the frequency domain can be derived.

Coupling of the Modules

The evaluation of Green's tensors relies on two primary methods. The first approach involves direct integration of the wavenumber k_r along its real axis. The second method applies the contour integration technique, offering an alternative route to compute the tensors. Comprehensive explanations of these techniques are available in the work by Peng et al. [12].
Once the Green's tensors are evaluated, the direct boundary element method is utilized to establish the coupling between the sound generation and propagation modules. In-depth information regarding this coupling process can be found in Peng et al. [12].

3.2.5 Implementation of Air-Bubble Curtains

The integration of air-bubble curtain modeling into the semi-analytical SILENCE model involves a series of interconnected steps. The approach, inspired by the multi-physics framework developed by Peng et al. [42], consists of four key modules, each addressing a specific aspect of the noise mitigation process:

- **Compressible Flow Model:** This module simulates the flow of compressed air from the injection vessel to the perforated hose located on the seabed. The output from this module serves as the basis for subsequent modeling steps.
- **Hydrodynamic Model:** Using the results of the compressible flow model, this module captures the generation and evolution of air bubbles with respect to depth and range, providing critical inputs for acoustic analysis.

- **Acoustic Model:** This model predicts the sound transmission loss caused by the air-bubble curtain. The transmission loss quantifies the reduction in sound energy as it propagates through the bubble layer.
- **Vibroacoustic Model:** The vibroacoustic model uses the transmission loss calculated by the acoustic model to predict the resulting underwater noise levels. Coupling between these models is achieved through a boundary integral formulation, ensuring a seamless interaction between modules.

By linking these modules, the SILENCE model provides a comprehensive framework for evaluating the effectiveness of air-bubble curtains in mitigating underwater noise. Figure 3.7 offers a visual overview of the coupled modeling process, including the sound generation, reduction, and propagation stages.

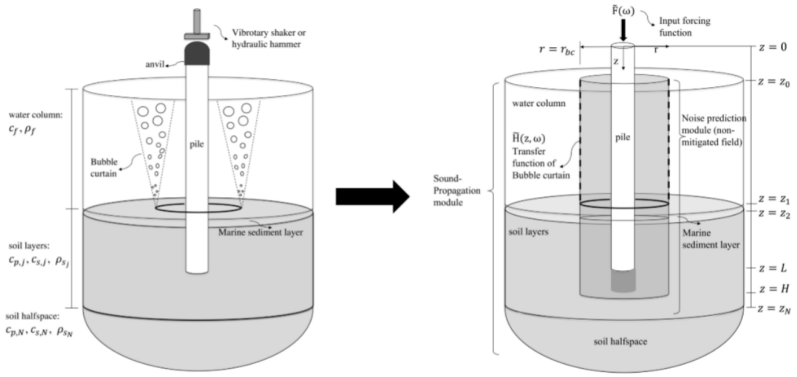

Figure 3.7: Left: Schematic representation of the complete system with an air-bubble curtain. Right: the coupled model incorporating the transfer function for transmission losses caused by the air-bubble curtain [42].

3.3 Computational methods for drivability

To determine whether a monopile can reach the target penetration depth, a drivability analysis is performed. The analysis also evaluates the driving stresses that develop during installation. The in-house wave-equation program DYNPAC, developed by Heerema Engineering Solutions, is used for this purpose. It requires soil, pile and hammer data as input and returns a range of blow-count predictions (lower, expected and upper scatter). Results are usually displayed as blow-count curves and hammer-energy curves versus depth. If the blow count for a given pile-soil-hammer combination exceeds a specified threshold (defined in the internal *HMC refusal criteria*, expressed as blows / 0.25 m), the pile is considered to have reached refusal.

A brief comparison with alternative drivability tools and a concise summary of DYNPAC's modelling assumptions are given below, followed by the theoretical background.

3.3.1 State-of-the-art overview

Current drivability tools can be grouped into three tiers.

(i) 1-D wave-equation programs (e.g. GRLWEAP, AllWave-PDP, TNOWAVE) are the most widely used in practice because they run quickly and need only simplified soil input.[69, 70].

(ii) Finite-element (FE) models capture full 2- or 3-D pile-soil interaction, rate effects and pore-pressure build-up [71], but are computationally demanding and therefore used mainly in research or for special back-analyses.

(iii) Hybrid approaches couple, for instance, an FE pile to simplified soil springs or boundary elements, aiming to bridge the accuracy gap of 1-D tools without the full cost of FE [72].

3.3.2 Position of DYNPAC

DYNPAC belongs to tier (i): a 1-D wave-equation code developed for offshore projects. Its main assumptions are:

- the pile is modelled as an elastic rod; only axial stress waves are considered [69];
- soil resistance is represented by non-linear springs in parallel with dashpots (velocity-dependent damping) [73];
- ultimate shaft and toe resistances are user-supplied, typically from CPT/API correlations.

Distinctive features include an optional non-linear Coyle-Gibson damping law [74] and a signal-matching mode for PDA data [75]. Limitations mirror those of other 1-D tools: no bending or lateral effects, simplified rate dependence, and reduced accuracy for very large monopiles where wave dispersion and soil plugging become significant [71]. In practice, DYNPAC gives blow-count and stress predictions comparable to GRLWEAP [70] but lacks the extensive hammer database and modern GUI of commercial packages.

Theory behind DYNPAC

DYNPAC is based on the wave-equation method for simulating dynamic interactions during pile driving [69]. The program models the propagation of stress waves generated by a hammer impact through the pile and its interaction with the surrounding soil.

The key concepts include:

- **Wave propagation:** Stress waves travel along the pile, reflecting at the tip and head. These are modelled with the one-dimensional wave equation

$$\frac{\partial^2 u}{\partial t^2} = c^2 \frac{\partial^2 u}{\partial x^2},$$

  where u is displacement, t time, x position and c wave speed.

- **Pile-soil interaction:** Soil response is idealised as a spring-dashpot system,

$$F = k\,u + c\,\frac{du}{dt},$$

  with stiffness k and damping c.

- **Hammer energy transfer:** The program computes energy transfer from hammer to pile and evaluates the resulting stress distribution and blow count required for penetration.

- **Numerical method:** DYNPAC solves the wave equation via an explicit finite-difference scheme, discretising the pile into segments to simulate wave propagation and soil interaction [69].

This approach provides insight into drivability, blow counts, energy transfer and stress distribution during offshore monopile installation.

4 | Modeling configuration and approach

This chapter outlines the configuration and approach used to assess the impact of different operational hammer settings on cumulative underwater noise emissions during monopile installation. The analysis is based on scenario simulations combining the DYNPAC pile-driving model with the SILENCE acoustic model. First, Section 4.1 describes how SILENCE is configured and validated using a representative German North Sea monopile geometry and CPT-derived soil profiles. Then, Section 4.2 defines scenarios of single-blow simulations, with varying target blow count and impulse duration at key penetration depths, that form the basis for all subsequent noise assessments.

4.1 Configuration and validation of the acoustic model

This section presents the configuration and validation of the SILENCE acoustic model. The model input is based on a monopile geometry representative of offshore practice in the German North Sea. Soil conditions are derived from cone penetration test (CPT) data from the German Bight, providing a realistic acoustic environment for simulation.

Subsection 4.1.1 introduces the main input parameters required for the simulation, including the geometry and material properties of the monopile, the stratification of the water and soil layers, the frequency- and time-domain discretisation, and the definition of the force input.

Subsection 4.1.2 outlines modeling assumptions and limitations. The chapter concludes with a validation study in Section 4.1.3, where model outputs are compared to field measurements. This includes the comparison of key acoustic metrics, evaluation of arrival time, and general interpretation of the results.

4.1.1 Model Setup and Input Parameters

This subsection outlines the key input parameters required for the modeling process. These include monopile geometry, material properties, water and soil characteristics, and the parameters for frequency- and time-domain analyses.

Geometry and material properties of the monopile

Monopiles typically have a tapered shape, with larger diameters at the base and smaller diameters near the top. The embedded section of the pile generally has a greater diameter than the exposed part. For modeling purposes, an average diameter over the submerged section is used to ensure consistency in calculations.

In addition to diameter variations, the wall thickness of the monopile also changes along its length. Data from a recent project in the German North Sea is used, where the monopile diameter ranges from 7.3 m to 9.2 m, and the wall thickness varies between 80 mm and 100 mm.

Since the submerged section, including both the water-exposed and soil-embedded parts, plays a crucial role in sound propagation [31], this part is the primary focus in the modeling approach.

In addition to geometric properties, modeling the monopile in SILENCE requires material parameters such as density, Young's modulus, and Poisson's ratio. The monopile is made of S355 steel, and the corresponding material properties are as follows:

- **Density** (ρ): 7850 kg/m^3.
- **Young's Modulus** (E): 210 GPa.
- **Poisson's Ratio** (ν): 0.28.

The material properties are based on the values specified in Eurocode 3 for the design of steel structures [76].

The parameters for the monopile geometry are outlined in Table 4.1.

Description	Parameter	Value	Unit
Steel kind	-	S355	-
Young's modulus	E	210	GPa
Poisson's ratio	ν	0.28	-
Density	ρ	7850	kg/m^3
Thickness	d	0.089	m
Pile diameter	D	8.8	m
Pile length	L	69.5	m

Table 4.1: Parameters for the monopile geometry.

Water and soil stratification

The representation of water and soil properties is critical for accurate modeling of acoustic wave propagation. The following assumptions are made:

- **Seawater as a homogeneous fluid**: For the frequency range analyzed in this study (up to 1000 Hz), dominant sound channels are not expected [77]. Consequently, layering within the water column does not need to be considered, and seawater is modeled as a homogeneous fluid with uniform temperature and salinity throughout the water depth [77]. Additionally, given the relatively shallow water depth, the influence of increasing hydrostatic pressure on the speed of sound propagation is minimal. As a result, the speed of sound is assumed to remain constant throughout the water column.
- **Density of seawater** (ρ_w): 1028 kg/m^3, based on the assumption of well-mixed saltwater conditions at the study location.
- **Speed of sound in seawater** (c_w): 1510 m/s.
- **Soil stratification**: Soil layers are modeled as stratified, with acoustic properties based on location-specific data.

The soil profile in the model is based on a CPT test, which revealed multiple sand layers of varying compactness. To simplify the input, the data was first depth-averaged into a single representative layer. However, a pronounced increase in cone resistance was observed at a depth of 11 m, justifying a two-layer interpretation. As a result, the soil is modeled as two distinct sand layers with different properties: Layer 1 extends from the seabed to 11 m depth, and Layer 2,

representing a more compacted sand, spans from 11 m to 50 m below the seabed. The CPT-based properties of both layers are summarized in Table 4.2.

The target penetration depth in the model is 27.5 m LAT (Lowest Astronomical Tide), indicating that the pile tip is positioned 27.5 metres beneath the lowest expected tidal water level. Above the sand layers, a water column is present, providing the interface between the monopile and the surrounding environment. The distinct acoustic properties of Layer 1 and Layer 2 are incorporated into the model to ensure an accurate representation of soil-induced sound propagation.

A schematic representation of the soil and water setup for the model, including the required water depths z_0, z_1, z_2, and z_3, is shown in Figure 4.1. The corresponding water depths for the fully penetrated pile are shown in Table 4.3.

Layer	q_c **[MPa]**	f_s **[MPa]**	q_t **[MPa]**	u **[MPa]**
Layer 1 (<11 m)	12.96	0.08580	13.08	0.06993
Layer 2 (>11 m)	65.27	0.4355	65.45	0.3182

Table 4.2: CPT-derived soil layer properties.

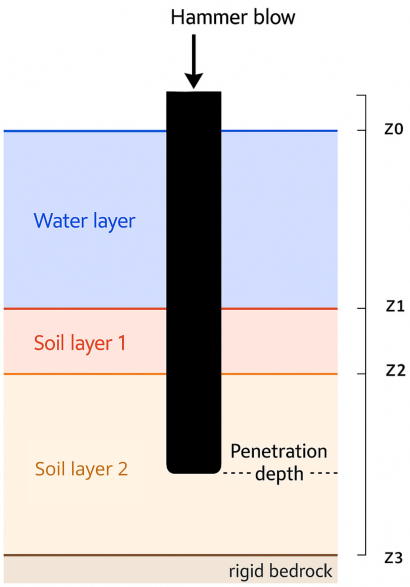

Figure 4.1: Schematic representation of the soil and water setup in the model, showing the water layer and soil layer 1 and 2.

Description	**Parameter**	**Value**	**Unit**
Target penetration depth	L_p	27.5	m
Sea surface from top pile	z_0	2.5	m
Water depth from top pile	z_1	42.0	m
Soil layer 1 depth from top pile	z_2	53.0	m
Soil layer 2 depth from top pile	z_3	92.0	m

Table 4.3: Required water depths for the fully penetrated pile in the model.

All soil parameters are listed in Table 4.4 and have been derived from the Cone Penetration Test (CPT) data of a sand profile corresponding to a recent project in Germany. The parameters v_s, v_p, and the Poisson's ratio (ν) were directly obtained from the CPT measurements, while the density (ρ) was derived from the same dataset. Using these known values, the Young's modulus (E) was calculated with the following equations for compressional and shear wave velocity:

$$v_p = \sqrt{\frac{E(1-\nu)}{\rho(1+\nu)(1-2\nu)}} \tag{4.1}$$

$$v_s = \sqrt{\frac{E}{2\rho(1+\nu)}} \tag{4.2}$$

According to Aziman et al. [78], typical compressional wave velocities for sands and clays range between 300 and 1900 m/s, while shear wave velocities typically lie between 100 and 500 m/s. The obtained values for v_p and v_s in this model fall within these ranges, indicating consistency with sandy soil conditions. Specifically, for Soil Layer 1, $v_p = 1750$ m/s and $v_s = 288$ m/s, while for Soil Layer 2, $v_p = 1886.36$ m/s and $v_s = 304.45$ m/s.

The compressional wave velocity v_p is highly sensitive to variations in the Poisson's ratio, meaning that even small changes in its value can have a significant impact on v_p. Therefore, the Poisson's ratio is carefully evaluated to ensure it remains within a realistic range in the aforementioned equations. According to Aziman et al. [78], the Poisson's ratio should approach 0.5 but must not be exactly 0.5, as this would result in division by zero in Equation 4.6. The values for soil layers 1 and 2, 0.486 and 0.487, are considered realistic based on the calculated shear and compressional wave velocities reported by Aziman et al. [78].

In addition to the aforementioned soil parameters, soil-damping properties must be considered. These properties are incorporated into the model using complex Lamé constants, as defined in Equations 4.3 and 4.4, where λ and μ represent the real parts. i represents the imaginary unit, while α_p and α_s denote the damping coefficients for compressional and shear waves, respectively. The imaginary components account for energy dissipation in the model.

$$\lambda^* = \lambda(1 + i\alpha_p) \tag{4.3}$$

$$\mu^* = \mu(1 + i\alpha_s) \tag{4.4}$$

The values of λ and μ are determined using Equations 4.5 and 4.6, as presented by Peng et al. [13]:

$$v_s = \sqrt{\frac{\mu}{\rho_s}} \tag{4.5}$$

$$v_p = \sqrt{\frac{\lambda + 2\mu}{\rho_s}} \tag{4.6}$$

In SILENCE, the damping coefficients α_p and α_s are expressed as percentages. Based on Jensen et al. [77], the corresponding values are presented in Table 4.4.

Description	Parameter	Soil layer 1	Soil layer 2	Unit
Young's modulus	E	477	576	MPa
Poisson's ratio	ν	0.49	0.49	-
Soil density	ρ	1937	2090	kg/m^3
Damping ratio of compressional waves	α_p	2.48	1.85	%
Damping ratio of shear waves	α_s	6.85	4.63	%
Compressional wave velocity	V_p	1750	1886	m/s
Shear wave velocity	V_s	288	304	m/s

Table 4.4: Parameters for soil properties and wave characteristics for soil layer 1 and soil layer 2.

Frequency and time domain analyses

Frequency and time domain analyses in the SILENCE model require careful selection of parameters:

- **Frequency Intervals (N_f)**: Calculated as half the number of time intervals (N_t).

$$N_f = \frac{N_t}{2} \tag{4.7}$$

- **Time Step (Δt)**: Determined as the inverse of twice the maximum frequency ($f_{\max}$).

$$\Delta t = \frac{1}{2 f_{\max}} \tag{4.8}$$

  The maximum frequency is set to 1000 Hz, as higher frequencies are unlikely to significantly contribute to pile noise generation in this study.

- **Number of time steps (N_t)**: The total number of time intervals, N_t, is determined by dividing the analysis duration t by the time step Δt:

$$N_t = \frac{t}{\Delta t} \tag{4.9}$$

- **Total time duration (t)**: In this study, the modeling is done for a position of 750 m from the monopile. The analysis duration must therefore be sufficient for sound waves to propagate across this distance. Given that the speed of sound in water is approximately 1510 m/s, the minimum required duration is:

$$t_{\min} = \frac{750}{1510} = 0.5 \text{ s} \tag{4.10}$$

  To ensure accuracy and account for potential variations, a conservative duration of 1 second is selected for t.

- **Frequency Resolution (Δf)**: Defined as:

$$\Delta f = \frac{f_{\max}}{N_f} \tag{4.11}$$

All required parameter values for the frequency and time analyses are summarized in Table 4.5.

Description	Parameter	Value	Unit
Number of frequency steps	N_f	1000	-
Time step size	Δt	0.0005	s
Number of time steps	N_t	2000	-
Total time duration	t	1	s
Maximum frequency	$f_{\max}$	1000	Hz
Frequency step size	Δf	1	Hz

Table 4.5: Parameters for the frequency and time analyses.

Force input

The hammer force is represented as a vertical load applied at the top of the monopile. The force varies over time and can be illustrated using a force-time diagram.

For this study a IHC S-5500 hydraulic hammer is used.

The force-time diagrams for the maximum hammer force, with and without pulse prolongation, are shown in Figure 4.2. The data is generated using DYNPAC, a computational model for drivability analysis, as described in Section 3.3.2.

The force-time data is transformed into force-frequency data using the discrete Fourier transform, as given in Equation 3.1. The force in the frequency domain, with and without pulse prolongation, is shown in the second figure in Figure 4.2.

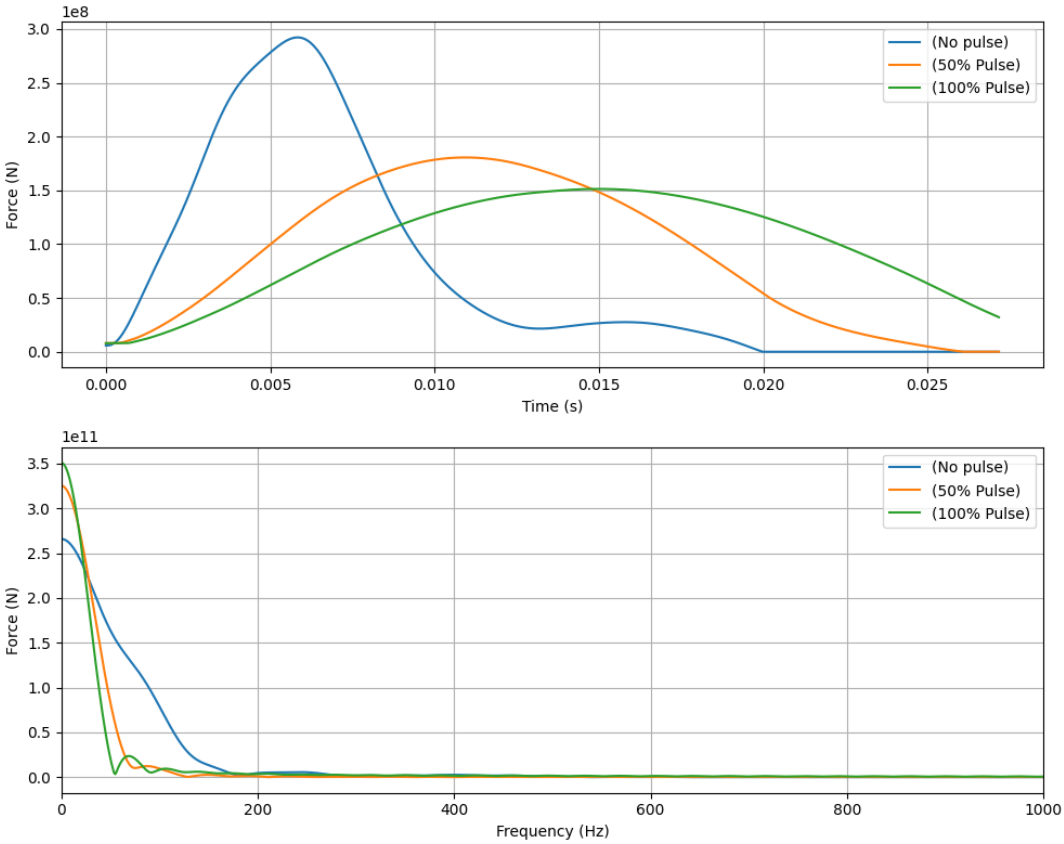

Figure 4.2: The force input for different settings of the hammer in the time domain (top) and the frequency domain (below).

Model implementation of the Double Big Bubble Curtain

In this study, a Double Big Bubble Curtain (DBBC) configuration is applied in Case 6 and Case 7. The DBBC parameters (nozzle diameter, spacing, hose diameter, and ring radius) are consistent with those used in Peng et al. (2023) and the CVOW-C mitigation plan by DEME and Prysmian (2023) [79, 80]. Section 3.2.5 explains how Air-Bubble Curtains are implemented in SILENCE, including how transmission losses are numerically integrated into the model.

Description	Value	Unit
Nozzle diameter	0.00200	m
Nozzle spacing	0.250	m
Hose diameter	0.102	m
Injected airflow	0.000283	m^3/s
Radius BBC 1	75	m
Radius BBC 2	150	m
Gas velocity at the nozzle	90	m/s

Table 4.6: Parameters for the double big bubble curtain system.

4.1.2 Model Assumptions and Limitations

Several simplifications and assumptions are made in the acoustic model setup, which introduce limitations to the interpretation of the results.

- **Soil characterisation**
  The soil parameters used in the SILENCE model are based on site-specific data from the German Bight, derived from cone penetration testing (CPT). However, soil conditions can vary significantly over small spatial scales due to natural heterogeneity in stratigraphy and compaction [81, 82]. This is particularly relevant because acoustic generation and propagation is highly sensitive to soil characteristics, as discussed in Section 2.3.2. Additionally, the SILENCE model applies a simplified soil stratification consisting of only two homogeneous layers. In reality, offshore soil profiles often contain a more complex layering of materials, each with varying stiffness, density, and damping behaviour. This simplification may result in deviations in the predicted pressure field, especially since reflections and refractions between layers are important.

- **Monopile geometry**
  The pile geometry used in the model is simplified to a uniform cylindrical monopile with constant outer diameter and wall thickness. In practice, monopiles are typically tapered and constructed from multiple segments with varying diameters and thicknesses. In this study, an averaged diameter and wall thickness were used based on the submerged part of the pile at full penetration. The resulting pile mass was verified to match that of the real pile to ensure the dynamic response remains realistic. However, this geometric simplification may influence the pile impedance and the way energy is transferred to the surrounding medium.

- **Numerical limitations**
  Due to computational constraints, the number of frequency steps in the model was limited to a maximum of 1000. Increasing the frequency resolution improves the accuracy of the pressure wave reconstruction in the time domain but also significantly increases computation time. This trade-off limits the precision of the temporal waveform, particularly in the case of sharp or short-duration impulses.

4.1.3 Validation of the model

To ensure the credibility of the simulation results, the acoustic model is validated against field data and subjected to basic sanity checks. This step is essential to assess whether the model outputs are within a realistic range and whether the implemented physics adequately capture the behaviour of underwater sound propagation during impact piling. The validation focuses exclusively on the unmitigated case, as this is the only configuration for which comparable field data is available. No pulse prolongation or bubble curtain systems were used during these particular blows.

Comparison to field data

The modeled data are compared to field measurements from a project conducted in the German North Sea, in which the same pile type was driven into geotechnically similar soil. In that project, several noise-mitigation systems were available but, for validation purposes, a subset test of 100 blows was performed without any mitigation measures. These unmitigated SEL values therefore provide a directly comparable basis for assessing the model's unmitigated predictions.

Hydrophones were positioned at a distance of 750 meters from the source. In total, four hydrophones were deployed. For comparison purposes, the average of the hydrophone measurements is used. The recorded SEL values are first converted to pressure using Equation 4.12, after which the average pressure is computed. Subsequently, the averaged pressure is converted back to SEL using Equation 2.4. The differences in measured sound levels between the hydrophones can be attributed to slight variations in their precise positioning, which can lead to differences in sound wave interactions and interference patterns despite all hydrophones being at the same distance from the pile.

$$X = X_{\text{ref}} \cdot 10^{\frac{\text{Decibel Level}}{10}} \tag{4.12}$$

Although the complete field dataset cannot be disclosed in this report due to confidentiality, the modeled $L_{\text{E,p}}$ and $L_{\text{p,pk}}$ levels show close agreement with the measured, unmitigated values. On average, the difference between model and field averages remains within $\pm 2, \text{dB}$, well inside typical measurement uncertainty [83], confirming the validity of the model under the same pile and comparable soil conditions.

Selection of representative penetration depths

Due to the long computational time of each SILENCE simulation (approximately 7 hours), it is not feasible to simulate every individual blow. To ensure that the selected penetration depths capture the main physical transitions in pile-soil-water interaction, sensitivity runs were performed at multiple penetration depths. The aim was to verify whether acoustic trends such as SEL decay, frequency shifts, and drivability characteristics could be interpolated reliably between selected depths. The results of this sensitivity analysis are provided in Appendix A.

As shown in Table A.1, the SEL values remain relatively stable across the examined penetration depths. While deeper embedment increases the contact area between the pile and surrounding soil, potentially introducing more energy dissipation through friction and plastic deformation, this additional loss occurs primarily in the ground. Since the dominant underwater noise source is the supersonic radial expansion of the pile wall (Mach-wave radiation), which originates in the upper, unburied part of the pile, the influence of increased embedment on the radiated SEL is limited. Both field data and modelling studies confirm that, beyond a certain minimum embedment length, increasing penetration depth does not substantially affect the underwater

SEL measured at a fixed distance [84, 85, 34, 14]. Reinhall and Dahl [34] show that the Mach-cone mechanism is relatively insensitive to soil coupling, while Trimoreau et al. [86] demonstrate that SEL variation between 10 and 18 m embedment remains below 2 dB.

Based on this sensitivity analysis, six representative depths were chosen: 5 m, 10 m, 12 m, 18.5 m, 23 m, and 27.5 m. These depths span critical geotechnical transitions (e.g., soil layering at 11 m), increasing embedded pile length, and varying hammer energy input. The selection provides a balance between physical coverage and computational efficiency and enables accurate reconstruction of cumulative noise levels using the method described in Chapter 4.

Arrival time of the impulse

To verify that frequency-domain results from the model are accurately transformed into the time domain, the arrival time of the impulse can be examined. Given the radius of interest for this research is 750 m and assuming a sound propagation speed of 1510 m/s, the impulse should arrive at approximately 0.5 seconds:

$$\text{Arrival time} = \frac{\text{distance}}{\text{speed of sound}} = \frac{750\,\text{m}}{1510\,\text{m/s}} \approx 0.5\,\text{s} \tag{4.13}$$

As shown in Figure 4.3, the simulated impulse reaches the system at about 0.5 seconds, in agreement with the predicted arrival time.

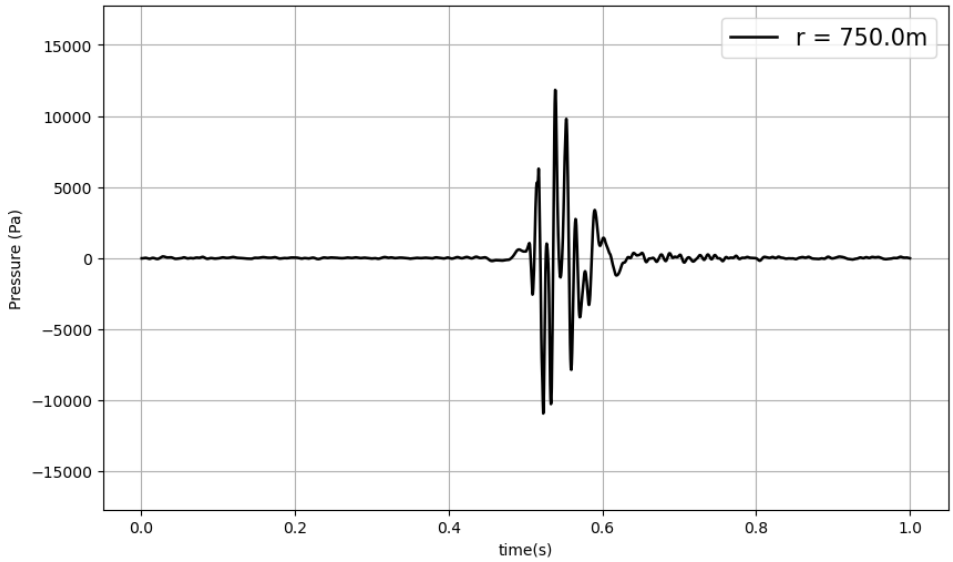

Figure 4.3: Time-domain pressure evolution of the modeled impulse generated by an IHC S-5500 hammer without mitigation measures, modeled at 2 meters above the seabed for a penetration depth of 27.5 m.

4.2 Scenario definition

To explore how variations in target blow count and impulse duration influence both the drivability of the pile and the resulting Sound Exposure Levels (SEL), three scenario sets are defined. Each scenario consists of a series of single-blow simulations at selected penetration depths. The section begins by describing the structure of these scenarios and the parameters that are varied.

The scenarios defined in this section form the foundation for all subsequent simulations.

4.2.1 Overview of scenarios

To address the research objectives, three sets of scenarios are developed: one focusing on variation in target blow count, one on pulse prolongation, and the other on the combination with a Double Big Bubble Curtain (DBBC). These scenarios are evaluated in terms of their effect on cumulative underwater noise.

Additionally, to explore the influence of the soil type for impulse prolongation, two of the scenarios are repeated using a clay-sand stratigraphy (soft clay over very dense sand) instead of medium dense sand over very dense sand. The parameters for the soil properties and wave characteristics for these layers are presented in Table E.1 in Appendix E.

Scenario	Description	Target blow count	Impulse elongation	Soil type
1	Lower target blow count	20 / 25 cm	No	Sand
2	Baseline industry practice	25 / 25 cm	No	Sand
3	Higher target blow count	30 / 25 cm	No	Sand
4	Medium impulse elongation	25 / 25 cm	50%	Sand
5	Maximum impulse elongation	25 / 25 cm	100%	Sand
6	Baseline with spatial mitigation	25 / 25 cm	No (DBBC only)	Sand
7	Combined temporal + spatial mitigation	25 / 25 cm	50% (with DBBC)	Sand
8	Baseline industry practice in clay-sand stratigraphy	25 / 25 cm	No	Clay-Sand
9	Medium impulse elongation in clay-sand stratigraphy	25 / 25 cm	50%	Clay-Sand

Table 4.7: Overview of all modelled scenarios. 8 and 9 are sensitivity runs in a two-layer clay-sand profile.

The scenario development relies on a two-step computational approach. First, the DYNPAC program is used to simulate the pile driving process based on a predefined pile and multi-layer soil profile. In DYNPAC, different target blow counts and hammer types, either with or without impulse shaping, can be selected which yield depth-specific values for hammer energy and number of blows. DYNPAC also generates the corresponding time-domain force signal for each hammer-soil-pile configuration.

In the second step, the time-domain force signals generated by DYNPAC are used as input for the SILENCE model to simulate the underwater noise radiation of individual hammer blows. Each SILENCE simulation calculates the vibro-acoustic response of a single blow, accounting for the coupled interaction between the pile, the surrounding water, and a simplified two-layer seabed model. Although the soil layering in SILENCE is fixed, the acoustic response varies with penetration depth due to two primary reasons. First, the embedded length of the pile increases with depth, altering its vibration behaviour and interaction with the surrounding media [14]. Second, the hammer energy typically increases with depth due to rising soil resistance, which affects the amplitude of the impact force.

For each selected penetration depth, DYNPAC provides the required hammer energy, number of blows, and the associated force-time signal. The rationale for selecting these representative depths, balancing computational efficiency with physical accuracy, is discussed in Section 4.1.3. Based on the resulting pressure output from SILENCE, the Sound Exposure Level (SEL) is determined for each depth. The cumulative Sound Exposure Level (cumSEL) for the entire installation is then calculated by combining the SEL values across all depths, weighted by the number of blows at each stage:

$$L_{E,\text{cum}} = 10\log_{10}\left(\sum_{i=24h}^{N} 10^{\text{SEL}_{\text{SS}}/10} \cdot N_i\right) \text{[dB re 1 } \mu\text{Pa]} \tag{4.14}$$

where SEL_{SS} is the single strike Sound Exposure Level, and N_i is the number of blows in 24 hours.

Figure 4.4 summarises the overall modelling workflow and shows where the hammer settings are adjusted.

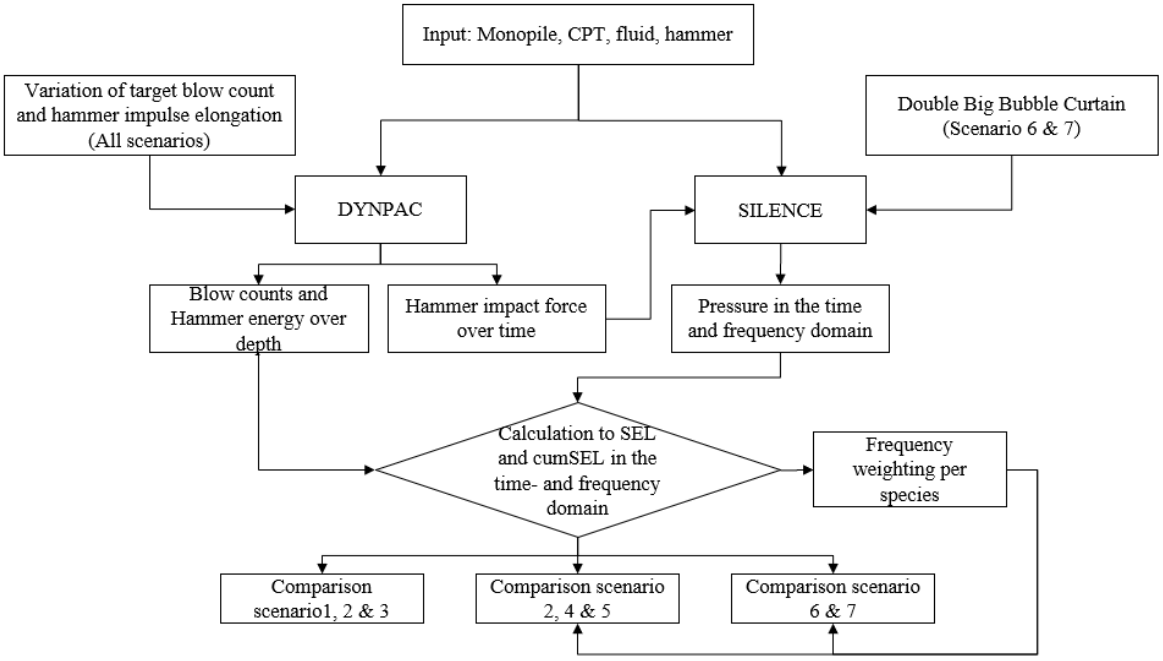

Figure 4.4: Workflow for scenario simulations: variation of hammer settings (1, 2, 3, 4, 5), spatial mitigation (6, 7), drivability in DYNPAC, acoustic response in SILENCE, and post-processing to SEL/cumSEL and species-weighted metrics before comparing scenario groups.

Variation in target blow counts

To evaluate how the choice of blow count strategy affects cumulative underwater noise emissions, a set of four scenarios is defined. These scenarios are based on different target blow counts, predefined values that indicate how many hammer blows should be applied to achieve 25 cm of pile penetration. In practice, the output energy of the hammer is regulated dynamically to reach the specified blow count target at each depth, depending on soil resistance. The total target penetration in all cases is 27.5 m.

The target blow count scenarios are:

1. 20 blows per 25 cm penetration
2. 25 blows per 25 cm penetration - reference case (industry baseline)
3. 30 blows per 25 cm penetration

The DYNPAC program is used to model the pile driving process for each scenario. Based on the given pile and multi-layer soil profile, and the specified target blow count, DYNPAC calculates

the required hammer energy at six selected penetration depths. This energy is adjusted such that the hammer can achieve the intended number of blows per 25 cm, accounting for the resistance of the soil at each depth.

In all scenarios, the pile geometry, soil layering, and target penetration depth remain constant. The only scenario variable is the target blow count, which affects both the hammer energy and the total number of blows. Within SILENCE, the only varying inputs are the penetration depth per blow and the corresponding force-time signal derived from DYNPAC.

This set of scenarios is intended to explore the trade-off between **fewer, more energetic blows** and **more, less energetic blows**, and how these strategies affect the cumulative noise footprint of the installation process.

Pulse prolongation

To investigate the effect of impulse shaping on the installation process and the resulting underwater noise levels, two pulse prolongation scenarios are defined. These scenarios are designed to evaluate how changes in the duration and shape of the impact force affect both the drivability of the pile and the noise levels emitted during installation.

In practice, pulse shaping is implemented by selecting a hammer configuration that elongates the impact duration through internal damping or energy absorption mechanisms. For this study, IQIP's PULSE is used, as elaborated on in Section 2.4.2. The DYNPAC program is used to model this effect by allowing the user to choose between different hammer types, including standard hammers and hammers that apply a pulse prolongation of 50% or 100%. These configurations yield different force-time data, with longer pulses showing lower peak forces but increased duration. The total energy delivered per blow is preserved, but the impulse shape is altered.

In each case, the force-time signal generated by DYNPAC is used as input for the SILENCE model. This approach ensures that the pulse shape reflects a physically consistent hammer-soil interaction based on the selected pile and soil profiles. By comparing the resulting underwater noise levels for different impulse durations, the analysis investigates whether impulse elongation not only reduces peak noise emissions, but also leads to a reduction in cumulative sound exposure.

The two scenarios investigated are:

4. Pulse prolongation by 50% - medium pulse
5. Pulse prolongation by 100% - maximum pulse

The pile geometry, soil layering, and target penetration depth are kept constant across all pulse prolongation scenarios. However, due to changes in the selected hammer type within DYNPAC, the resulting hammer energy and number of blows per penetration depth vary between scenarios. These values influence the cumulative SEL calculation. Within SILENCE, the only varying parameters are the penetration depth per blow and the corresponding force-time signal.

Combined use with a Double Big Bubble Curtain

The Double Big Bubble Curtain (DBBC) is frequently used in offshore pile driving operations because it is often the most effective way to ensure compliance with underwater noise regulations. In practice, most installations that aim to reduce acoustic emissions will apply a (D)BBC by default. It is therefore important to assess how such a mitigation system interacts with the operational strategies considered in this study.

From a physical perspective, both impulse shaping and bubble curtains influence the frequency spectrum of the radiated noise, albeit in different ways. Pulse prolongation tends to shift energy toward lower frequencies [43], while bubble curtains attenuate specific frequency bands through scattering and impedance effects [87]. Understanding the combined effect of these techniques is essential to evaluate whether their joint application provides additive benefits, or whether certain combinations are more or less effective due to spectral overlap or interaction [79].
Two scenarios are defined to evaluate the effect of a DBBC: one in comparison to a reference case without PULSE, and one combining a DBBC with impulse elongation.
The two scenarios investigated are:

6. No pulse prolongation in combination with a DBBC
7. Pulse prolongation by 50% in combination with a DBBC

By comparing Case 6 (reference case with DBBC) and Case 7 (pulse prolongation with DBBC), the analysis provides insight into the relative impact of temporal versus spatial mitigation, and explores the potential synergies between the two. This comparison is especially relevant for real-world applications, where combined strategies are often necessary to meet increasingly strict underwater noise limits.

Clay-sand profile

A sensitivity analysis was conducted for the baseline scenario (Case 2) and the 50% PULSE scenario (Case 4) using a two-layer clay-sand stratigraphy. By applying the same hammer settings to a soft clay cap over dense sand, this additional case evaluates the influence of soil type on the relative performance of impulse elongation.

8. No pulse prolongation in clay-sand stratigraphy
9. Pulse prolongation by 50% in clay-sand stratigraphy

4.2.2 Frequency weighting

Both PULSE and the DBBC are expected to alter the frequency spectrum of radiated noise during pile driving. However, marine mammals do not perceive all frequencies equally. As discussed in Section 2.2.2, each hearing group has a distinct auditory sensitivity curve. For example, porpoises are highly sensitive to high-frequency sounds, while baleen whales primarily detect low-frequency noise.

To assess the actual perceptual impact of piling noise, regulatory frameworks such as those by NOAA and NMFS recommend applying frequency weighting to the cumulative sound exposure level (SEL). This means adjusting the spectral energy distribution to reflect what a specific hearing group would effectively hear. In practice, this involves attenuating frequency bands outside the species' hearing range and preserving those within their sensitivity window.

The purpose of frequency weighting is thus to convert a physical measure (acoustic energy) into a biologically relevant metric. Without weighting, a high-energy signal at an irrelevant frequency could overestimate risk, while an impactful signal at a sensitive frequency might be overlooked.

In this study, frequency weighting is applied to the cumSEL for all scenarios to evaluate whether the spectral changes introduced by PULSE and the DBBC reduce acoustic exposure in the frequency bands that matter most for each hearing group. This makes it possible to compare not only overall noise reduction but also species-specific effectiveness of mitigation strategies.

5 | Numerical study on cumulative underwater noise

This chapter presents the results of varying hammer configurations on underwater noise emissions. The analysis is structured in five parts: (1) the effect of target blow count variation, (2) the effect of impulse elongation, (3) the combined effect of impulse elongation with a Double Big Bubble Curtain (DBBC), (4) the frequency weighting of the cumulative Sound Exposure Level (cumSEL), and (5) the effect of impulse elongation in a different soil profile.

For the blow count variation, results are expressed in terms of unweighted cumSEL at a distance of 750 m. For impulse elongation, both unweighted and frequency-weighted cumSEL values are evaluated for all five NOAA marine mammal hearing groups. The influence of impulse elongation is first examined independently, followed by the combined PULSE+DBBC configuration. In each case, results include frequency-domain analysis, with and without the application of species-specific weighting functions.

5.1 The effect of target blow count variation

This section presents the results regarding the impact of varying the target blow count on the cumulative underwater noise emissions generated during pile driving. Three target blow counts, specifically 20, 25 (baseline), and 30 blows per 0.25 m penetration, are analysed. Results are reported in terms of cumulative Sound Exposure Level (cumSEL) at a reference distance of 750 m from the monopile. Prior to acoustic modelling, drivability simulations were conducted to establish hammer energy requirements and blow distributions.

5.1.1 Drivability analysis

The drivability analysis was conducted using the dynamic piling analysis software DYNPAC. The outcomes of these simulations, required hammer energy and the number of blows per incremental penetration depth, are depicted in Figures 5.1a, 5.1b, and 5.1c.

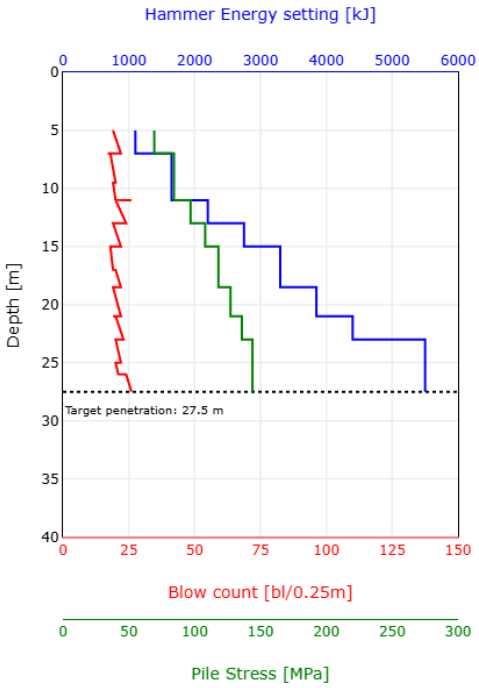

(a) Target blow count: 20 blows/0.25 m

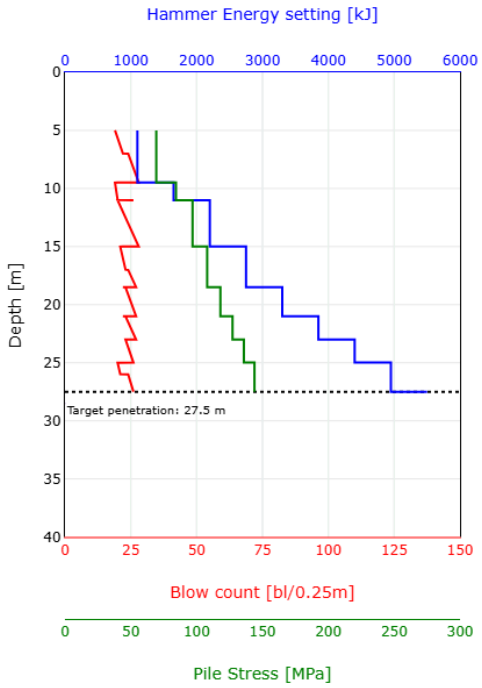

(b) Target blow count: 25 blows/0.25 m (baseline)

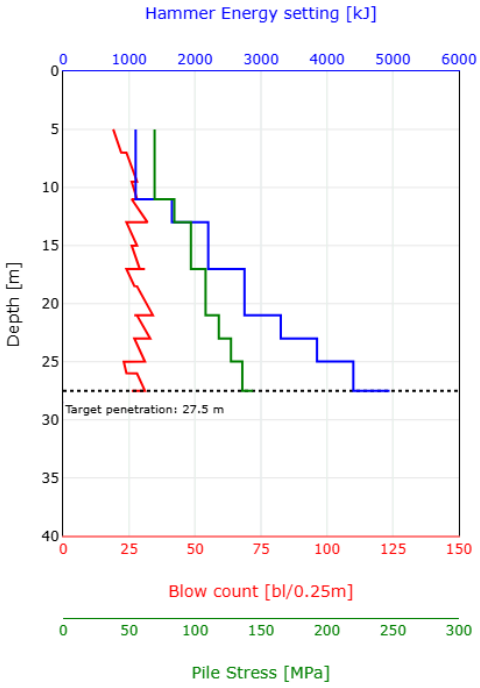

(c) Target blow count: 30 blows/0.25 m

Figure 5.1: DYNPAC drivability curves indicating the required hammer energy (blue lines) and blow count (red lines) for three different target blow count scenarios: (A) 20 blows/0.25 m, (B) 25 blows/0.25 m (baseline scenario), and (C) 30 blows/0.25 m.

The drivability curves presented in Figure 5.6 highlight distinct differences in the energy distribution and number of hammer blows required for each configuration. Table 5.1 summarises

the total number of blows and the corresponding total duration of each scenario to reach the designated penetration depth of 27.5 m. The variation in the total blow count ranges from -13.4% (1966 blows) to +15.8% (2632 blows), relative to the baseline scenario of 2272 blows. Detailed tables containing blow counts and corresponding hammer energy at incremental depths are provided in Appendix B.

Scenario	**Total number of blows**	**Duration (min)**
20 blows/0.25 m	1966	77.5
25 blows/0.25 m (baseline)	2272	87.8
30 blows/0.25 m	2632	101.1

Table 5.1: Summary of total blow count and corresponding duration for each blow count scenario to achieve a penetration depth of 27.5 m.

Differences observed in Table 5.1 demonstrate how variations in the target blow count significantly affect the total driving duration. A reduction in blow count (shorter driving durations) corresponds to higher average hammer energy per blow, whereas an increase in blow count (longer driving durations) results in reduced hammer energy per blow. This inverse relationship between blow count and hammer energy per blow aligns with established literature on pile drivability [38]. Specifically, Lippert et al. (2018) reported similar findings, noting that fewer hammer blows inherently necessitate higher individual blow energy.

The subsequent sections investigate the acoustic implications of these blow count and hammer energy variations by examining the resulting Sound Exposure Levels (SEL) and cumulative acoustic impact.

5.1.2 Single strike sound levels

To evaluate how variations in the target blow count affect acoustic emissions, the SEL values associated with the loudest blow per scenario are analyzed first. Figure 5.2 shows the SEL as a function of horizontal distance from the monopile for each scenario (20, 25, and 30 blows per 0.25 m).

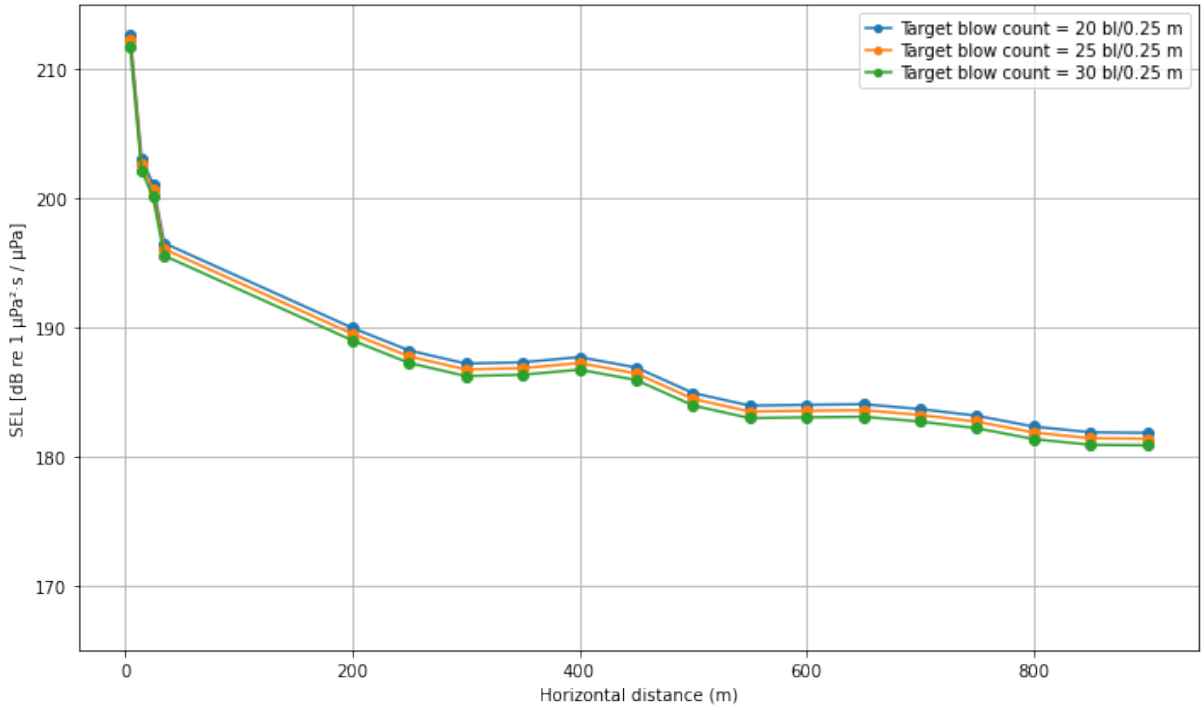

Figure 5.2: Comparison of modelled maximum SEL values as a function of horizontal distance from the monopile for three target blow count variations (penetration depth = 27.5 m, receiver positioned 2 m above seabed).

Small incremental increases in SEL values are evident around distances of approximately 350 m and again near 600 m in Figure 5.2. These localized peaks result from the complex interaction of direct and reflected acoustic paths, a phenomenon extensively documented in acoustic propagation literature [32, 34].

Acoustic propagation significantly affects underwater noise distribution. Several factors, such as water depth, seabed composition, and the presence of reflective surfaces, contribute to distinct acoustic modes that propagate within the water column. The interference between these modes can either be constructive or destructive depending on the relative phase relationships between sound waves. At approximately 350 m and 600 m distances from the pile, constructive interference occurs, causing an increase in local sound pressure levels due to aligned phases of direct and reflected waves [32, 38].

Detailed SEL and L_{peak} values per penetration depth are provided in Table C.1 in Appendix C. Table 5.2 summarizes the maximum SEL and L_{peak} values at 750 m distance from the monopile, at 2 m above the seabed, along with their variations relative to the baseline scenario (25 blows/0.25 m). The scenario with 20 blows per 0.25 m employs fewer blows but higher energy per blow, resulting in slightly higher SEL and peak sound levels. Conversely, the scenario with 30 blows per 0.25 m, involving more blows with lower energy per blow, yields marginally lower SEL and peak sound levels.

Scenario	SEL [dB re 1 µPa^{2}s]	SEL variation [dB]	L_{peak} [dB re 1 µPa]	L_{peak} variation [dB]
20 blows/0.25 m	183.16	+0.46	201.46	+0.46
25 blows/0.25 m (baseline)	182.70	[-]	201.00	[-]
30 blows/0.25 m	182.19	-0.51	200.49	-0.51

Table 5.2: Maximum SEL and L_{peak} values and their variation relative to the baseline scenario (25 blows/0.25 m), modelled at 750 m horizontal distance and 2 m above the seabed.

These findings correspond with the theoretical expectations that distributing the same total pile-driving energy over more blows reduces individual blow energy, consequently lowering per-blow SEL and peak sound levels [32, 38]. However, the effect on cumulative noise exposure, incorporating total blow count, requires separate consideration and will be explored in subsequent sections.

5.1.3 Cumulative sound exposure

Having determined the blow counts and corresponding single-strike SEL values, the cumulative Sound Exposure Level (cumSEL) is computed for each target blow count configuration across a range of horizontal distances from the monopile. The results are illustrated in Figure 5.3.

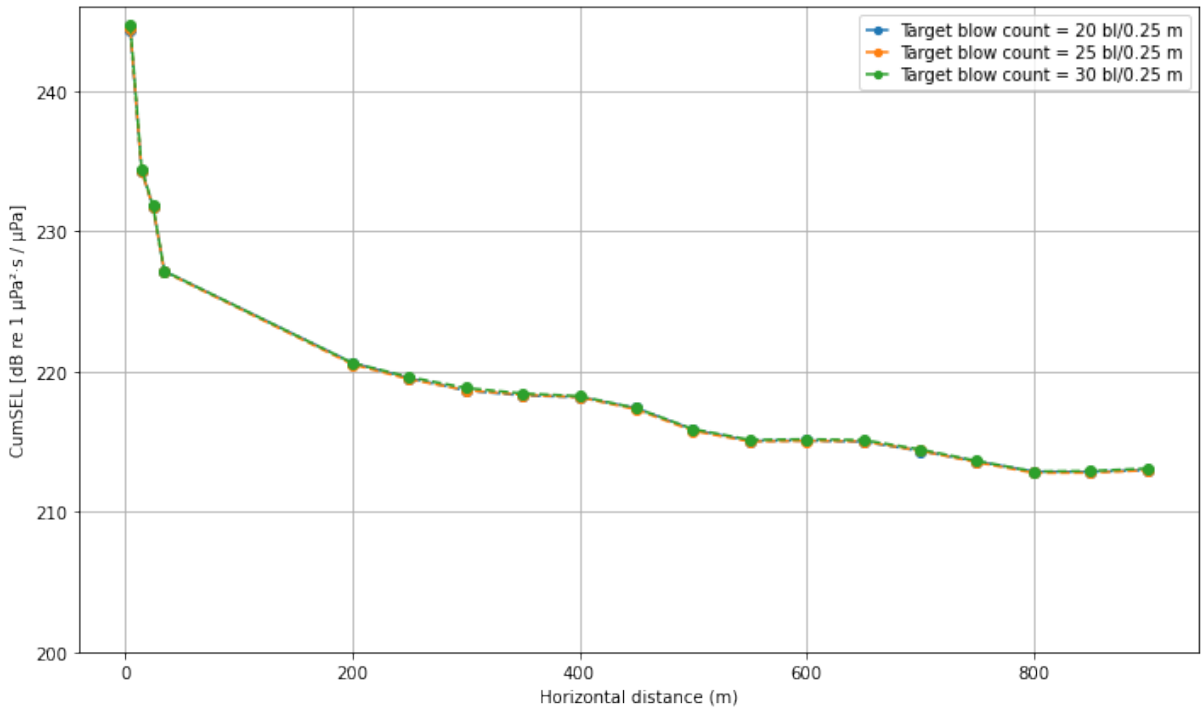

Figure 5.3: Comparison of the modelled cumulative SEL values for three target blow count scenarios. Modelled at 2 m above the seabed.

As shown in the figure, the differences in cumSEL among the three cases are minimal, with maximum deviations below 0.1 dB. This outcome is consistent with theoretical expectations. When the total energy delivered by the hammer remains approximately constant, increasing the number of blows spreads the energy across a longer duration, reducing the energy per strike but maintaining the overall acoustic energy (logarithmic sum). This trade-off can be described by the following relationship:

$$\mathrm{SEL}_{\mathrm{cum}} = \mathrm{SEL}_{\mathrm{single}} + 10 \cdot \log_{10}(N_{\mathrm{strikes}})$$

where N_{strikes} represents the total number of hammer blows.

The corresponding values at 750 m from the pile, 2 m above the seabed, are summarised in Table 5.3.

Scenario	**cumSEL** [dB re 1 µPa^{2}s]	**cumSEL variation** [dB]
20 blows/0.25 m	213.59	+0.06
25 blows/0.25 m (baseline)	213.53	[-]
30 blows/0.25 m	213.63	+0.10

Table 5.3: Cumulative SEL values and variation relative to the baseline (25 blows/0.25 m), modelled at 750 m horizontal distance and 2 m above the seabed.

These results indicate that altering the target blow count alone, without significantly changing total energy input, has negligible influence on overall cumSEL levels.

5.1.4 Spectral distribution

To assess the frequency-dependent effects of target blow count variation, the SEL and cumSEL are also analysed in the frequency domain. The resulting third-octave band spectra are shown in Figure 5.4 and Figure 5.5.

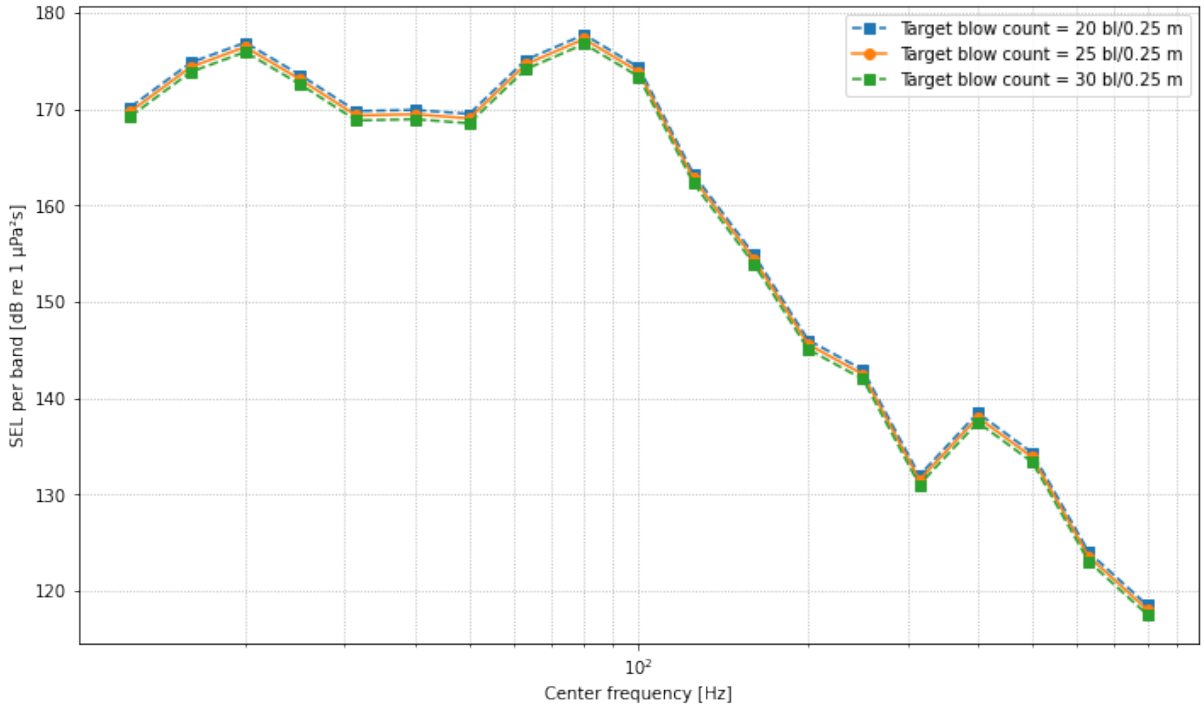

Figure 5.4: Third-octave band SEL spectra for the three blow count scenarios, modelled at 750 m from the monopile and 2 m above the seabed.

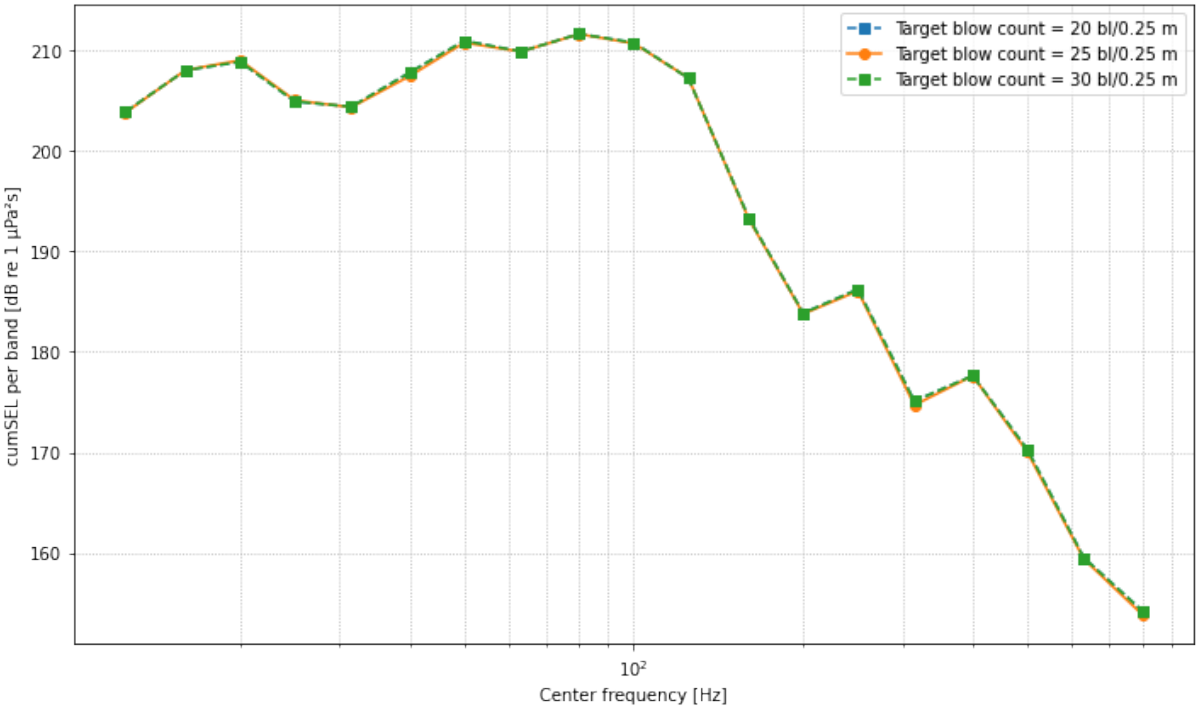

Figure 5.5: Third-octave band cumSEL spectra for the three blow count scenarios, modelled at 750 m from the monopile and 2 m above the seabed.

The spectra indicate that variations in blow count have a negligible effect on the spectral distribution of radiated sound. Over the whole frequency range, the spectral energy levels remain similar. The results suggest that when the total impact energy remains approximately constant, spectral shaping through blow count adjustment alone is limited.

5.2 Impact of impulse elongation

As explained in Section 2.4.2, pulse prolongation systems extend the contact time between the hammer and the monopile by modifying the shape of the force signal. This adjustment redistributes the same total impact energy over a longer duration, resulting in lower peak amplitudes but extended impulse durations.

This redistribution is expected to affect both the radiated underwater noise and the drivability of the pile. While lower peak amplitudes may reduce instantaneous sound pressure levels, the cumulative acoustic impact over time (e.g., 24-hour SEL) may still increase or decrease depending on changes in drivability, such as a potential increase in the number of blows or in hammer energy required to achieve target penetration. Because these effects interact, it is not immediately clear whether impulse elongation will lead to an overall increase or decrease in cumulative noise.

Moreover, the frequency content of the emitted sound is likely to shift due to the modified time profile of the impact. As discussed in Chapter 2, some regulatory frameworks, such as those used in the United States, apply frequency weighting based on species-specific hearing sensitivities. This means that both the magnitude and spectral distribution of the noise are relevant for assessing environmental impact.

This section explores how the elongation of the impulse duration affects these parameters, using the simulation setup introduced in Chapter 4.

5.2.1 Drivability analysis

As discussed in Chapter 4, a drivability analysis is first conducted using the dynamic piling analysis software (DYNPAC) to determine the required hammer energy and number of blows per penetration depth. The results of this analysis are shown in Figures 5.6b, 5.6a, and 5.6c.

These figures indicate that both Case 4 and the reference configuration successfully reach the target penetration depth of 27.5 m. However, Case 5 shows refusal [2] at a certain depth, meaning that the pile can no longer be driven further. This is evident from the red line in the drivability plot, which represents the number of blows required per 25 cm of penetration. In this case, the red line never reaches the target penetration depth of 27.5 m, indicating that the applied hammer energy is insufficient to overcome soil resistance beyond a certain depth. In this case, the prolonged pulse appears to work counter-productively, preventing sufficient energy transfer for continued penetration. As a result, this configuration is not considered technically feasible for the full installation process using a 100% pulse system. This scenario is therefore excluded from further analysis.

[2]Refusal occurs when the blow count surpasses a specified threshold set by the *HMC refusal criteria*; see Section 3.3 for elaboration.

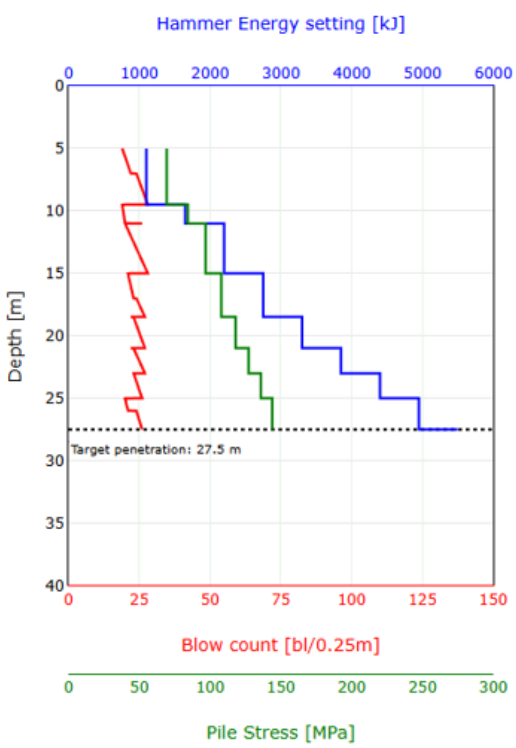

(a) No pulse (baseline)

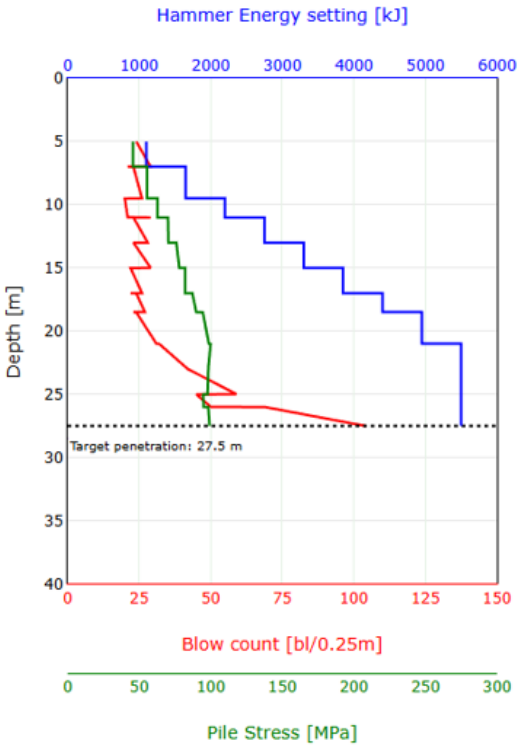

(b) Pulse 50%

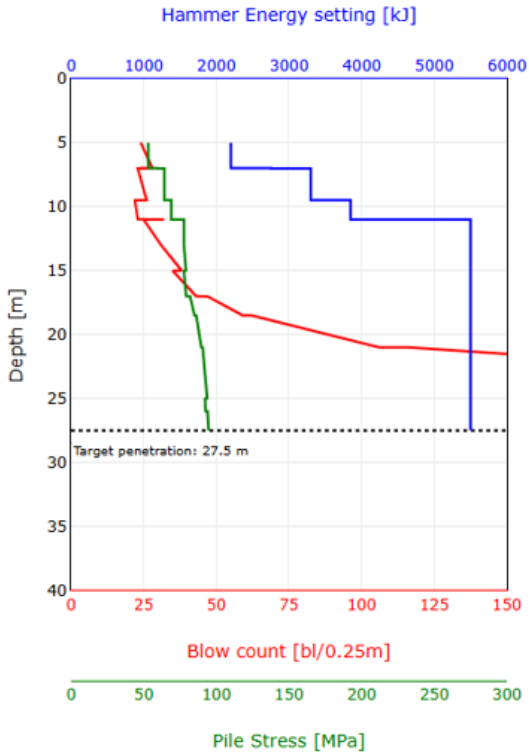

(c) Pulse 100%

Figure 5.6: Drivability curves for different pulse configurations: (A) No pulse (baseline), (B) Pulse 50%, and (C) Pulse 100%.

The DYNPAC drivability analysis reveals noticeable differences between the hammer configura-

tions. The Pulse 50% scenario requires 3386 blows to reach the full penetration depth of 27.5 m and takes 133.9 minutes. The reference scenario (without pulse shaping) achieves the same depth with only 2272 blows in 87.8 minutes. The Pulse 100% scenario does not reach the target depth at all, indicating refusal; hence, the total number of blows and driving duration are undefined. An overview of the blow counts and hammer energy per depth increment is provided in Appendix B, and the total blow counts and corresponding durations are summarised in Table 5.4.

It can be observed from Figure 5.6b (and more in detail in the appendix tables) that the increase in required blows for the Pulse 50% configuration primarily arises in the final 6.5 m of penetration. This depth range exhibits significantly higher blow counts compared to the reference case, indicating reduced energy transfer efficiency during deeper penetration stages when using elongated impulses.

This effect can be explained by soil-structure interaction principles: as the pulse duration increases, the peak force transmitted to the pile decreases, reducing the capacity to overcome static tip resistance. Additionally, dense sand exhibits increasing resistance with depth due to compaction and confinement. A softer, prolonged impulse dissipates more energy into soil damping and causes local densification in front of the pile, both of which further hinder penetration. These effects compound near refusal, where high static and dynamic resistance require short, high-intensity impacts to maintain penetration efficiency. As a result, elongated impacts such as those from Pulse 50% become progressively less effective in the final meters. This phenomenon is consistent with findings in dynamic pile driving literature for dense granular soils [38, 88].

Scenario	Number of blows	Duration (min)
No PULSE	2272	87.8
50% PULSE	3386	133.9

Table 5.4: Blow count and duration for target penetration depth of 27.5 m.

5.2.2 Single strike sound levels

To establish a quantitative comparison between the PULSE and reference hammer configurations, the Sound Exposure Level (SEL) per individual strike is first assessed. For each configuration, the loudest single blow, typically occurring near maximum penetration, is selected. Figure 5.7 presents the spatial decay of SEL with distance from the monopile.

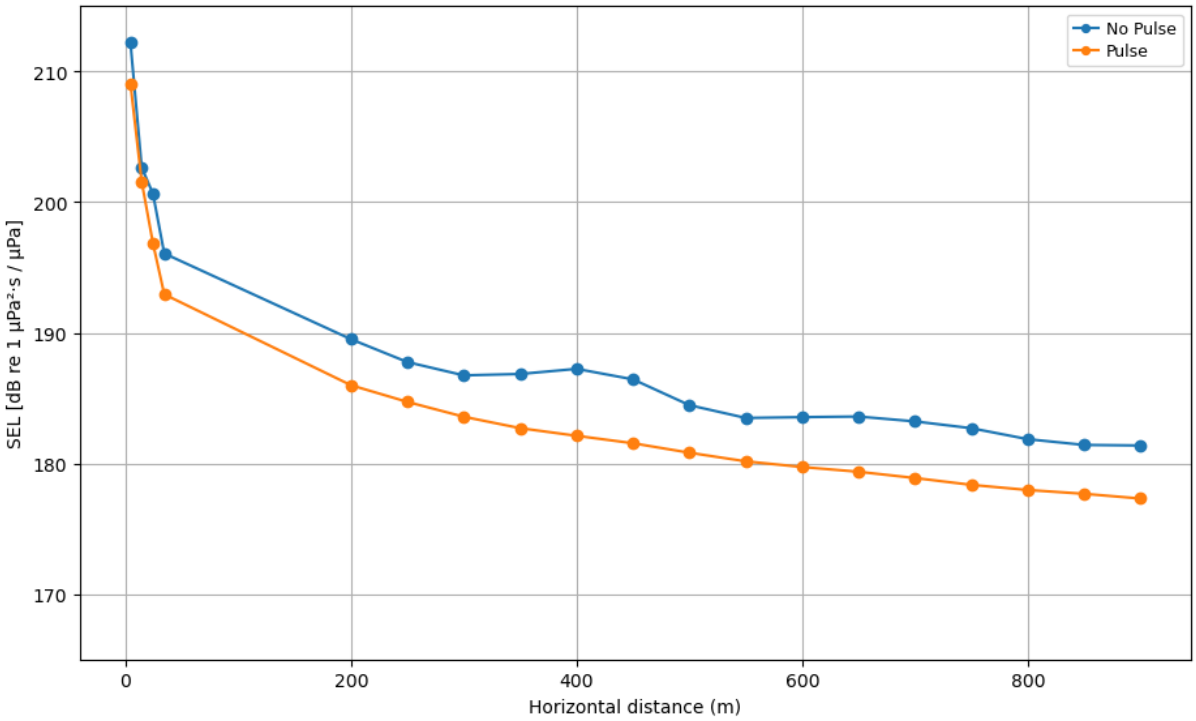

Figure 5.7: Comparison of modelled maximum SEL values as a function of horizontal distance from the monopile for two scenarios: no PULSE and PULSE (penetration depth = 27.5 m, receiver positioned 2 m above seabed)

Table 5.5 lists the SEL values measured at 750 m for both scenarios. The reduction in SEL achieved through the use of PULSE is also provided. These results show that the PULSE configuration yields a reduction of 4.34 dB in the per-strike SEL relative to the baseline configuration. Across all distances, PULSE reduces the per-strike SEL relative to the reference case. Notably, the no-PULSE scenario exhibits local peaks in the SEL field that are absent in the PULSE case. These peaks likely result from constructive interference between direct and reflected wave paths, which can locally elevate SEL values and thus contribute to higher cumulative noise levels in specific regions. The smoother decay in the PULSE configuration indicates a more gradual energy distribution and reduced interference patterns.

5.2.3 Cumulative sound exposure

Once the per-strike SEL and blow count are known, the cumulative Sound Exposure Level (cumSEL) over the full pile installation can be determined. Figure 5.8 shows the cumSEL as a function of distance from the monopile.

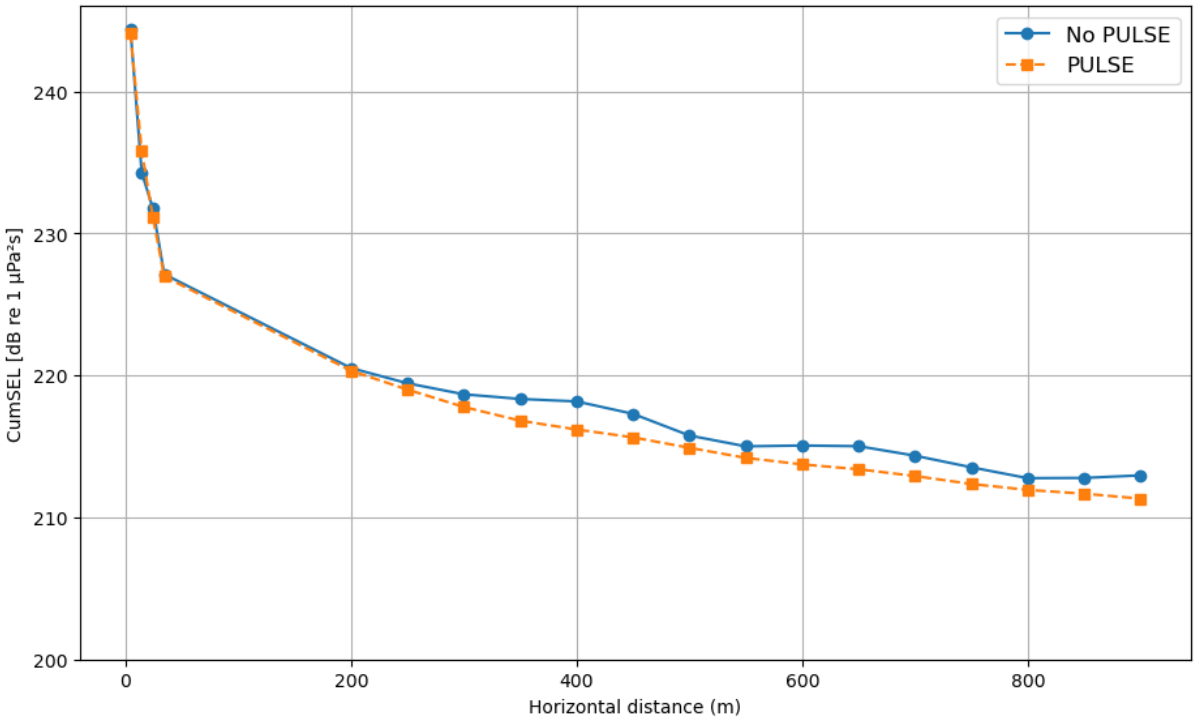

Figure 5.8: Comparison of the modelled cumulative SEL values for two scenarios: no PULSE and PULSE, 2 m above the seabed.

Scenario	**SEL** [dB re 1 µPa^{2}s]	**SEL variation** [dB]	**cumSEL** [dB re 1 µPa^{2}s]	**cumSEL variation** [dB]
No PULSE (baseline)	182.70	[-]	213.53	[-]
PULSE (50%)	178.36	-4.34	212.35	-1.18

Table 5.5: Modelled SEL and cumSEL values at 750 m distance from the monopile, 2 m above the seabed. Reductions are expressed relative to the no-PULSE baseline scenario.

Compared to the results in Figure 5.7, it is observed that the reduction in cumulative SEL is smaller than the SEL reduction observed for individual blows. Specifically, PULSE results in only a 1.18 dB reduction in cumulative SEL at 750 m. This limited reduction can be explained by the cumulative nature of SEL, which is governed by both the energy per blow and the total number of blows:

$$\mathrm{SEL}_{\mathrm{cum}} = \mathrm{SEL}_{\mathrm{single}} + 10 \cdot \log_{10}(N_{\mathrm{strikes}})$$

In the PULSE case, the increased number of strikes (+49%) offsets much of the reduction achieved per individual blow, leading to only a modest net improvement in cumulative noise emissions.

5.2.4 Spectral distribution

To better understand the spectral effects of PULSE, both the SEL and cumSEL values are analyzed in the frequency domain. Figures 5.9 and 5.10 show the respective 1/3-octave band levels for SEL and cumSEL at 750 m.

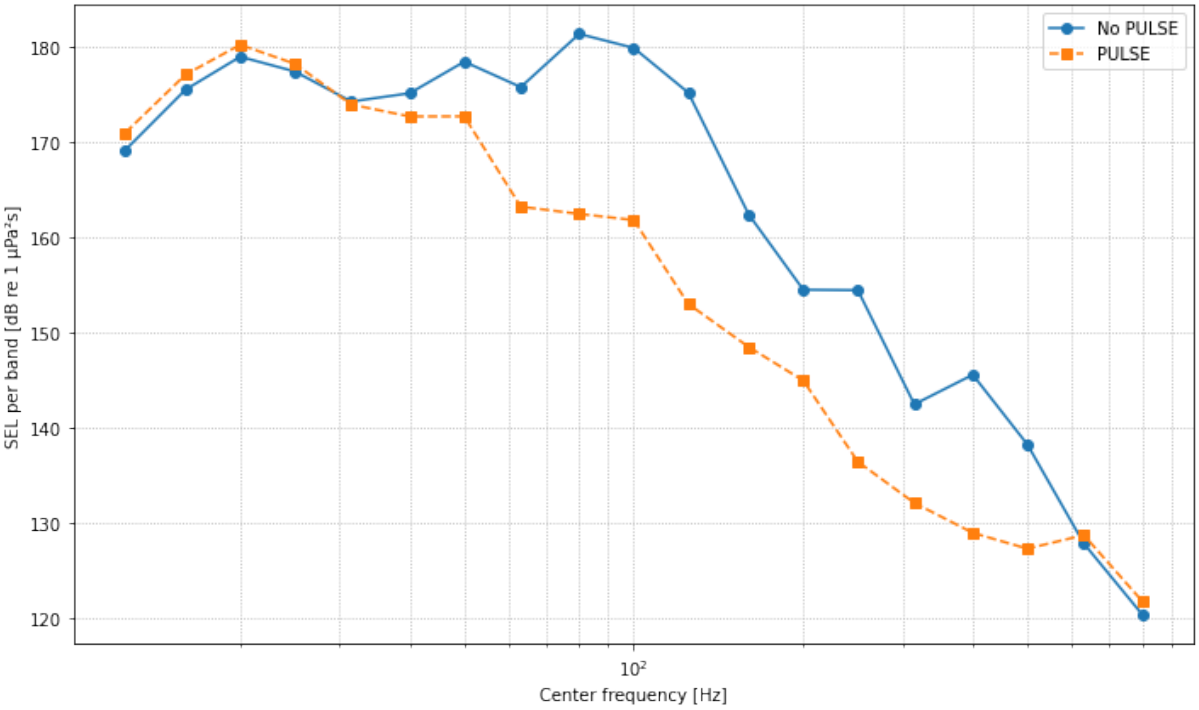

Figure 5.9: 1/3-octave band SEL at 750 m from the monopile. Comparison between PULSE and no PULSE configurations.

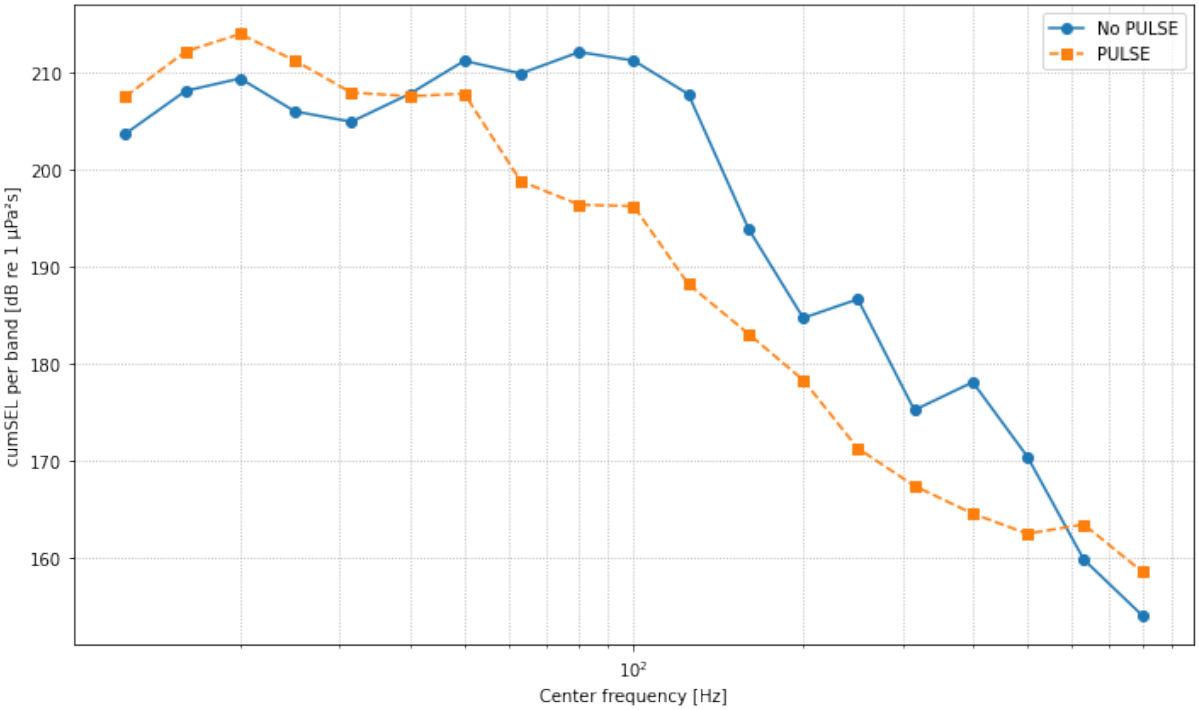

Figure 5.10: 1/3-octave band cumulative SEL at 750 m from the monopile. Comparison between PULSE and no PULSE configurations.

These figures confirm that the application of PULSE shifts a portion of the energy spectrum toward lower frequencies (<40 Hz). This spectral redistribution is a direct consequence of the elongated impulse shape, which increases signal duration and reduces high-frequency components

due to the time-frequency uncertainty principle [31]. The reduced slope in the high-frequency tail and the relative increase below 40 Hz confirm that energy is concentrated in the lower bands. The presence of increased low-frequency energy is acoustically relevant for two reasons. First, low-frequency sound propagates with lower attenuation and therefore contributes disproportionately to far-field noise levels. Second, some marine mammal species, particularly low-frequency cetaceans, retain hearing sensitivity in these bands. This underscores the importance of applying frequency-weighting functions when assessing ecological impact, which is addressed in Section 5.4.

5.3 Combined impact of PULSE and a Double Big Bubble Curtain (DBBC)

This section evaluates the cumulative acoustic impact of impulse elongation (PULSE) in combination with a Double Big Bubble Curtain (DBBC). First, the cumulative and per-strike sound levels are assessed to quantify the reduction achieved by the DBBC with and without PULSE. Subsequently, the spectral response is examined to determine whether synergistic or counteractive behaviour arises from the combined configuration.

5.3.1 Single strike and cumulative sound levels

Figure 5.11 presents the modelled maximum Sound Exposure Level (SEL) per blow for four scenarios: baseline (no PULSE, no DBBC), PULSE only, DBBC only, and PULSE combined with DBBC. The SEL values are computed at a receiver height of 2 m above the seabed.

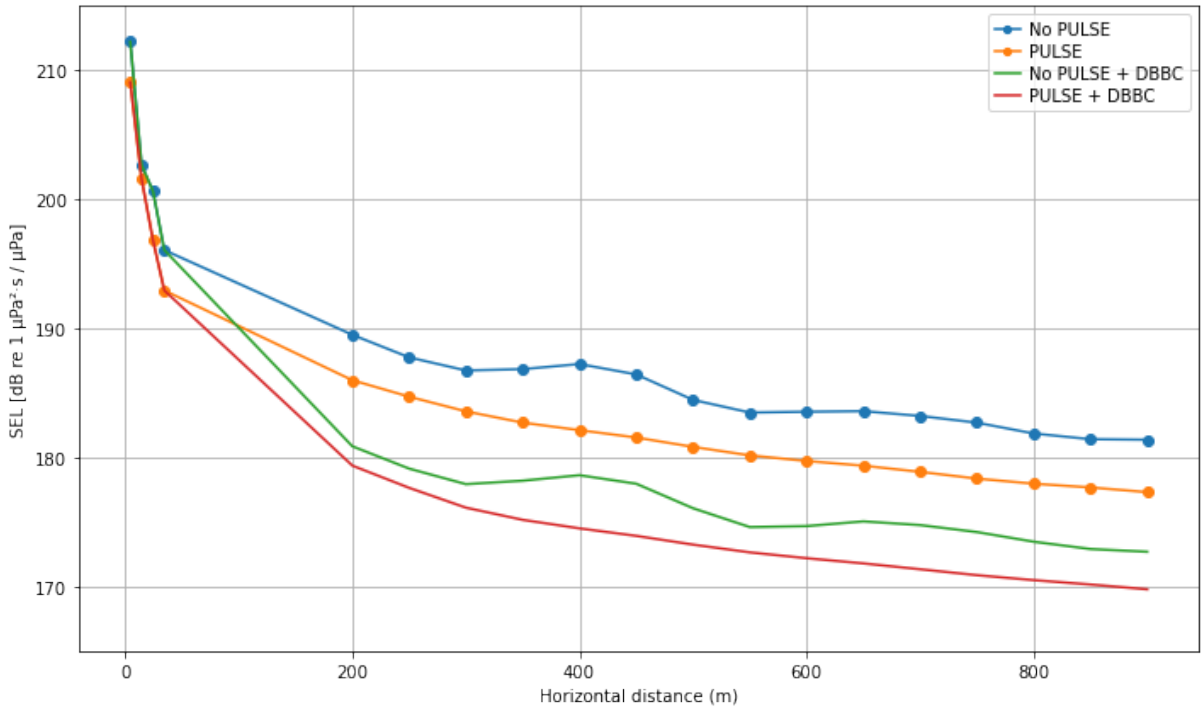

Figure 5.11: Modelled per-strike SEL values for four configurations: no PULSE, no PULSE + DBBC, PULSE (50%), and PULSE + DBBC. Receiver at 2 m above seabed.

The results indicate that the DBBC significantly reduces SEL for both PULSE and no-PULSE configurations across all distances from the source. These reductions are consistent with literature, which reports that bubble curtains are particularly effective in the mid- to high-frequency

range due to their interaction with wavelengths comparable to or smaller than the bubble diameters [42, 89]. In contrast to PULSE, the DBBC does not affect the mechanical drivability or the number of required blows, which contributes to its effectiveness in lowering cumulative levels.

Figure 5.12 shows the corresponding cumulative SEL (cumSEL) values for each configuration. For most distances from the monopile, the combination of PULSE and DBBC results in the lowest overall cumSEL.

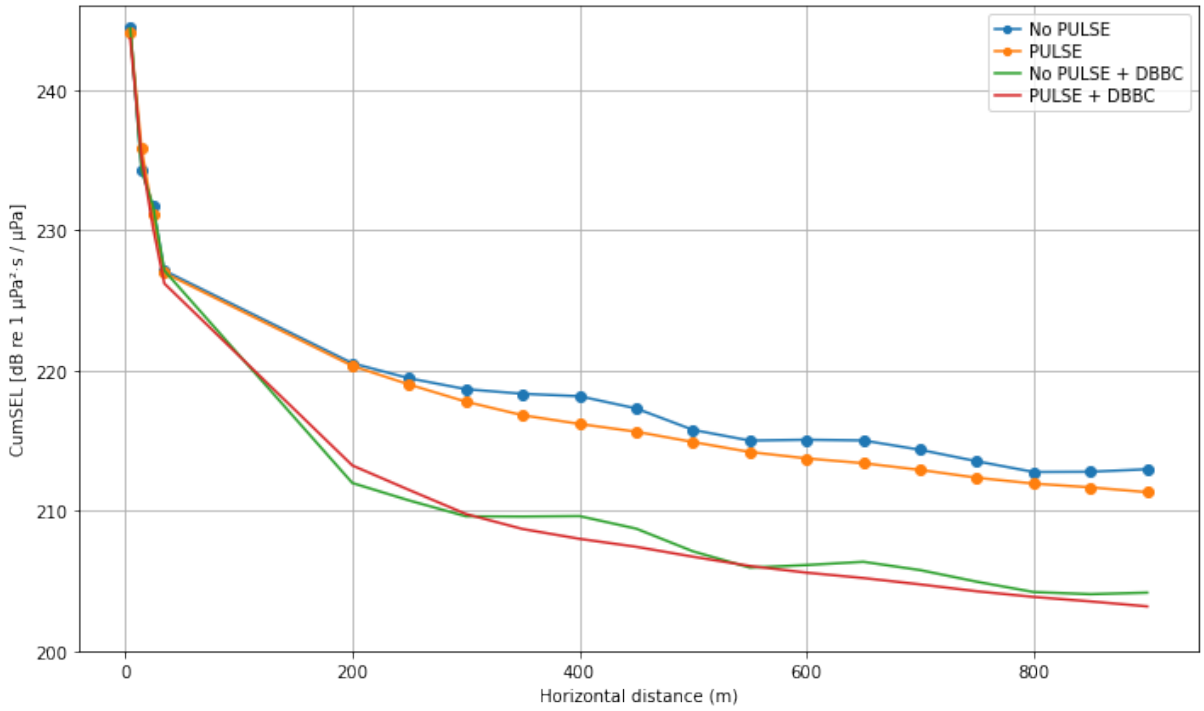

Figure 5.12: Modelled cumulative SEL values for four configurations: no PULSE, no PULSE + DBBC, PULSE (50%), and PULSE + DBBC. Receiver at 2 m above seabed.

Table 5.6 summarises the SEL and cumSEL values at 750 m distance for each scenario. Reductions relative to the baseline are also included. While PULSE alone results in a cumSEL reduction of 1.18 dB, the combination of PULSE with DBBC yields a reduction of only 0.58 dB compared to the DBBC-only case. This marginal gain suggests that, once the DBBC is in place, the additional benefit of PULSE becomes limited. However, since this is about small values, this could also be due to the sensitivity of the SILENCE model.

Scenario	**SEL** [dB re 1 µPa^{2}s]	**SEL variation** [dB]	**cumSEL** [dB re 1 µPa^{2}s]	**cumSEL variation** [dB]
No PULSE + DBBC	174.08	[-]	204.73	[-]
PULSE (50%) + DBBC	170.30	-3.78	204.15	-0.58

Table 5.6: SEL and cumSEL values for scenarios with DBBC, with and without PULSE. All values modelled at 750 m from the monopile, 2 m above the seabed. Reductions are given relative to the DBBC-only configuration.

5.3.2 Spectral distribution

Bubble curtains are widely known for their broadband noise attenuation, particularly effective at frequencies above 200 Hz due to resonance and scattering effects [87]. To examine the interaction

between PULSE and the DBBC across frequencies, the 1/3-octave band SEL and cumSEL values are shown in Figures 5.13 and 5.14.

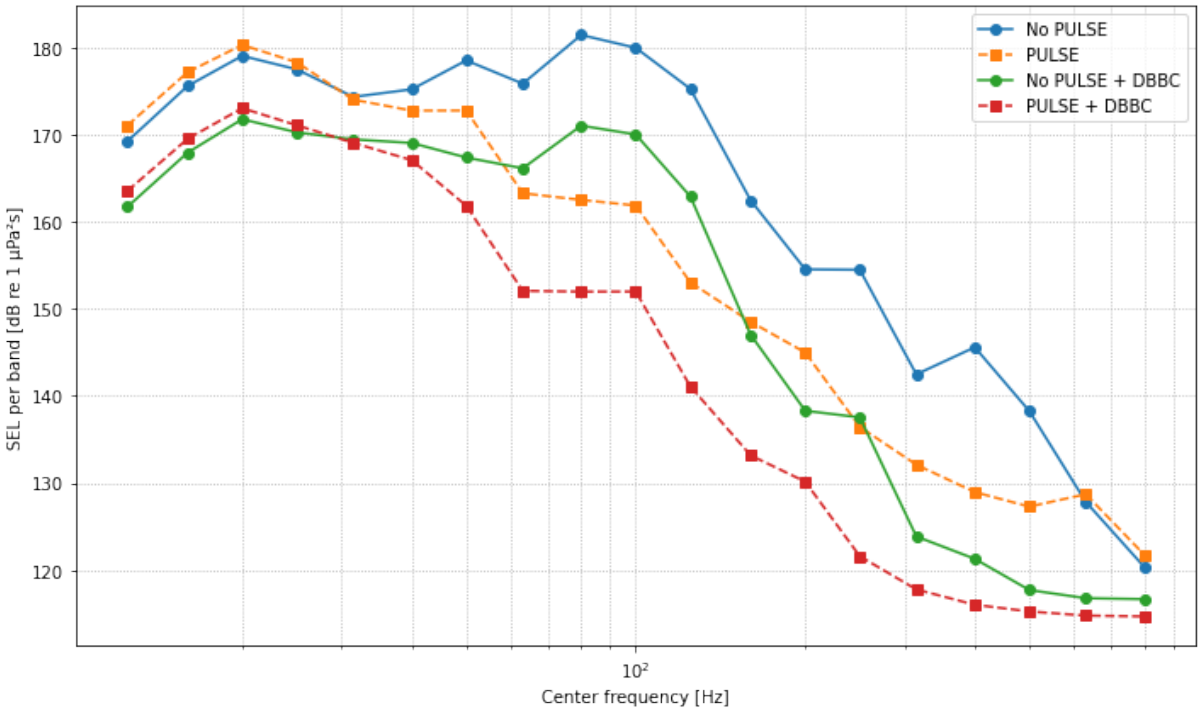

Figure 5.13: 1/3-octave band SEL at 750 m for all four configurations.

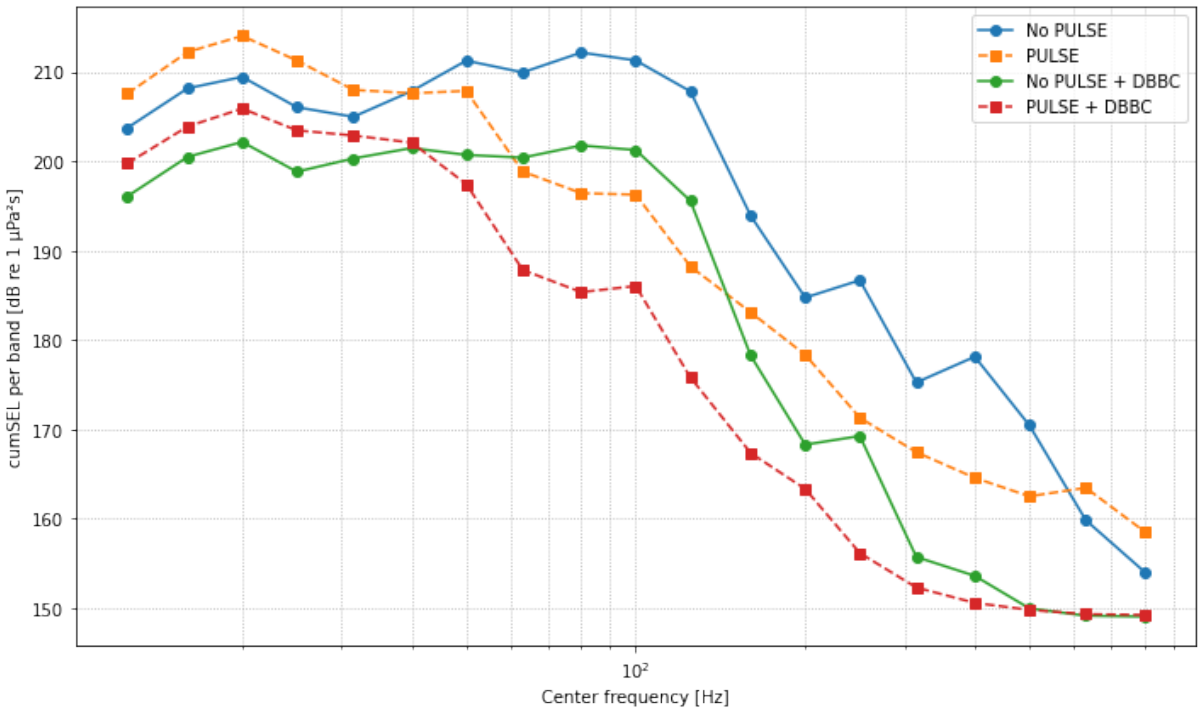

Figure 5.14: 1/3-octave band cumulative SEL at 750 m for all four configurations.

These spectral results confirm that the DBBC achieves substantial noise reduction across a wide frequency range. In particular, mid- and high-frequency energy is markedly suppressed. PULSE remains effective in lowering the mid-frequency peak associated with impulsive strikes,

but contributes less at lower frequencies. Notably, a small reduction in low-frequency bands (<40 Hz) is observed in the DBBC scenarios. This is contrary to common expectations, as bubble curtains are generally considered ineffective below 100 Hz due to the mismatch between wavelength and bubble size.

One possible explanation is that the effective acoustic thickness of the DBBC, enhanced by dual-ring placement, results in partial scattering even for longer wavelengths. A second, physically motivated explanation involves the shallow water cutoff frequency: below this critical frequency the channel ceases to behave as an efficient waveguide, and energy is preferentially refracted into, and absorbed by, the seabed rather than propagating through the water column. Because longer impulses contain more low-frequency energy that is likely to fall below this cutoff point, they suffer additional attenuation that is not mitigated by waterborne measures such as air bubble curtains. Finally, there is also a numerical consideration: the SILENCE model applies its own low-frequency cutoff that can introduce artificial attenuation below a user-defined threshold. Consequently, any apparent suppression in the low-frequency band should be interpreted with caution, as it may arise from a combination of genuine cutoff frequency physics and model-induced artefacts, and therefore may not accurately represent the true performance under field conditions.

The combination of PULSE and a DBBC results in cumulative noise reductions across all frequency bands. While the DBBC delivers the majority of the attenuation (approximately 8.8 dB), the additional benefit of PULSE when used in combination is limited to approximately 0.6 dB. In contrast, PULSE alone contributes a 1.18 dB reduction in the absence of any secondary mitigation. These results imply that DBBC is the dominant contributor to sound reduction in this combined strategy, while PULSE has most of its value when used independently. Nonetheless, no evidence was found that PULSE counteracts the DBBC. Instead, the methods appear complementary, with no adverse spectral interactions.

5.4 Frequency-weighted noise impact

The application of frequency weighting provides insight into the ecological relevance of the cumulative Sound Exposure Level (cumSEL) across different marine mammal hearing groups, as previously introduced in Section 2.2.2. This analysis evaluates the impact of PULSE and the DBBC on the weighted cumSEL values for all five NOAA-defined auditory groups. The weighting process reflects the frequency-dependent hearing sensitivity of each group, thereby enabling more accurate assessment of potential auditory impacts.

The results are shown in two steps: first, the frequency weighting is applied to scenarios without the DBBC (Figures D.1–D.5), followed by scenarios that include the DBBC (Figures D.6–D.10). The cumulative results per group are summarised in Table 5.7.

Scenario	No PULSE & No DBBC [dB re 1 µPa²s]	PULSE & No DBBC [dB re 1 µPa²s]	No PULSE & DBBC [dB re 1 µPa²s]	PULSE & DBBC [dB re 1 µPa²s]
Unweighted	213.53	212.35	204.73	194.17
Low-frequency (LF) cetaceans	209.68	202.08	199.50	194.17
Mid-frequency (MF) cetaceans	155.24	143.60	144.36	134.49
High-frequency (HF) cetaceans	142.77	130.63	131.69	120.92
Phocid pinnipeds	178.18	165.84	166.86	155.46
Otariid pinnipeds	191.61	183.42	181.29	175.42

Table 5.7: Frequency-weighted cumSEL values (in dB re 1 µPa²s) for the five NOAA hearing groups, modelled at 750 m from the monopile and 2 m above the seabed. The unweighted cumSEL is also included for reference.

Weighted cumulative noise (PULSE)

Figures D.1–D.5 present the frequency-weighted cumSEL spectra that compare baseline and 50% PULSE conditions for each marine-mammal hearing group. To illustrate the interpretation in the main text, the low-frequency cetacean spectrum (Figure 5.15) is reproduced here; the corresponding plots for mid-frequency cetaceans, high-frequency cetaceans, phocid pinnipeds, and otariid pinnipeds are provided in Appendix D.1 (Figures D.2–D.5).

The results confirm that PULSE lowers the cumulative noise levels across all hearing groups. The reductions are most pronounced for mid- and high-frequency cetaceans and phocid pinnipeds (between 11-13 dB), as the elongated impact pulse shifts energy away from their sensitive frequency bands. This effect is consistent with the known spectral redistribution caused by pulse elongation, which concentrates energy at lower frequencies while attenuating high-frequency content [31].

The reduction in frequency-weighted cumSEL due to PULSE is greater than the reduction in unweighted cumSEL, particularly for mid- and high-frequency hearing groups. This indicates that the spectral shift caused by impulse elongation removes energy from the frequency bands most relevant to these species. For low-frequency cetaceans, the weighted cumSEL reduction (7.6 dB) is still larger than the unweighted reduction (1.18 dB), suggesting that PULSE is more effective when assessed through auditory-weighted metrics than when using broadband levels alone.

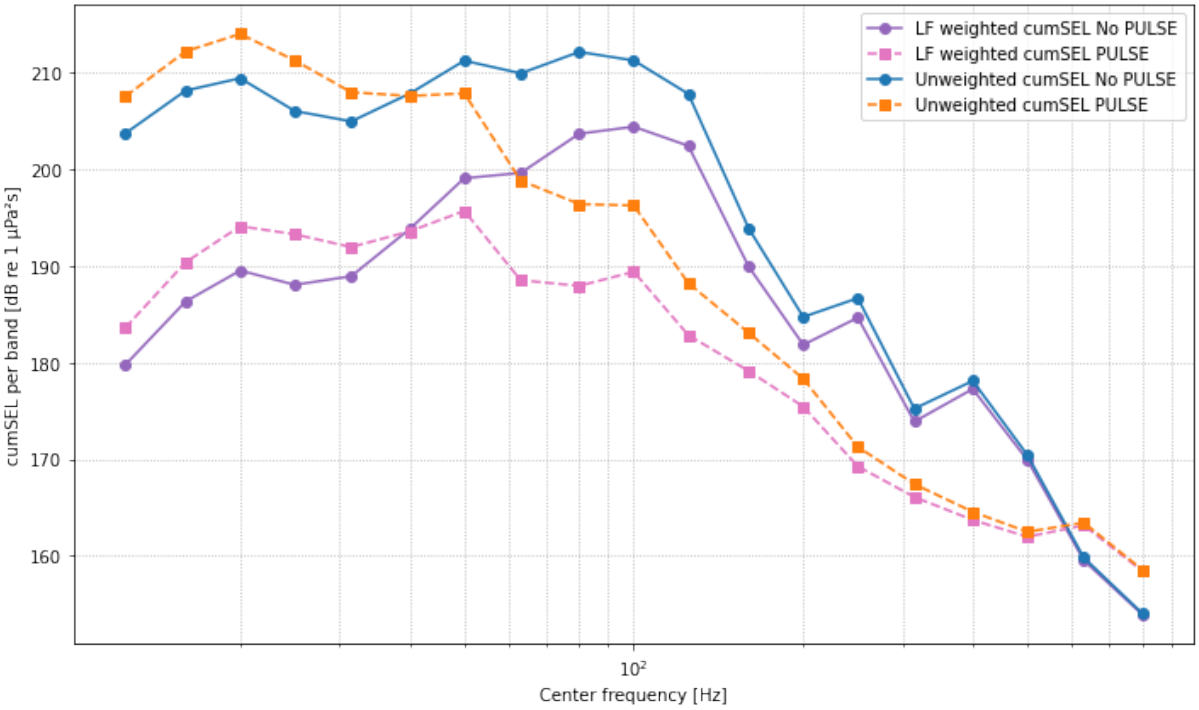

Figure 5.15: Frequency-weighted cumSEL spectrum for low-frequency cetaceans.[3]

Weighted cumulative noise (PULSE + DBBC)

Figure D.6–D.10 presents the frequency-weighted cumSEL for the scenarios that include a DBBC. To illustrate the interpretation in the main text, the low-frequency cetacean spectrum (Figure 5.16) is reproduced here; the corresponding plots for mid-frequency cetaceans, high-frequency cetaceans, phocid pinnipeds, and otariid pinnipeds are provided in Appendix D.2 (Figures D.6–D.10).

The data show that the DBBC provides further reduction in all hearing groups compared to PULSE alone. The effectiveness of the DBBC remains highest in the mid- to high-frequency range, consistent with theoretical and empirical findings that bubble curtains primarily attenuate frequencies above 200 Hz due to scattering and resonance effects [90, 91].

Although PULSE increases energy in the lower frequencies, the weighted cumSEL for LF cetaceans is still lower when both PULSE and the DBBC are used together. This suggests that their combined application does not lead to adverse interactions in the frequency domain.

[3]Modelled at 750 m from the monopile and 2 m above the seabed.

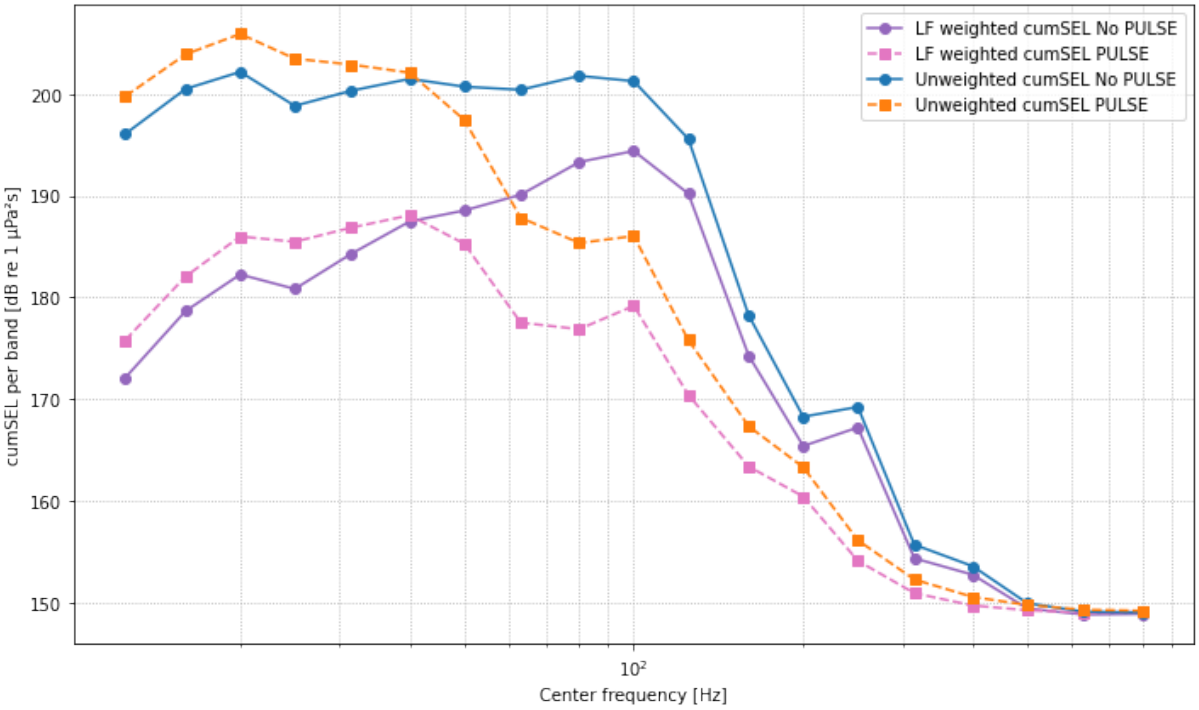

Figure 5.16: Frequency-weighted cumSEL spectrum for low-frequency cetaceans comparing the scenarios with and without DBBC.[3]

Frequency weighting highlights the variation in mitigation effectiveness across species. PULSE is most beneficial for species sensitive to mid- and high-frequency sound (MF, HF cetaceans and pinnipeds). The DBBC further enhances these reductions and compensates for the limited effectiveness of PULSE in the low-frequency range. For LF cetaceans, the weighted cumSEL remains above the threshold value, as specified in Table 2.4, indicating a potential need for additional mitigation beyond PULSE and DBBC.

5.5 Sensitivity to clay-sand stratigraphy

To evaluate how stratigraphic contrasts affect both installation performance and noise emission, the workflow for the pulse elongation scenarios was repeated for a two-layer clay-over-sand profile. The subsequent subsections report the drivability results, single-strike SELs, cumulative SELs, and frequency-weighted cumulative SELs, and they benchmark each outcome against the sand-only baseline.

5.5.1 Drivability analysis

The drivability assessment was repeated for the mixed clay-sand profile introduced in Section 4.2.1. Figure 5.17) and Table 5.8 summarise the outcome for the baseline hammer setting and the 50% PULSE configuration. As for the all-sand profile, the 100% PULSE proved technically infeasible: DYNPAC predicts refusal before the pile reaches the target penetration depth. In contrast, a 50% PULSE remains technically feasible, but the associated increase in required blow count, and thus the impact on drivability performance, is markedly smaller than in the sand-only case. The elongated impulse now requires 2400 blows, approximately 23% more than the 1946 blows of the baseline, whereas the same pulse setting demanded a 49% increase in the sand profile. The reduction in penalty is attributed to the soft clay cap, which lowers the static

[3]Modelled at 750 m from the monopile and 2 m above the seabed.

tip resistance during the early stages of driving; consequently, less additional hammer energy is needed to compensate for the longer, lower-amplitude impacts. Overall, the clay-sand sensitivity run shows that the variation in the magnitude of the blow-count is strongly site dependent.

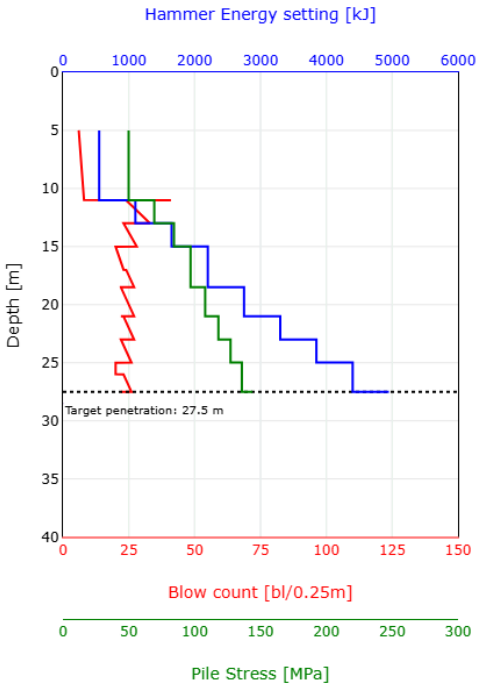

(a) No pulse (baseline)

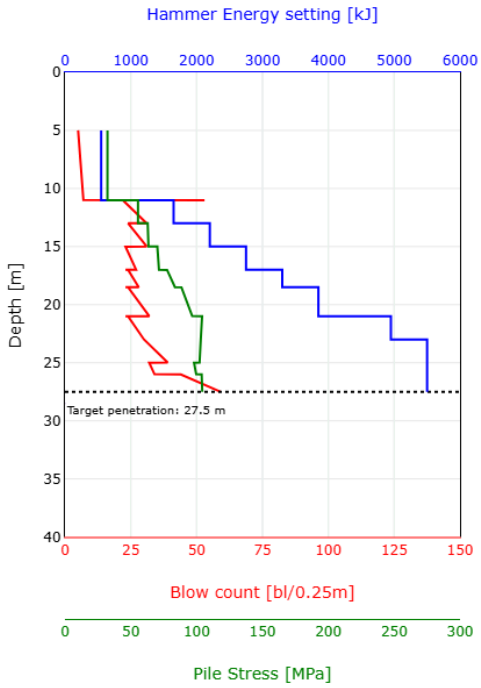

(b) Pulse 50%

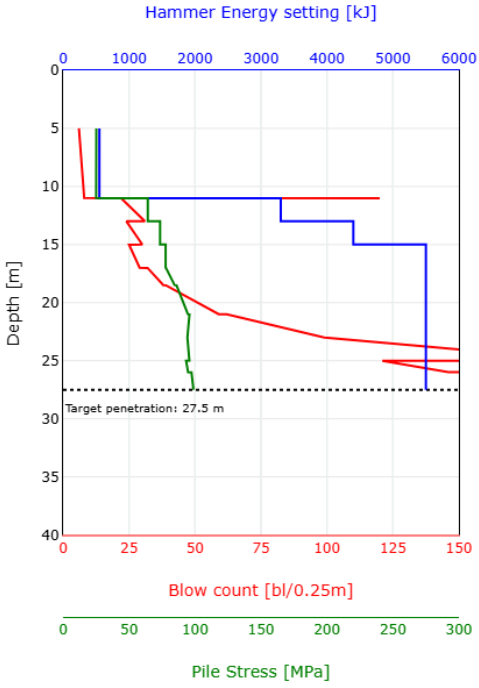

(c) Pulse 100%

Figure 5.17: Drivability curves for different pulse configurations: (A) No pulse (baseline), (B) Pulse 50%, and (C) Pulse 100% in a clay-sand soil configuration.

Scenario	Number of blows	Δ blows vs. full-sand	Duration (min)
No PULSE	1946	−326	74.0
50 % PULSE	2400	−986	94.2

Table 5.8: Blow count and total driving time to reach 27.5 m penetration for the clay-sand profile.

5.5.2 Single strike and cumulative sound levels

To quantify the combined influence of hammer setting and soil composition, single-strike Sound Exposure Levels (SEL) and cumulative Sound Exposure Levels (cumSEL) are evaluated for four cases: baseline hammer in the medium dense over very dense sand profile (case 2), 50% PULSE in that same sand profile (case 4), baseline hammer in the soft clay over very dense sand profile, and 50% PULSE in the clay-sand profile.

For each case the acoustically most energetic blow, typically recorded near the final penetration stage, is selected for the SEL comparison. Figure 5.18 plots the radial decay of SEL with distance from the monopile, enabling direct comparison of both the PULSE effect and the stratigraphic effect.

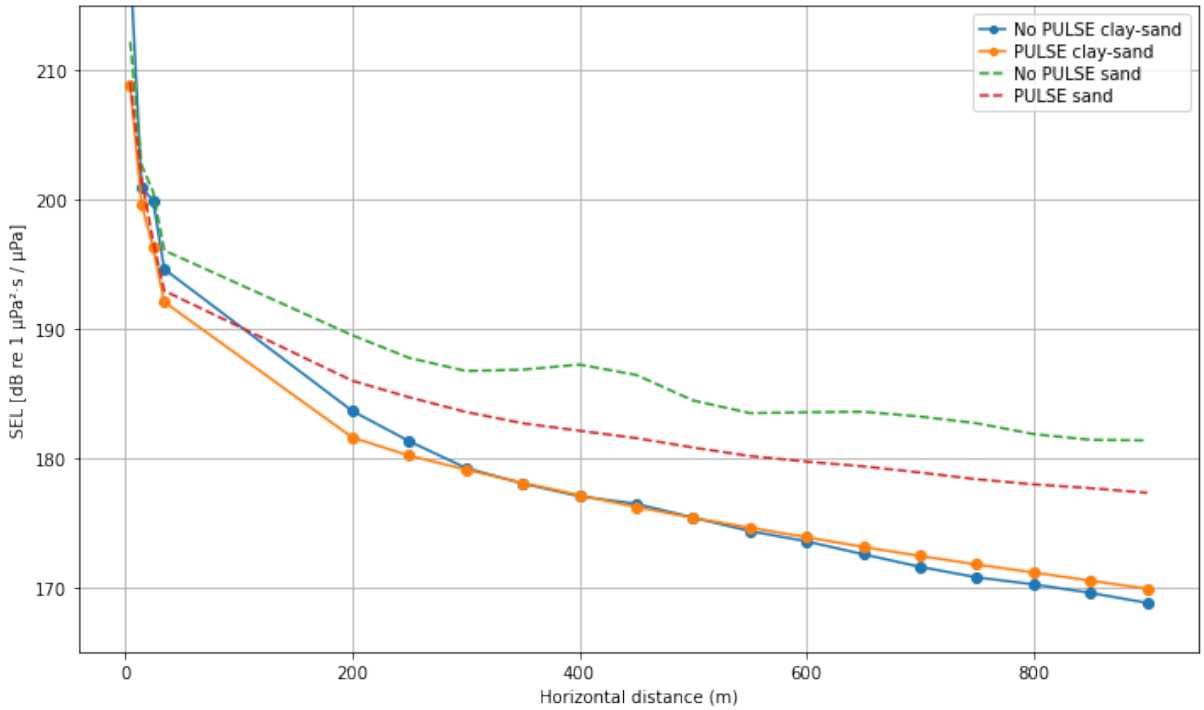

Figure 5.18: Comparison of modelled maximum SEL values as a function of horizontal distance from the monopile for two scenarios: no PULSE and PULSE (clay-sand profile, penetration depth = 27.5 m, receiver positioned 2 m above seabed)

The cumulative SEL as a function of distance is plotted in Figure 5.19, which compares the baseline and 50% PULSE configurations for the clay-sand profile.

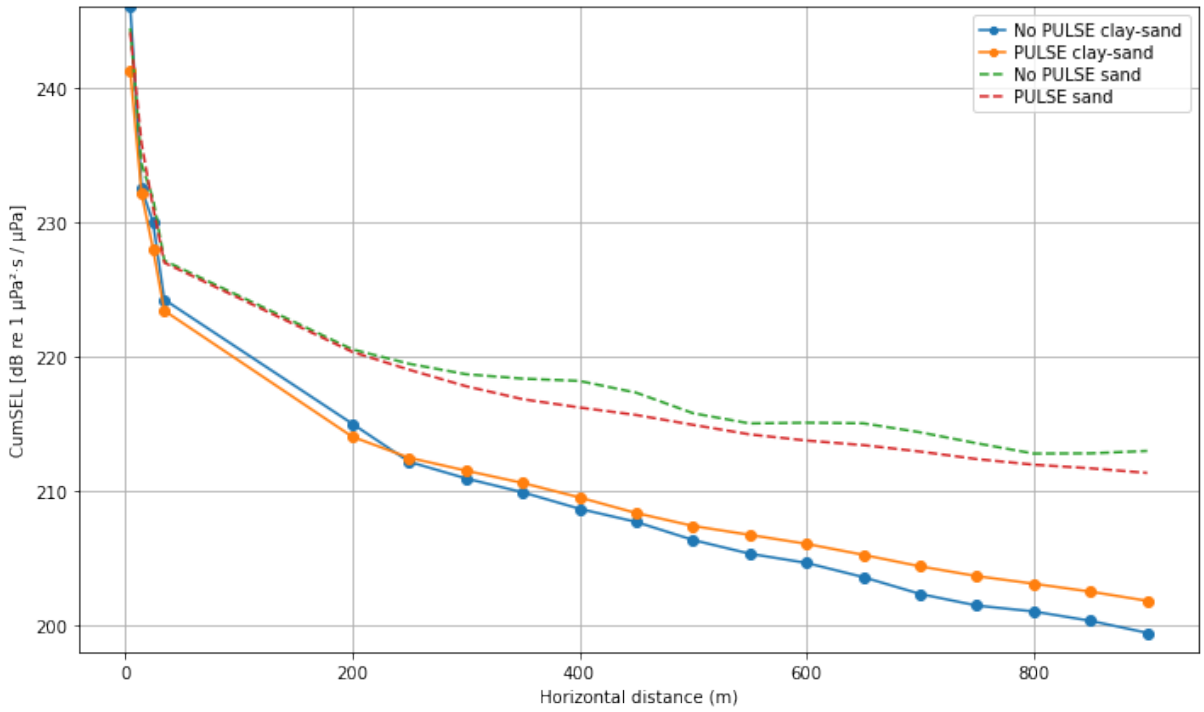

Figure 5.19: Comparison of the modelled cumulative SEL values for two scenarios: no PULSE and PULSE, 2 m above the seabed. Comparison between clay-sand profile and full sand profile.

Table 5.9 compares the single-strike SEL and cumulative SEL (cumSEL) at a range of 750 m for the clay-sand stratigraphy, contrasting the 50% PULSE configuration with the no-PULSE baseline. The right-hand column lists the differences between the two cases. For this soil profile, the elongated pulse increases the single-strike SEL by roughly 1 dB and, because it also requires more blows to reach full penetration, leads to a correspondingly higher cumSEL (+2.19 dB) than the baseline.

It is noteworthy that the clay-sand profile shows a net increase in single-strike SEL for the 50% PULSE case at 750 m from the source, even though a modest reduction ($\approx$ 2 dB) is observed in the immediate vicinity of the pile. The benefit diminishes with range, and beyond roughly 300 m the trend reverses, yielding slightly higher SEL than the baseline. A plausible explanation is that the elongated pulse redistributes energy toward lower frequencies, which undergo less geometric and viscous attenuation in the water column and are partly re-radiated by the stiff underlying sand. In the near field, the lower peak force still dominates and produces a small reduction, but at mid-range the reduced high-frequency loss and constructive interference at the clay-sand interface offset, and ultimately outweigh, the initial gain.

This adverse behaviour only emerges once the pile tip has penetrated well into the lower sand layer (penetrations $\gtrsim$ 18 m). For shallower stages (5-13 m), where the clay cap still separates the pile wall from the sand substratum, the 50% PULSE configuration does reduce single-strike SEL relative to the baseline, see Appendix E.3 for reference. In this depth interval the impedance contrast between water and clay remains the dominant control on radiation, reflections at the clay-sand boundary are weaker, and the low-frequency shift produced by PULSE therefore translates into a net SEL decrease at all analysed ranges.

By contrast, the all-sand profile continues to exhibit a small decrease in single-strike SEL under identical PULSE conditions at every penetration depth. Because the impedance contrast between the two sand layers is minor, reflections at the internal interface are weak and do not reinforce the

low-frequency content re-radiated into the water column. Consequently, the overall single-strike SEL remains lower for PULSE in the sand-sand case.

Scenario	**SEL** [dB re 1 µPa^{2}s]	**SEL variation** [dB]	**cumSEL** [dB re 1 µPa^{2}s]	**cumSEL variation** [dB]
No PULSE (baseline)	170.77	[-]	201.46	[-]
PULSE (50%)	171.77	+1.00	203.65	+2.19

Table 5.9: Modelled SEL and cumSEL values at 750 m distance from the monopile, 2 m above the seabed. Reductions are expressed relative to the no-PULSE baseline scenario.

5.5.3 Spectral distribution

To better understand the spectral effects of PULSE in the clay-sand stratigraphy, both the SEL and cumSEL values are analyzed in the frequency domain. Figures 5.20 and 5.21 show the respective 1/3-octave band levels for SEL and cumSEL at 750 m.

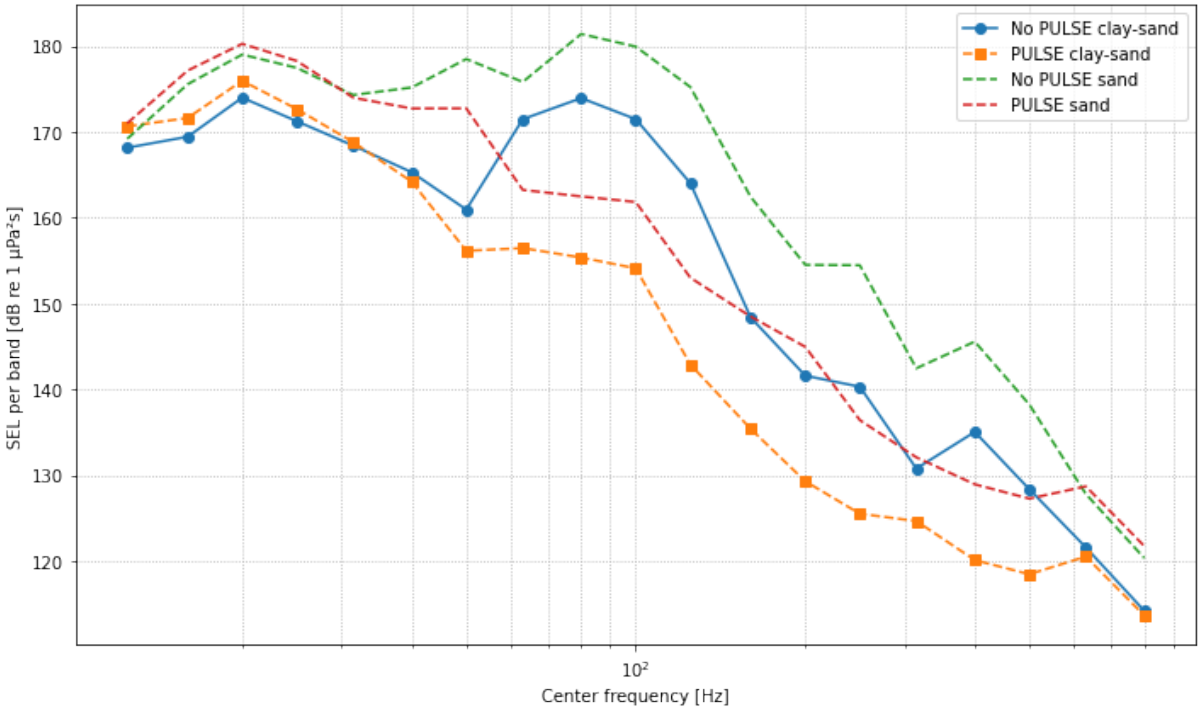

Figure 5.20: 1/3-octave band SEL at 750 m from the monopile. Comparison between PULSE and no PULSE configurations. Comparison between clay-sand profile and full sand profile.

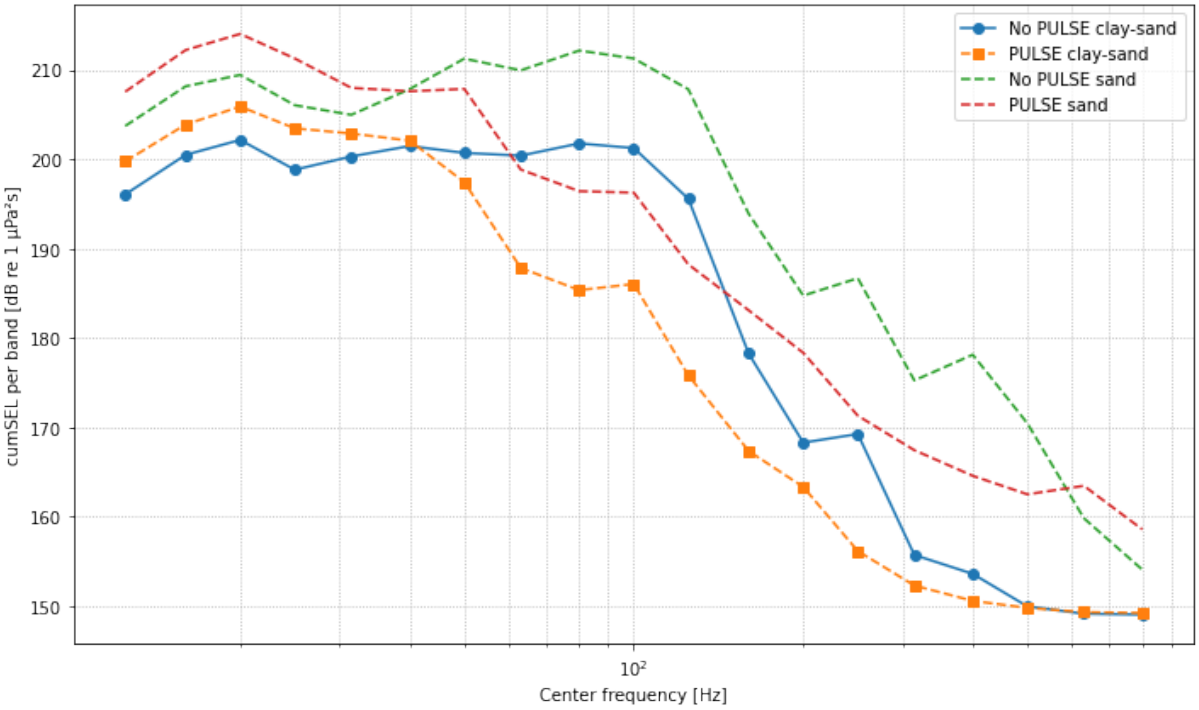

Figure 5.21: 1/3-octave band cumulative SEL at 750 m from the monopile. Comparison between PULSE and no PULSE configurations. Comparison between clay-sand profile and full sand profile.

The clay-sand simulations exhibit the same qualitative behaviour as the all-sand case: pulse elongation suppresses high-frequency content and redistributes acoustic energy into the lower bands. Both the single-strike SEL and the cumulative SEL curves display this spectral shift, confirming that the elongated time history again trades peak amplitude for longer, low-frequency radiation.

A minor deviation appears around 70 Hz in the single-strike spectra: the no-PULSE curve shows a local trough that is absent in the sand-sand results. This dip is likely a site-specific interference effect, destructive superposition of direct and clay-sand interface-reflected waves, which selectively attenuates energy in that narrow band. Aside from this feature, the relative PULSE-vs-baseline trends remain consistent with those observed for the all sand profile, supporting the conclusion that impulse elongation primarily alters the spectrum rather than its overall shape, even when a pronounced impedance contrast is present.

5.5.4 Frequency-weighted noise impact

Figure E.1–E.5 presents the frequency-weighted cumSEL for the scenarios in the clay-sand stratigraphy. To illustrate the interpretation in the main text, the low-frequency cetacean spectrum (Figure 5.22) is reproduced here; the corresponding plots for mid-frequency cetaceans, high-frequency cetaceans, phocid pinnipeds, and otariid pinnipeds are provided in Appendix E.4 (Figures E.1–E.5).

The cumulative results per group for the clay-sand stratigraphy are summarised in Table 5.10.

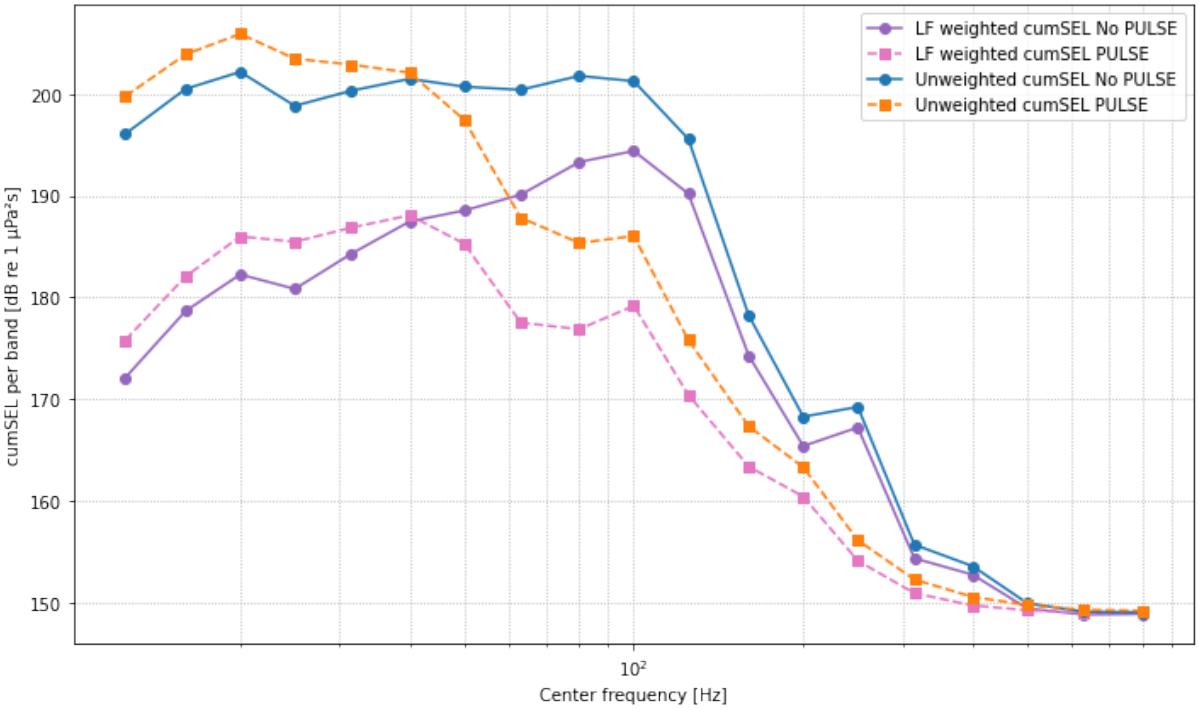

Figure 5.22: Frequency-weighted cumSEL spectrum for low-frequency cetaceans comparing the scenarios with and without PULSE in a clay-sand stratigraphy.[3]

Scenario	**No PULSE & No DBBC** [dB re 1 µPa²s]	**PULSE & No DBBC** [dB re 1 µPa²s]
Unweighted	201.46	203.65
Low-frequency (LF) cetaceans	199.50	194.17
Mid-frequency (MF) cetaceans	144.36	134.49
High-frequency (HF) cetaceans	131.69	120.92
Phocid pinnipeds	166.86	155.46
Otariid pinnipeds	181.29	175.42

Table 5.10: Frequency-weighted cumSEL values (in dB re 1 µPa²s) for the five NOAA hearing groups, modelled at 750 m from the monopile and 2 m above the seabed. The unweighted cumSEL is also included for reference.

For the clay–sand stratigraphy, a 50 % pulse elongation still yields clear ecological benefits once species-specific weighting is applied. Although the unweighted cumulative level rises by ≈ 2 dB – because the softer impact requires 23 % more blows and partly shifts energy into low-loss, low-frequency bands – the weighted cumSEL decreases for every NOAA hearing group.

Reductions range from ≈ 5 dB for low-frequency cetaceans to ≈ 11 dB for mid- and high-frequency cetaceans, with pinniped groups lying in between (Table 5.10). The gains are 1–2 dB smaller than in the all-sand case, reflecting additional low-frequency re-radiation at the clay-sand interface, yet the overall pattern remains: pulse shaping is acoustically neutral in broadband terms but markedly advantageous when judged with biologically relevant, frequency-weighted metrics.

6 | Discussion, Conclusions, and Recommendations

6.1 Discussion and Conclusions

The aim of this study was to investigate how variations in operational parameters affect the cumulative underwater noise generated during offshore impact pile driving. Pile installation for offshore wind farms produces high-intensity impulsive sound, posing a risk to marine life through behavioral disturbances, physical injury, or hearing damage. To mitigate such impacts and comply with regulatory thresholds, various technical solutions are employed, including impulse elongation (PULSE) and Double Big Bubble Curtains (DBBCs). Additionally, operational strategies like varying the target blow count during installation offer potential for noise control.

To quantify the influence of these interventions on cumulative acoustic impact, this study combined a dynamic drivability model (DYNPAC) with a semi-analytical underwater acoustics model (SILENCE). The findings underscore that the perceived effectiveness of mitigation strategies is fundamentally influenced by the choice of acoustic metric, particularly the application of species-specific frequency weighting. This chapter reflects on the key findings, elucidates their underlying mechanisms, and discusses model limitations and sources of uncertainty.

6.1.1 Operational Parameter Influence on Cumulative Sound Exposure Level (cumSEL)

Based on the simulations, the influence of operational settings on cumSEL can be explained by four primary mechanisms:

Target Blow Count Policy

Adjusting the target blow count had a negligible effect on both broadband and frequency-weighted cumSEL (varying by less than 0.1 dB across configurations). While reducing the blow count led to shorter installation durations requiring higher hammer energy per blow, and vice versa, the total hammer energy needed to achieve full penetration remained constant. Consequently, the logarithmic summation of sound exposure over all strikes resulted in comparable cumSEL values, irrespective of how the energy was delivered. Spectral analysis further confirmed minimal differences in energy distribution across the frequency range. This indicates that modifying the target blow count alone, without altering total hammer energy, is ineffective for significantly modifying underwater noise profiles.

Impulse Elongation (PULSE)

Impulse elongation (e.g., 50% PULSE configuration) significantly alters the pile driving and radiated underwater sound. Drivability analysis revealed a substantial increase (up to 49%) in

the number of required hammer blows, particularly during final penetration where reduced peak force was insufficient against rising soil resistance. The 100% PULSE scenario even led to refusal, highlighting a technical limitation where diminished impact force compromises penetration capacity.

From an acoustic perspective, PULSE notably reduced per-strike Sound Exposure Level (SEL) (e.g., 4.34 dB reduction for 50% PULSE at maximum penetration) due to lowered peak amplitude and slower rise time. However, considering cumulative SEL (cumSEL) over the full installation process, the net reduction was modest (only 1.18 dB for unweighted cumSEL), as the increased number of strikes largely counteracted the per-strike benefit.

Crucially, PULSE shifts acoustic energy towards lower frequency bands (<40 Hz) due to its elongated time profile. This redistribution is acoustically relevant as low-frequency sound propagates further and affects sensitive species. When species-specific frequency weighting was applied, this spectral shift translated into substantial reductions in weighted cumSEL (8-13 dB) for mid- and high-frequency sensitive groups, illustrating the strong metric-dependence of perceived effectiveness. Conversely, for low-frequency cetaceans, the benefit was more modest (7.6 dB reduction), but still significant, as their hearing overlaps with the slightly increased low-frequency energy. This demonstrates that pulse shaping is indeed effective when assessed through auditory-weighted criteria. Overall, while PULSE reduces per-strike noise and redistributes energy favorably, its drivability penalty and limited impact on unweighted cumSEL suggest its standalone utility for long-term acoustic impact reduction, when unweighted metrics are the sole concern, is limited. This underscores the need to balance acoustic mitigation with installation efficiency and consider combining pulse shaping with additional measures.

Double Big Bubble Curtain (DBBC) and its Interaction with PULSE

The combined application of PULSE and a Double Big Bubble Curtain (DBBC) proved complementary, operating through distinct physical mechanisms to reduce underwater noise. The DBBC consistently lowered Sound Exposure Levels (SEL and cumSEL), particularly in the mid- to high-frequency range where bubble resonance and scattering are most pronounced. Spectral analysis confirmed its broadband attenuation, suppressing energy across most frequencies above 100 Hz.

While a DBBC alone significantly reduced SEL, adding PULSE yielded further, albeit modest, additional benefits. For instance, at 750 meters, the combined PULSE+DBBC case resulted in only a 0.58 dB further reduction in unweighted cumSEL compared to the DBBC-only configuration. This suggests that once broadband attenuation is provided by the bubble curtain, the incremental gains from modifying the pulse shape become marginal. Importantly, no adverse spectral interactions were observed between PULSE and the DBBC; on the contrary, the combined strategy produced the lowest cumulative levels for all hearing groups, including low-frequency cetaceans.

Notably, the PULSE+DBBC combination also resulted in a small but measurable reduction of low-frequency energy (<40 Hz), contrary to common assumptions about bubble curtain performance. This unexpected attenuation might be attributed to enhanced scattering from the dual-ring DBBC's combined acoustic thickness, shallow-water cutoff effects, or the numerical low-frequency cutoff in the SILENCE model. However, conclusions regarding sub-100 Hz performance should be interpreted cautiously due to potential model artifacts.

Despite the broad effectiveness of both methods, weighted cumSEL values for low-frequency cetaceans remained elevated compared to other species. This suggests that even combined strategies might be insufficient for this group, necessitating additional measures like using a Triple Big

Bubble Curtain (TBBC), longer ramp-up periods, or exclusion zones to ensure regulatory compliance and species protection.

Stratigraphic Control

The sensitivity study involving a clay-sand stratigraphy revealed that soil layering significantly influences mitigation effectiveness. At shallow embedment (5-13 m), the 50% PULSE configuration still achieved approximately 2-3 dB single-strike SEL reduction. However, at full penetration (25-27.5 m), the same configuration unexpectedly increased SEL by approximately 1 dB due to low-frequency reflections at the clay-sand interface. Consequently, both single-strike SEL and blow count rose, resulting in cumSEL values approximately 2 dB higher for medium PULSE in comparison to no PULSE. This underscores the critical importance of stratigraphy-matched mitigation design.

While peak pressure (L_{peak}) still showed a slight decrease in this layered seabed, cumulative metrics increased. This demonstrates that in such layered seabeds, reflections at soil interfaces can offset, or even reverse, the acoustic benefits of impulse elongation. Site-specific soil characterisation is therefore essential before adopting impulse shaping as a noise mitigation measure. For frequency-weighted impact, weighted cumSEL still decreased by 5-11 dB with PULSE, further reaffirming that metric choice governs the "success" of any measure.

6.1.2 Impact of Acoustic Metrics on Perceived Effectiveness

This study consistently highlights that the choice of acoustic metric fundamentally influences the perceived effectiveness of mitigation strategies. While unweighted cumSEL often showed only minor reductions from impulse elongation, frequency-weighted cumSEL values revealed substantially larger reductions, particularly for species with mid- or high-frequency hearing sensitivity. This discrepancy underscores that underwater sound is not a neutral physical measure; its biological significance depends entirely on how it is evaluated and by the specific receiver.

Regulatory frameworks, such as those applied by NOAA, embed species-specific assumptions through frequency weighting. These weightings prioritize biologically relevant frequencies and suppress others, effectively redefining which parts of the acoustic spectrum are considered impactful. Consequently, a mitigation strategy's perceived effectiveness may hinge less on its absolute physical noise reduction and more on its alignment with regulatory metrics. This implies that any comparison of mitigation outcomes – between techniques, projects, or countries – must always be interpreted in light of the specific acoustic metrics and weighting criteria applied. What is considered "less noisy" for a porpoise may not be "less noisy" for a baleen whale, and compliance under one framework may be insufficient under another.

Thus, operational settings can materially reduce underwater noise, but their apparent efficacy depends on the regulatory metric applied; unweighted and weighted cumSEL may rank the same measure differently.

These conclusions are drawn chiefly from a medium-dense over very-dense sand profile and one soft clay-over-sand sensitivity run. Because impedance, damping, and layering govern both drivability and acoustics, the numerical values cannot be generalized to other soils (e.g. stiff clays, silts) or strongly stratified sites without further analysis. Extending the workflow to a wider set of soil conditions is required before universal design rules can be issued.

6.2 Limitations of the study

Several model limitations and assumptions affect the precision and generalisability of the results. These must be considered when interpreting the findings of this study.

6.2.1 DYNPAC model limitations

Limitation	Anticipated influence	Physical explanation
Fixed target blow count	Limited impact on cumulative predictions; may bias local blow count curves.	The energy per blow is recomputed in DYNPAC to satisfy a single target count value over the full penetration. In field practice the target is adjusted with depth, but cumulative blow energy, which controls SEL, is preserved; only the depth-by-depth distribution may deviate.
One-dimensional axial rod assumption	Low influence on overall drivability trends for the vertical pile analysed; potentially larger for tilted or eccentric impacts.	The pile is modelled as a vertical, concentric elastic rod; bending modes are therefore secondary. Exclusion of flexural waves does not alter the axial energy budget that drives noise radiation.
Simplified strain-rate damping	Low–moderate uncertainty ($< 2\,\mathrm{dB}$) in the resulting acoustic L_{peak} when the DYNPAC–derived force-time signal is used as input; $< 1\,\mathrm{dB}$ effect on cumSEL.	Strain-rate effects are lumped into a single dashpot in DYNPAC, shifting the peak force by only a few percent; such small changes in the hammer pulse translate to $\leq 2\,\mathrm{dB}$ variation in L_{peak} computed by SILENCE.
Limited applicability to very large diameters ($\geq 8\,\mathrm{m}$)	Negligible in this study (D $\approx 8.8\,\mathrm{m}$ shows no measurable dispersion); uncertainty increases for piles $\geq 10\,\mathrm{m}$.	Stress-wave dispersion and soil plugging become measurable only when $L/D \lesssim 6$; the analysed pile has $L/D \approx 8$.

Table 6.1: DYNPAC model limitations and their expected influence on the results.

6.2.2 SILENCE model limitations

Limitation	Anticipated influence	Physical explanation
Two-layer soil profile[4]	Adds ∼1-5 dB uncertainty in SEL at typical monitoring ranges.	Real seabeds are stratified; the uppermost layer dominates noise generation. Neglecting deeper strata mainly removes weak reverberations and low-frequency modes, usually altering far-field SEL by a few dB [31].
Uniform monopile geometry	Broadband difference expected to be <1 dB; high-order modes may shift slightly.	The dominant acoustic response is set by overall diameter; minor tapers or stiffeners merely perturb higher modes.
Prescribed hammer force (no hammer-pile interaction)	Differences are typically $<1-2$ dB at 750 m, provided that the input force curve accurately represents the total energy.	The hammer is modelled as a prescribed force input, without capturing feedback dynamics or structural response of the pile.
Free-free boundary assumption	Small variations in predicted noise due to deviations from actual conditions.	In reality, boundary conditions lie between clamped-free and free-free conditions, affecting vibration modes and resulting sound radiation.
Rigid soil bottom (finite layer depth)	Negligible (<1 dB) if the rigid base is placed many wavelengths below the pile toe.	Reflections from a deep rigid interface arrive late and are highly attenuated, contributing little to the early-time acoustic field.
Empty monopile interior	Effect on exterior SEL is expected to be <1 dB.	The steel shell dominates vibration; whether the cavity contains air, water or grout only marginally alters high-frequency radial modes, which couple weakly to the water column.
Horizontal uniformity	Exact impact site-specific but usually $\leq$1-2 dB in averaged far-field levels.	Axisymmetric models ignore sloping bathymetry or lateral soil contrasts. Such asymmetries mainly cause directional variations rather than large changes in worst-case or averaged SPL.
Low-frequency cut-off (∼40 Hz)	Underestimates broadband SEL by $\lesssim$1-2 dB.	Pile-driving energy below 40 Hz is small; omitting it removes long-wavelength modes that contribute little to far-field pressure except very near the pile.

Table 6.2: SILENCE model limitations and their expected influence on offshore pile-driving noise predictions (sources as indicated).

[4]The full (non-student) SILENCE version can handle multiple soil layers; the two-layer restriction applies only to the software edition used in this study.

6.2.3 Study-wide limitations

Limitation	Anticipated influence	Physical explanation
No environmental dynamics	Low for relative trends; moderate for absolute levels.	Currents $\leq 0.5\ \mathrm{m\,s^{-1}}$ modify transmission loss by < 1 dB at 750 m. Temperature stratification is minor in the shallow German Bight.
Limited validation (unmitigated only)	Moderate.	Agreement within ± 2 dB for the baseline increases confidence in trend predictions; absolute levels for PULSE or DBBC remain unverified.
Parameter sensitivity (CPT-based soil set)	High for absolute SPL; low for inter-scenario ranking.	Wave-speed perturbations of $\pm 10\%$ cause approximately 3 dB shift in SEL, yet the ranking of scenarios is robust.
Single soil profile and monopile	Moderate–high for external generalisation; low within North-Sea sands; the clay-sand sensitivity test (App. E) already shows different results, illustrating this limitation.	Conclusions hold for medium-dense North-Sea sands; clay- or silt-rich or strongly layered sites may behave differently.
Single DBBC configuration	Low for qualitative conclusions; unknown for alternative designs.	Higher gas flux or different ring spacing could enhance low-frequency attenuation; current results therefore represent a lower-bound estimate.

Table 6.3: Study-wide constraints and their estimated influence on the results.

6.3 Recommendations

The study's findings translate into several immediate actions for researchers, practitioners, and regulators. Because each stakeholder group influences underwater-noise management in a different way – through fundamental research, project execution, or policy design – the recommendations are organised in three parts. First, the academic section highlights modelling and validation work that would most improve predictive accuracy. Second, the industry section focuses on practical steps developers and contractors can take when planning or executing offshore piling campaigns. Finally, the regulatory section outlines measures that authorities could adopt to ensure that noise limits remain both ecologically relevant and technically achievable.

6.3.1 Academic perspective

1. **Refine stratigraphic representation.** Two-layer seabed schemes unavoidably smooth out the multiple impedance interfaces that a realistic sediment column presents; literature indicates this simplification can shift cumulative SEL by several decibels. Subsequent work should apply the full multi-layer capability of SILENCE.

2. **Validate combined mitigation strategies in field conditions.** Empirical data for installations using combined PULSE and DBBC mitigation are currently lacking. Instrumented field trials would enable validation and benchmarking of models, particularly focusing on frequencies below 100 Hz, where numerical limitations and shallow-water phenomena introduce uncertainties.

3. **Investigate frequency-weighted effects of monopile dimensions.** Future research should explicitly explore how increased monopile diameter affects the spectral distribution of radiated sound energy. Larger piles produce a spectral shift toward lower frequencies, potentially influencing cumulative SEL outcomes differently depending on species-specific hearing sensitivity. This spectral shift might lead to reduced weighted cumSEL for marine fauna, since frequency weighting mainly reduces low-frequency noise. This nuanced effect warrants further investigation to inform regulatory assessments and optimise monopile designs in offshore wind installations.

4. **Broaden soil condition scenarios.** Investigate diverse soil profiles, including layered sediments, and heterogeneous mixtures, to better understand the variability of acoustic emissions and drivability responses across a wider range of geotechnical conditions.

5. **Explore alternative DBBC configurations.** Investigations into variations such as increased gas flux rates, larger curtain radii, or modified bubble spacing configurations could improve noise attenuation effectiveness.

6. **Include environmental dynamics.** Assess the effects of currents, temperature gradients, and other dynamic environmental parameters on acoustic propagation and bubble curtain performance, enhancing the realism and predictive accuracy of acoustic models.

7. **Evaluate different monopile geometries.** Given that changes in monopile diameter and wall thickness can shift acoustic energy into different frequency bands, systematic studies exploring various monopile configurations and their acoustic consequences would provide valuable insights, particularly for species-specific mitigation.

8. **Empirical validation of model assumptions.** Field measurements are critical for validating assumptions inherent in drivability and acoustic models such as DYNPAC and SILENCE. Empirical studies comparing real-world installation scenarios with model predictions should be prioritised to improve confidence in simulation-based assessments.

6.3.2 Industry perspective

1. **Select mitigation measures based on local regulatory metrics.** Before selecting noise mitigation strategies, developers and contractors should carefully consider the acoustic metrics enforced by local regulations (L_{peak}, SEL, cumSEL, or frequency-weighted cumSEL). The effectiveness of mitigation measures, such as impulse elongation (PULSE), depends significantly on the metric used for compliance. For instance, PULSE shows limited reduction in unweighted cumSEL but substantial benefits when frequency-weighted metrics are applied. Aligning mitigation strategies closely with the specific regulatory context ensures optimal ecological benefit and regulatory compliance.

2. **Update geotechnical investigation practices.** Industry site surveys should routinely include high-resolution seismic CPTs or direct measurements of P-wave and S-wave velocities. Accurate characterisation of these parameters will significantly enhance the reliability of acoustic predictions and aid in optimising mitigation strategies.

3. **Develop low-frequency mitigation techniques.** Current mitigation measures predominantly attenuate mid- to high-frequency noise. Innovative solutions specifically designed to mitigate low-frequency acoustic emissions are necessary to protect species sensitive to these frequencies effectively.

6.3.3 Regulatory perspective

1. In this study, even weighted cumSEL values remain too high for low-frequency marine mammals, despite the use of mitigation measures such as double bubble curtains and pulse elongation. Therefore, it is particularly important to complement acoustic mitigation with behavioural displacement strategies, such as soft-start procedures, allowing animals to detect and vacate the area before full-energy piling begins.

Bibliography

[1] Eurostat. *Share of Energy from Renewable Sources*. 2024. URL: https://ec.europa.eu/eurostat/databrowser/view/nrg_ind_ren/default/table?lang=en.

[2] Global Wind Energy Council (GWEC). *Global Wind Report 2024*. Global Wind Energy Council (GWEC), 2024. URL: https://gwec.net/.

[3] Soren Krohn. *Wind Energy Policy in Denmark: Status 2002*. 2002.

[4] S. Sanchez et al. "Foundations in Offshore Wind Farms: Evolution, Characteristics and Range of Use. Analysis of Main Dimensional Parameters in Monopile Foundations". In: *Journal of Marine Science and Engineering* 7.12 (2019). DOI: 10.3390/jmse7120441.

[5] Arthur N. Popper and Anthony D. Hawkins. *The Effects of Noise on Aquatic Life II*. Springer New York, 2016.

[6] B.L. Southall et al. "Marine Mammal Noise Exposure Criteria: Initial Scientific Recommendations". In: *Aquatic Mammals* 33.4 (2007), pp. 411–521.

[7] Christine Erbe. *International Regulation of Underwater Noise*. Tech. rep. Centre for Marine Science and Technology, Curtin University, 2013. URL: https://www.acoustics.asn.au/journal/2013/2013-1.pdf.

[8] National Marine Fisheries Service. *Draft Technical Memorandum Guidance: Acoustic Guidance for Fisheries, Version 3.0*. Tech. rep. NOAA Fisheries, 2024. URL: https://www.fisheries.noaa.gov/s3/2024-05/NMSFAcousticGuidance-DraftTECHMEMOGuidance-3.0-FEB-24-OPR1.pdf.

[9] Ronald A. Kastelein, Robin Gransier, and Leah Hoek. "Effects of repeated exposure to underwater noise on harbor porpoise hearing". In: *Journal of the Acoustical Society of America* 127.2 (2010), pp. 1139–1145. DOI: 10.1121/1.3290996.

[10] Danish Energy Agency. *Energistyrelsens Guidelines for Underwater Noise — Installation of Impact or Vibratory Driving Piles*. 2023. URL: https://ens.dk/sites/ens.dk/files/Vindmoller_hav/energistyrelsens_guidelines_for_underwater_noise_-_installation_of_impact_or_vibratory_driving_piles_2023.pdf.

[11] Yaxi Peng, Antonio Jarquin, and Apostolos Tsouvalas. "A multi-physics approach for modelling noise mitigation using an air-bubble curtain in impact pile driving". In: *Front. Mar. Sci.* 10 (2023), p. 1134776. DOI: 10.3389/fmars.2023.1134776. URL: https://www.frontiersin.org/articles/10.3389/fmars.2023.1134776.

[12] Y. Peng et al. "A fast computational model for near- and far-field noise prediction due to offshore pile driving". In: *The Journal of the Acoustical Society of America* 149.3 (Mar. 2021), pp. 1772–1790. ISSN: 0001-4966. DOI: 10.1121/10.0003752.

[13] Y. Peng et al. "Study of the Sound Escape with the Use of an Air Bubble Curtain in Offshore Pile Driving". In: *Journal of Marine Science and Engineering* 9.2 (Feb. 2021), p. 232. ISSN: 2077-1312. DOI: 10.3390/JMSE9020232. URL: https://www.mdpi.com/2077-1312/9/2/232.

[14] M. A. Bellmann et al. *Underwater Noise During the Impulse Pile-Driving Procedure: Influencing Factors on Pile-Driving Noise and Technical Possibilities to Comply with Noise Mitigation Values*. Tech. rep. Federal Maritime and Hydrographic Agency (BSH), 2020.

[15] Lawrence E. Kinsler et al. *Fundamentals of Acoustics*. 4th. New York: John Wiley & Sons, 2000.

[16] Herman Medwin and Clarence S. Clay. *Fundamentals of Underwater Sound*. 3rd. San Diego, CA: Academic Press, 1998.

[17] A. Thompson and B. Taylor. *Guide for the Use of the International System of Units*. National Institute of Standards and Technology, 2008.

[18] European Parliament. *Marine Strategy Framework Directive 2008/56/EC*. https://eur-lex.europa.eu/legal-content/EN/TXT/?uri=CELEX:32008L0056. Directive establishing a framework for community action in the field of marine environmental policy. 2008.

[19] Umwelt Bundesamt. *Underwater Noise*. https://www.bsh.de/EN/TOPICS/Offshore/Environmental_assessments/Underwater_sound/underwater_sound_node.html. 2020.

[20] Government of the Netherlands. *Waterwet (Water Act)*. https://wetten.overheid.nl/BWBR0025458/2024-01-01. 2024.

[21] Klaus Lucke and Marije Siemensma. *International Regulations on the Impact of Pile Driving Noise on Marine Mammals: A Literature Review*. Tech. rep. C044.13. The Hague, The Netherlands: IMARES Wageningen UR, 2013. URL: https://edepot.wur.nl/306911.

[22] NOAA Fisheries. *Offshore Wind Energy: Protecting Marine Life*. 2021. URL: https://www.fisheries.noaa.gov.

[23] BOEM. *Proposed Mitigations for Offshore Wind Energy Development*. 2020. URL: https://www.boem.gov.

[24] D. Wartzok and D. Ketten. "Marine Mammal Sensory Systems". In: *Biology of Marine Mammals*. Ed. by J.E. Reynolds and S.A. Rommel. Washington, DC: Smithsonian Institution Press, 1999, pp. 117–175.

[25] W.J. Richardson et al. *Marine Mammals and Noise*. San Diego, CA: Academic Press, 1995.

[26] W.W.L. Au and M.C. Hastings. *Principles of Marine Bioacoustics*. New York: Springer, 2008.

[27] National Marine Fisheries Service. *Technical Guidance for Assessing the Effects of Anthropogenic Sound on Marine Mammal Hearing: Underwater Acoustic Thresholds for Onset of Permanent and Temporary Threshold Shifts*. NOAA Technical Memorandum NMFS-OPR-55. Silver Spring, MD: NOAA, 2016.

[28] NOAA Fisheries. *ESA All Species Sound Threshold Summary*. 2023. URL: https://www.fisheries.noaa.gov/s3/2023-02/ESA%20all%20species%20threshold%20summary_508_OPR1.pdf.

[29] NOAA Fisheries. *Marine Mammal Protection Act Policies, Guidance, and Regulations*. 2020. URL: https://www.fisheries.noaa.gov/national/marine-mammal-protection/marine-mammal-protection-act-policies-guidance-and-regulations.

[30] G. Jonker. "Vibratory Pile Driving Hammers for Pile Installations and Soil Improvement Projects". In: *Proceedings of the Offshore Technology Conference*. Houston, Texas, Apr. 1987. DOI: 10.4043/5422-MS.

[31] A. Tsouvalas. "Underwater Noise Generated by Offshore Pile Driving". Promotor: A.V. Metrikine. Doctoral Thesis. Delft University of Technology, 2015. URL: http://resolver.tudelft.nl/uuid:55776f60-bbf4-443c-acb6-be1005559a98.

[32] Apostolos Tsouvalas. "Underwater Noise Emission Due to Offshore Pile Installation: A Review". In: *Energies* 13.12 (2020). Final published version, Article 3037. DOI: 10.3390/en13123037.

[33] Christian Kuhn et al. "Dynamic Measurements of Pile Deflections as a Source of Underwater Sound Emissions During Impact Driving of Offshore Pile Foundations". In: *Proceedings of the Conference on Offshore Pile Foundations*. 2014.

[34] Per G. Reinhall and Peter H. Dahl. "Underwater Mach Wave Radiation from Impact Pile Driving: Theory and Observation". In: *Journal of the Acoustical Society of America* 130.3 (2011), pp. 1209–1216. DOI: 10.1121/1.3614540.

[35] M. B. Fricke and R. Rolfes. "Towards a complete physically based forecast model for underwater noise related to impact pile driving". In: *The Journal of the Acoustical Society of America* 137 (2015). DOI: 10.1121/1.4908241.

[36] G. D. Meegan et al. "Nonlinear Stoneley and Scholte Waves". In: *The Journal of the Acoustical Society of America* 106 (1999). DOI: 10.1121/1.427920.

[37] D. Kong et al. "Analysis of influencing factors of lateral soil resistance distribution characteristics around monopile foundation for offshore wind power". In: *Applied Ocean Research* 97 (2020). DOI: 10.1016/j.apor.2020.102106. URL: https://doi.org/10.1016/j.apor.2020.102106.

[38] T. Lippert, M. A. Ainslie, and O. von Estorff. "Pile driving acoustics made simple: Damped cylindrical spreading model". In: *The Journal of the Acoustical Society of America* 143 (2018). DOI: 10.1121/1.5011158. URL: https://doi.org/10.1121/1.5011158.

[39] S. Schecklman et al. "A computational method to predict and study underwater noise due to pile driving". In: *The Journal of the Acoustical Society of America* 138 (2015). DOI: 10.1121/1.4922333. URL: https://doi.org/10.1121/1.4922333.

[40] Jonas von Pein et al. "Scaling laws for mitigated pile driving: Dependence of underwater noise on strike energy, pile diameter, ram weight, water depth, and mitigation system". In: *Journal of the Acoustical Society of America* 156.3 (Sept. 2024), pp. 2045–2059. DOI: 10.1121/10.0030302.

[41] BBC Future. *The Big Bubble Curtains Protecting Porpoises from Wind Farm Noise*. Nov. 2023. URL: https://www.bbc.com/future/article/20231106-the-big-bubble-curtains-protecting-porpoises-from-wind-farm-noise.

[42] Y. Peng, A. J. Laguna, and A. Tsouvalas. "A Multi-Physics Approach for Modelling Noise Mitigation Using an Air-Bubble Curtain in Impact Pile Driving". In: *Frontiers in Marine Science* 10 (Oct. 2023). ISSN: 2296-7745.

[43] Apostolos Tsouvalas and Andrei Metrikine. "Noise Reduction by the Application of an Air-Bubble Curtain in Offshore Pile Driving". In: *Journal of Sound and Vibration* 371 (June 2016), pp. 150–170. ISSN: 0022-460X. DOI: 10.1016/J.JSV.2016.02.025.

[44] Discovery of Sound in the Sea (DOSITS). *Bubble Curtain: Anthropogenic Sounds*. 2023. URL: https://dosits.org/galleries/audio-gallery/anthropogenic-sounds/bubble-curtain/.

[45] K. Brandt et al. *The Mitigation of Noise by a Big Bubble Curtain: A Study into the Optimization of a Big Bubble Curtain Configuration and a Contribution to Noise Mitigation Modelling*. Technical Report. 2022. URL: https://repository.tudelft.nl/islandora/object/uuid%5C%3A8710dd87-e05a-44d2-9d14-3052306108fa.

[46] S. Koschinski and K. Lüdemann. *Noise Mitigation for the Construction of Increasingly Large Offshore Wind Turbines: Technical Options for Complying with Noise Limits*. Report. 2020.

[47] IQIP. *PULSE®*. URL: https://iqip.com/products/pile-driving-equipment/piling-underlimited-stress-equipment/.

[48] IQIP. *PULSE Piling Brochure*. 2021. URL: https://windeurope.org/ElectricCity2021/files/exhibition/exhibitor-highlight/iqip/iqip-pulse-piling-brochure.pdf.

[49] Bureau of Ocean Energy Management (BOEM). *Empire Offshore Wind: Construction and Operations Plan, Appendix M-1: Underwater Acoustic Report*. Sept. 2023. URL: https://www.boem.gov/sites/default/files/documents/renewable-energy/Public_EOW_COP_App%20M-1_UW%20Acoustic_Sept%202023.pdf.

[50] M.A. Bellmann et al. "Underwater noise during percussive pile driving: Influencing factors on pile-driving noise and technical possibilities to comply with noise mitigation values". In: *Journal of Marine Science and Engineering* 9.8 (2021), p. 819. DOI: 10.3390/jmse9080819.

[51] *Inventory of measures to mitigate the emission and environmental impact of underwater noise*. OSPAR Publication 706/2016. OSPAR Commission, 2020. URL: https://tethys.pnnl.gov/sites/default/files/publications/OSPARCommission.pdf.

[52] A. MacGillivray. "Finite difference computational modeling of marine impact pile driving". In: *The Journal of the Acoustical Society of America* 136 (June 2015). DOI: 10.1121/1.4900002.

[53] H. Masoumi, G. Degrande, and G. Lombaert. "Prediction of free field vibrations due to pile driving using a dynamic soil-structure interaction formulation". In: *Soil Dynamics and Earthquake Engineering* 27.2 (Jan. 2007), pp. 126–143. DOI: 10.1016/j.soildyn.2006.05.005.

[54] H. Masoumi and G. Degrande. "Numerical modeling of free field vibrations due to pile driving using a dynamic soil-structure interaction formulation". In: *Journal of Computational and Applied Mathematics* 215 (June 2008), pp. 503–511. DOI: 10.1016/j.cam.2006.03.051.

[55] H. Masoumi, S. François, and G. Degrande. "A non-linear coupled finite element–boundary element model for the prediction of vibrations due to vibratory and impact pile driving". In: *International Journal for Numerical and Analytical Methods in Geomechanics* 33 (Feb. 2009), pp. 245–274. DOI: 10.1002/nag.719.

[56] M. V. Hall. "An analytical model for the underwater sound pressure waveforms radiated when an offshore pile is driven". In: *The Journal of the Acoustical Society of America* 138 (2015), pp. 795–806.

[57] A. Tsouvalas and A. V. Metrikine. "A semi-analytical model for the prediction of underwater noise from offshore pile driving". In: *Journal of Sound and Vibration* 332 (2013), pp. 3232–3257.

[58] Z. Y. Zhang and C. T. Tindle. "Improved equivalent fluid approximations for a low shear speed ocean bottom". In: *The Journal of the Acoustical Society of America* 98 (1995), pp. 3391–3396.

[59] A. Tsouvalas and A. Metrikine. "A three-dimensional vibroacoustic model for the prediction of underwater noise from offshore pile driving". In: *Journal of Sound and Vibration* 333 (Apr. 2014), pp. 2283–2311. ISSN: 0022-460X. DOI: 10.1016/J.JSV.2013.11.045.

[60] H. Kim. "Prediction of Structure Borne Noise Radiation and Propagation from Offshore Impact Pile Driving". PhD thesis. Kingston, RI, USA: University of Rhode Island, 2014.

[61] C. Pop, V. Zania, and B. Trimoreau. "Numerical modelling of offshore pile driving". In: *Proceedings of the XVI European Conference on Soil Mechanics and Geotechnical Engineering (ECSMGE 2015)*. Edinburgh, UK: ICE Publishing, Sept. 2015.

[62] D. R. Wilkes and A. Gavrilov. "Numerical Modelling of Sound Radiation from Marine Pile Driving over Elastic Seabeds". In: *Lecture Notes in Mechanical Engineering*. Berlin/Heidelberg, Germany: Springer, 2016, pp. 107–112.

[63] M. A. Wood. "Modelling and Prediction of Acoustic Disturbances from Offshore Piling". PhD thesis. Southampton, UK: University of Southampton, 2016.

[64] M. Zampolli et al. "Validation of finite element computations for the quantitative prediction of underwater noise from impact pile driving". In: *Journal of the Acoustical Society of America* 133.1 (2013), pp. 72–81.

[65] J. Kaplunov, L. Y. Kossovich, and E. Nolde. *Dynamics of Thin Walled Elastic Bodies*. New York: Academic Press, 1998, pp. 129–134.

[66] A. A. Bakr. *Axisymmetric Potential Problems*. Berlin: Springer, 1986, pp. 6–38.

[67] Milton Abramowitz and Irene A. Stegun. *Handbook of Mathematical Functions with Formulas, Graphs, and Mathematical Tables*. Tenth Printing, with corrections. Vol. 55. Applied Mathematics Series. Issued June 1964, Tenth Printing December 1972, Price $11.35 domestic postpaid, or $10.50 GPO Bookstore. Washington, D.C.: National Bureau of Standards, 1964. ISBN: N/A.

[68] J. D. Achenbach. *Wave Propagation in Elastic Solids*. Amsterdam: North Holland, 1973.

[69] E. A. L. Smith. "Pile Driving Analysis by Wave Methods". In: *Journal of Geotechnical Engineering* 86.GT4 (1960), pp. 1–23.

[70] G. G. Goble, F. Rausche, and G. Likins. "Dynamic Analysis of Pile Driving — Case Studies". In: *Journal of the Geotechnical Engineering Division, ASCE* 102.GT9 (1976), pp. 951–972.

[71] P. C. Meijers et al. "The Effect of Stress Wave Dispersion on the Drivability Analysis of Large-Diameter Monopiles". In: *Procedia Engineering* 199 (2017), pp. 2390–2395.

[72] K. Asche et al. "Numerical Modelling of Offshore Pile Driving". In: *XVI European Conference on Soil Mechanics and Geotechnical Engineering*. 2015.

[73] M. F. Randolph and H. A. Simons. "An Analysis of Driving Pile into Dense Sand". In: *Géotechnique* 36.4 (1986), pp. 551–562.

[74] H. M. Coyle and P. Gibson. "A Modified Quake-Dashpot Model for Pile Driving Analysis". In: *Advanced Piling Techniques* 2 (1986), pp. 45–53.

[75] P. Middendorp and C. van Zandwijk. "Accuracy and Reliability of Dynamic Pile Testing Techniques". In: *4th Int. Conf. on Behavior of Offshore Structures (BOSS)*. 1985.

[76] European Committee for Standardization. *EN 1993-1-1: Eurocode 3: Design of Steel Structures - Part 1-1: General Rules and Rules for Buildings*. Available at https://eurocodes.jrc.ec.europa.eu. Brussels, Belgium: CEN, 2005.

[77] Finn B. Jensen et al. *Computational Ocean Acoustics*. Second Edition. Springer, 2011. ISBN: 978-1-4419-8677-1. DOI: 10.1007/978-1-4419-8678-8.

[78] M. Aziman et al. "Compressive and Shear Wave Velocity Profiles using Seismic Refraction Technique". In: *Journal of Physics: Conference Series* 710 (2016), p. 012011.

[79] Yaxi Peng et al. "Numerical assessment of double bubble curtain performance for underwater noise mitigation during impact pile driving". In: *Frontiers in Marine Science* 10 (2023), p. 1123173. DOI: 10.3389/fmars.2023.1123173.

[80] DEME Offshore and Prysmian Group. *Double Big Bubble Curtain Noise Attenuation Plan – Coastal Virginia Offshore Wind Commercial (CVOW-C)*. Submitted to the U.S. Bureau of Ocean Energy Management (BOEM). 2023. URL: https://www.boem.gov/sites/default/files/documents/renewable-energy/state-activities/CVOW-C-DBBC-Attenuation-Plan.pdf.

[81] Ray Kirby and Wenbo Duan. "Modelling sound propagation in the ocean: a normal mode approach using finite elements". In: *Proceedings of Acoustics 2018*. Adelaide, Australia, Nov. 2018, pp. 1–10.

[82] Oleg A. Godin. "Underwater sound propagation over a layered seabed with weak shear rigidity". In: *Journal of the Acoustical Society of America* 157.1 (2025), pp. 314–327. DOI: 10.1121/10.0034864.

[83] V. Humphrey et al. "Variability of underwater radiated ship noise measured using two hydrophone arrays". In: *Proceedings of OCEANS 2015—Genova*. Genova, Italy, May 2015, pp. 1–10.

[84] J. von Pein, T. Lippert, and M.A. Bellmann. "Field measurements and predictions of underwater noise during offshore pile driving: Comparison and uncertainty assessment". In: *Marine Pollution Bulletin* 182 (2022), p. 113935.

[85] James D. Wood, E. Topham, and M.J. Witt. "Acoustic field measurements during impact pile driving: implications for marine mammal mitigation". In: *Bioacoustics* 22.3 (2013), pp. 250–271.

[86] A. Trimoréau, J.H. Bettencourt, and W.A. Kuperman. "Modeling of underwater pile driving noise in a sloping seabed: Effect of pile penetration depth". In: *Applied Acoustics* 79 (2014), pp. 60–69.

[87] B. Würsig, Jr. Greene C. R., and T. A. Jefferson. "Development of an air bubble curtain to reduce underwater noise of percussive piling". In: *Mar. Environ. Res.* 49 (2000), pp. 79–93. DOI: 10.1016/S0141-1136(99)00050-1. URL: https://www.sciencedirect.com/science/article/pii/S0141113699000501.

[88] Zongyu Fan et al. "Experimental study on pile driving responses in dense sand using different impact waveforms". In: *Marine Structures* 79 (2021), p. 102976. DOI: 10.1016/j.marstruc.2021.102976.

[89] M. Dǒ0e4hne et al. "Bubble curtains attenuate noise from offshore wind farm construction and reduce temporary habitat loss for harbour porpoises". In: *Mar. Ecol. Prog. Ser.* 580 (2017), pp. 221–237. DOI: 10.3354/meps12257. URL: https://www.int-res.com/abstracts/meps/v580/p221-237/.

[90] S. Koschinski and K. Lüdemann. *Development of Noise Mitigation Measures in Offshore Wind Farm Construction*. Tech. rep. Federal Agency for Nature Conservation (BfN), Germany, 2013. URL: https://www.cbd.int/doc/meetings/mar/mcbem-2014-01/other/mcbem-2014-01-submission-noise-mitigation-en.pdf.

[91] G. Dies et al. "Analysis of bubble curtain effectiveness in the coastal Virginia offshore wind turbine installation". In: *J. Acoust. Soc. Am.* 155.3, Supplement (2024), A319. DOI: 10.1121/10.0027660. URL: https://pubs.aip.org/asa/jasa/article/155/3_Supplement/A319/3301863/Analysis-of-bubble-curtain-effectiveness-in-the.

[92] Michael A. Ainslie. *Principles of Sonar Performance Modeling*. Praxis Books. Berlin: Springer, 2010. ISBN: 978-3-540-87661-5.

A | Sensitivity study for the influence of the penetration depth on noise levels

A.1 SEL and L_{peak} values over the penetration depth at 750 m from the monopile

Penetration depth	**20 bl/0.25m**	
	SEL	L_{peak}
[m]	[dB re 1 μPa^{2}s]	[dB re 1 μPa]
5.0	183.08	203.87
7.0	182.73	203.06
11.0	182.32	201.64
13.0	182.24	201.14
15.0	182.52	201.02
18.5	182.70	200.92
21.0	182.91	200.99
23.5	183.15	201.07
27.5	183.16	201.46

Table A.1: SEL and L_{peak} values for different penetration depths with constant hammer energy (5500 kJ). Modelled at 750 m from the monopile and 2 m above the seabed. Scenario: Target blow count = 20 bl/0.25 m.

A.2 SEL and L_{peak} values over the penetration depth in the frequency domain

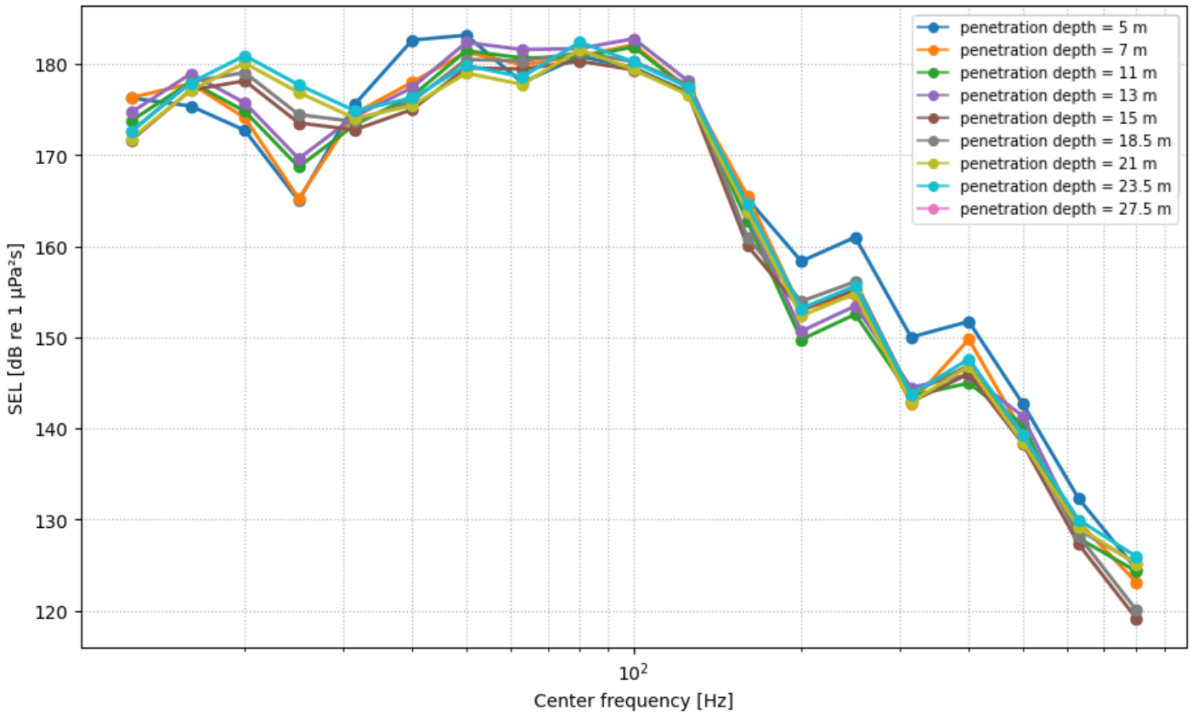

Figure A.1: SEL values in the frequency domain for different penetration depths with constant hammer energy (5500 kJ). Modelled at 750 m from the monopile and 2 m above the seabed.

B | Effect of operational parameters on the drivability

B.1 Drivability results for target blow count variation

Penetration [m]	Energy [kJ]	Blows
6.99	1100	175
6.99	1650	175
7.01	1650	176
9.49	1650	374
9.51	1650	376
10.99	1650	494
11.01	1650	496
11.01	2200	496
13.00	2200	687
13.00	2750	687
14.99	2750	862
14.99	3300	862
15.01	3300	863
16.99	3300	1013
17.01	3300	1015
18.49	3300	1145
18.49	3849	1145
18.51	3849	1147
20.99	3849	1365
20.99	4400	1365
21.01	4400	1367
23.00	4400	1550
23.00	5500	1550
24.99	5500	1725
25.01	5500	1727
25.99	5500	1809
26.01	5500	1811
27.50	5500	1966
Total		**1966**

(a) (A) 20 bl/0.25 m

Penetration [m]	Energy [kJ]	Blows
6.99	1100	175
7.01	1100	177
9.49	1100	455
9.49	1650	455
9.51	1650	457
10.99	1650	575
11.01	1650	577
11.01	2200	577
13.00	2200	768
14.99	2200	991
14.99	2750	991
15.01	2750	993
16.99	2750	1175
17.01	2750	1177
18.49	2750	1337
18.49	3300	1337
18.51	3300	1339
20.99	3300	1607
20.99	3849	1607
21.01	3849	1609
23.00	3849	1824
23.00	4400	1824
24.99	4400	2031
24.99	4950	2031
25.01	4950	2033
25.99	4950	2115
26.01	4950	2117
27.50	4950	2272
27.50	5500	2272
Total		**2272**

(b) (B) 25 bl/0.25 m

Penetration [m]	Energy [kJ]	Blows
6.99	1100	175
7.01	1100	177
9.49	1100	455
9.51	1100	457
10.99	1100	623
11.01	1100	626
11.01	1650	626
13.00	1650	881
13.00	2200	881
14.99	2200	1104
15.01	2200	1106
16.99	2200	1336
17.01	2200	1338
17.01	2750	1338
18.49	2750	1498
18.51	2750	1500
20.99	2750	1837
20.99	3300	1837
21.01	3300	1839
23.00	3300	2102
23.00	3849	2102
24.99	3849	2349
24.99	4400	2349
25.01	4400	2351
25.99	4400	2445
26.01	4400	2447
27.50	4400	2632
27.50	4950	2632
Total		**2632**

(c) (C) 30 bl/0.25 m

Table B.1: Drivability output for target blow count variations.

B.2 Drivability results for impulse elongation

Penetration [m]	Energy [kJ]	Blows
6.99	1100	175
7.01	1100	177
9.49	1100	455
	1650	455
9.51	1650	457
10.99	1650	575
11.01	1650	577
	2200	577
13.00	2200	768
14.99	2200	991
	2750	991
15.01	2750	993
16.99	2750	1175
17.01	2750	1177
18.49	2750	1337
	3300	1337
18.51	3300	1339
20.99	3300	1607
	3849	1607
21.01	3849	1609
23.00	3849	1824
	4400	1824
24.99	4400	2031
	4950	2031
25.01	4950	2033
25.99	4950	2115
26.01	4950	2117
27.5	4950	2272
	5500	2272
Total		**2272**

(a) (A) Reference case (no pulse)

Penetration [m]	Energy [kJ]	Blows
6.99	1100	231
	1650	231
7.01	1650	233
9.49	1650	491
	2200	491
9.51	2200	493
10.99	2200	617
11.01	2200	619
	2750	619
13.00	2750	842
	3300	842
14.99	3300	1073
	3849	1073
15.01	3849	1075
16.99	3849	1281
	4400	1281
17.01	4400	1283
18.49	4400	1443
	4950	1443
18.51	4950	1445
20.99	4950	1753
	5500	1753
21.01	5500	1756
23.00	5500	2090
24.99	5500	2560
25.01	5500	2564
25.99	5500	2760
26.01	5500	2766
27.5	5500	3386
Total		**3386**

(b) (B) Medium PULSE case

Table B.2: Drivability output for reference case (A) and medium PULSE case (B).

C | Noise levels per hammer energy level

C.1 Noise levels for varying target blow counts

C.1.1 Without additional mitigation measures

Hammer energy	**20 bl/0.25m**		**25 bl/0.25m**		**30 bl/0.25m**	
	SEL	L_{peak}	SEL	L_{peak}	SEL	L_{peak}
[kJ]	[dB re 1 μPa^{2}s]	[dB re 1 μPa]	[dB re 1 μPa^{2}s]	[dB re 1 μPa]	[dB re 1 μPa^{2}s]	[dB re 1 μPa]
1100	176.09	196.88	176.09	196.88	176.09	196.88
1650	177.21	196.78	177.21	196.78	177.01	195.91
2200	178.26	197.16	178.26	197.16	178.26	197.16
2750	179.23	198.13	179.69	197.91	179.69	197.91
3300	180.48	198.71	180.48	198.71	180.93	198.85
3849	181.15	199.37	181.60	199.52	181.60	199.52
4400	182.18	200.10	182.18	200.10	182.19	200.49
4950	182.70	201.00	182.7	201	[-]	[-]
5500	183.16	201.46	[-]	[-]	[-]	[-]

Table C.1: SEL and L_{peak} values for different target blow counts.

C.1.2 In combination with a DBBC

Hammer energy	**20 bl/0.25m**		**25 bl/0.25m**		**30 bl/0.25m**	
	SEL	L_{peak}	SEL	L_{peak}	SEL	L_{peak}
[kJ]	[dB re 1 μPa^{2}s]	[dB re 1 μPa]	[dB re 1 μPa^{2}s]	[dB re 1 μPa]	[dB re 1 μPa^{2}s]	[dB re 1 μPa]
1100	167.54	186.88	167.54	186.88	167.54	186.88
1650	168.23	186.68	168.23	186.68	167.86	185.43
2200	169.11	186.68	169.11	186.68	169.11	186.68
2750	170.08	187.65	170.74	188.06	170.74	188.06
3300	171.53	188.85	171.53	188.85	172.24	190.41
3849	172.20	189.52	172.91	191.08	172.91	191.08
4400	173.49	191.66	173.49	191.66	173.56	192.15
4950	174.08	192.66	174.08	192.66	[-]	[-]
5500	174.53	193.12	[-]	[-]	[-]	[-]

Table C.2: SEL and L_{peak} values for different target blow counts in combination with a DBBC.

C.2 Noise levels for impulse elongation

C.2.1 Without additional mitigation measures

Hammer energy	**No PULSE**		**Medium PULSE**	
[kJ]	SEL [dB re 1 μPa^{2}s]	L_{peak} [dB re 1 μPa]	SEL [dB re 1 μPa^{2}s]	L_{peak} [dB re 1 μPa]
1100	176.09	196.88	170.26	187.33
1650	177.21	196.78	172.16	190.02
2200	178.26	197.16	173.41	191.27
2750	179.69	197.91	174.15	192.19
3300	180.48	198.71	174.94	192.98
3849	181.60	199.52	176.51	193.67
4400	182.18	200.10	177.09	194.25
4950	182.70	201.00	178.06	194.83
5500	[-]	[-]	178.36	195.38

Table C.3: SEL and L_{peak} values for PULSE without a DBBC.

C.2.2 In combination with a DBBC

Hammer energy	**No PULSE + DBBC**		**Medium PULSE + DBBC**	
[kJ]	SEL [dB re 1 μPa^{2}s]	L_{peak} [dB re 1 μPa]	SEL [dB re 1 μPa^{2}s]	L_{peak} [dB re 1 μPa]
1100	167.54	186.88	162.87	179.85
1650	168.23	186.68	163.77	182.37
2200	169.11	186.68	165.02	183.62
2750	170.74	188.06	165.52	184.57
3300	171.53	188.85	166.31	185.36
3849	172.91	191.08	168.31	185.29
4400	173.49	191.66	168.00	186.42
4950	174.08	192.66	169.60	187.02
5500	[-]	[-]	170.30	187.73

Table C.4: SEL and L_{peak} values for PULSE with a DBBC.

D | Frequency-weighted noise impact

D.1 Weighted cumulative noise (PULSE)

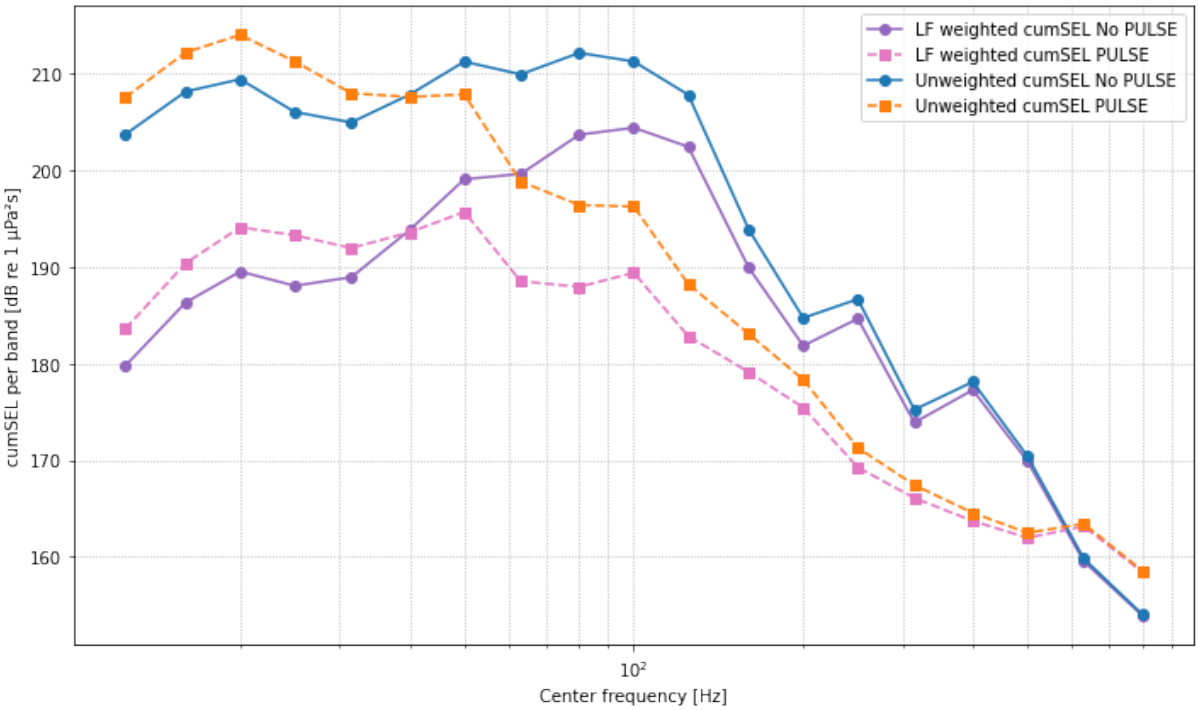

Figure D.1: Frequency-weighted cumSEL spectrum for low-frequency cetaceans.[3]

[3]Modelled at 750 m from the monopile and 2 m above the seabed.

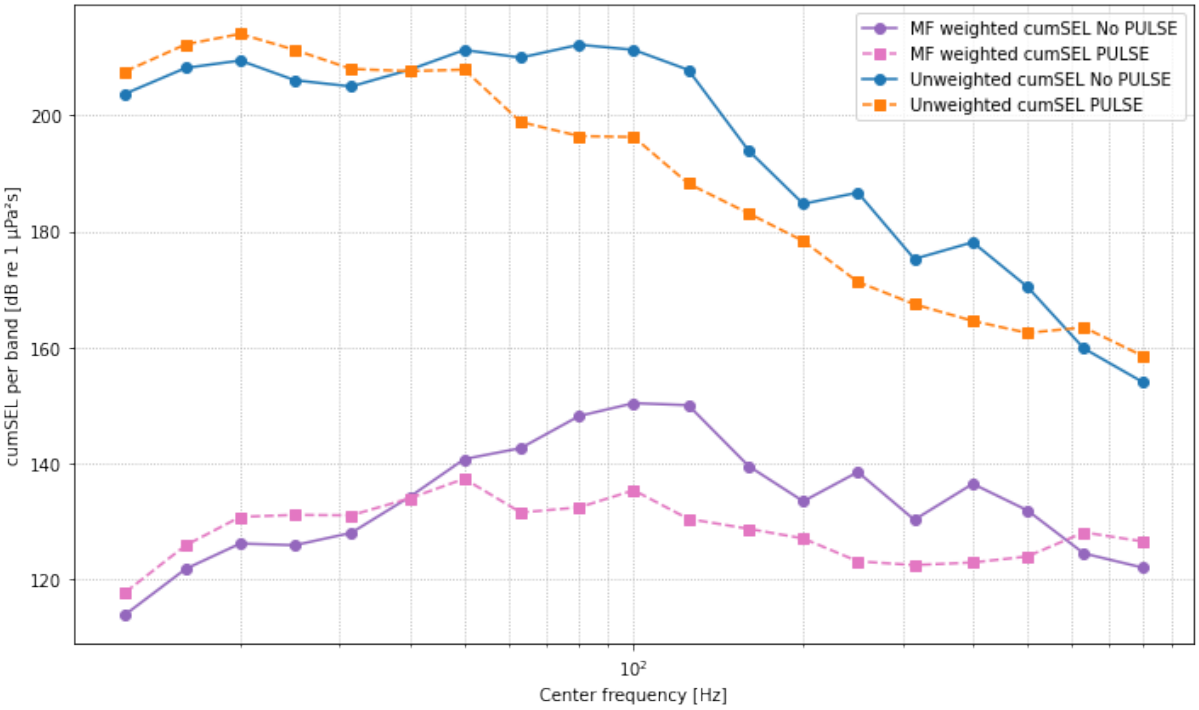

Figure D.2: Frequency-weighted cumSEL spectrum for mid-frequency cetaceans.[3]

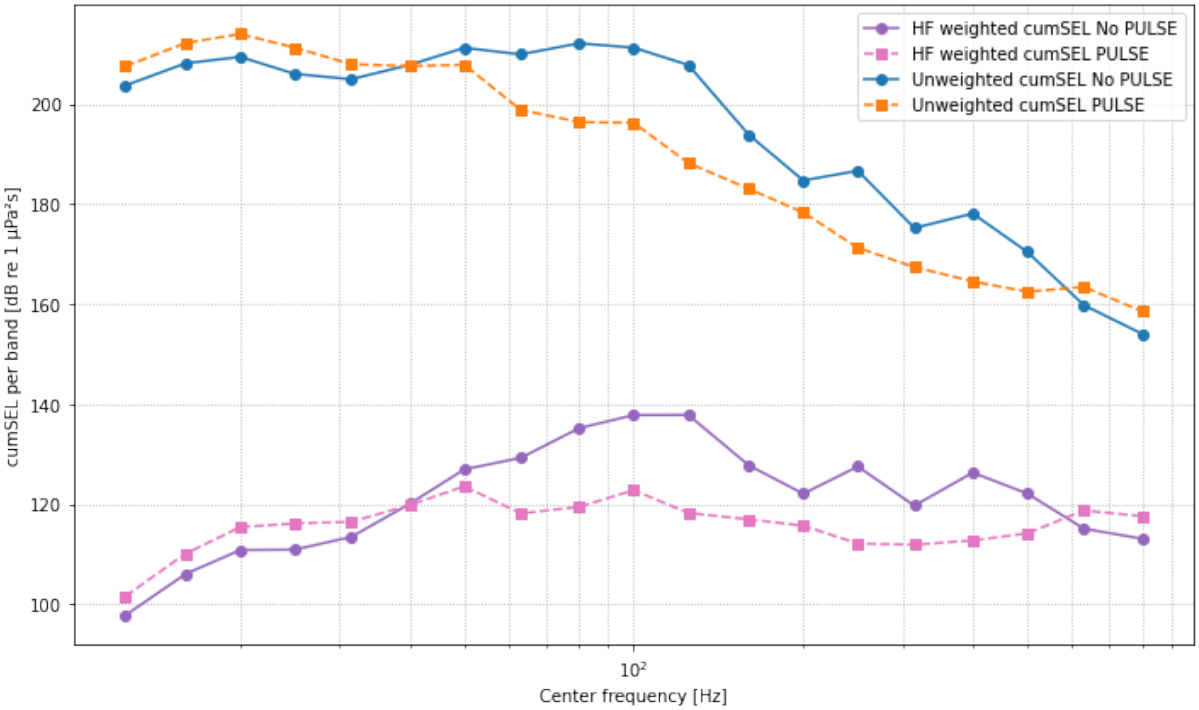

Figure D.3: Frequency-weighted cumSEL spectrum for high-frequency cetaceans.[3]

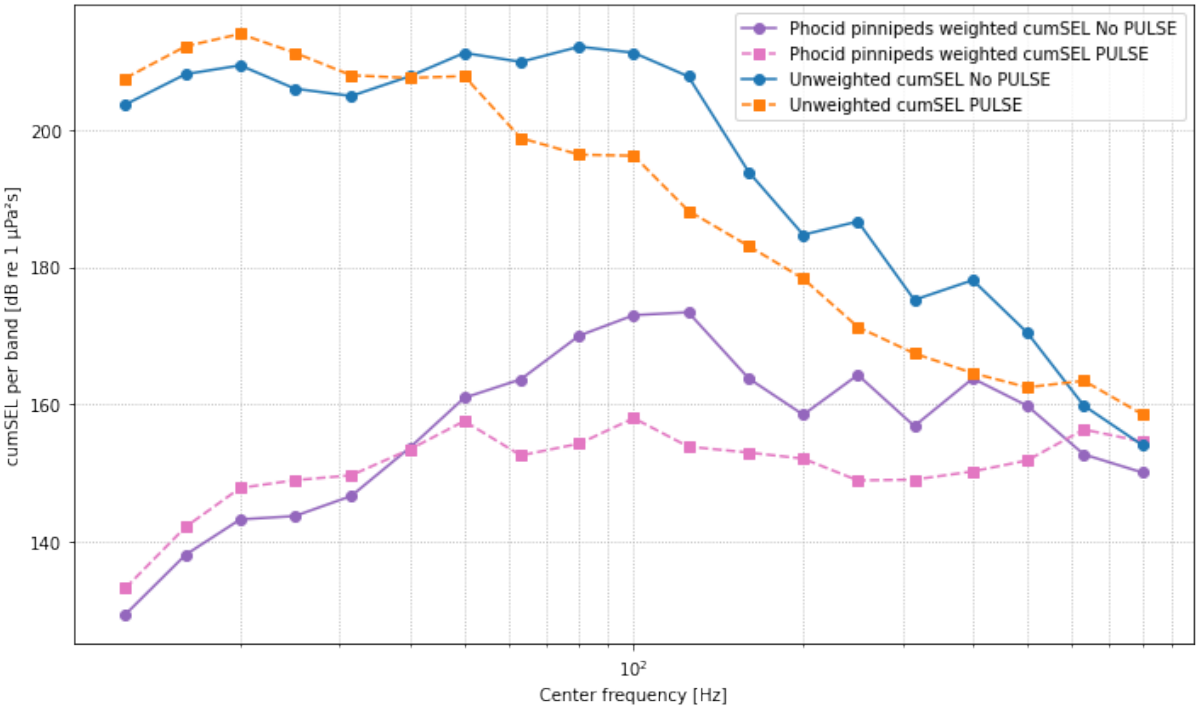

Figure D.4: Frequency-weighted cumSEL spectrum for phocid pinnipeds.[3]

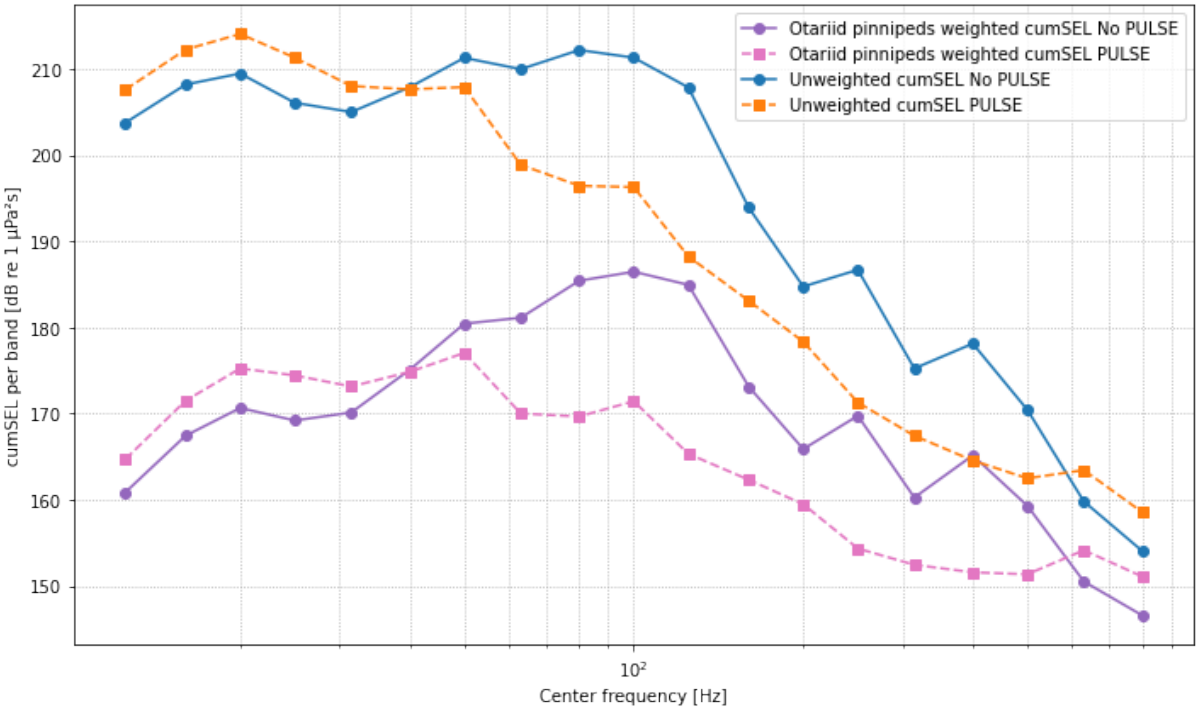

Figure D.5: Frequency-weighted cumSEL spectrum for otariid pinnipeds.[3]

D.2 Weighted cumulative noise (PULSE+DBBC)

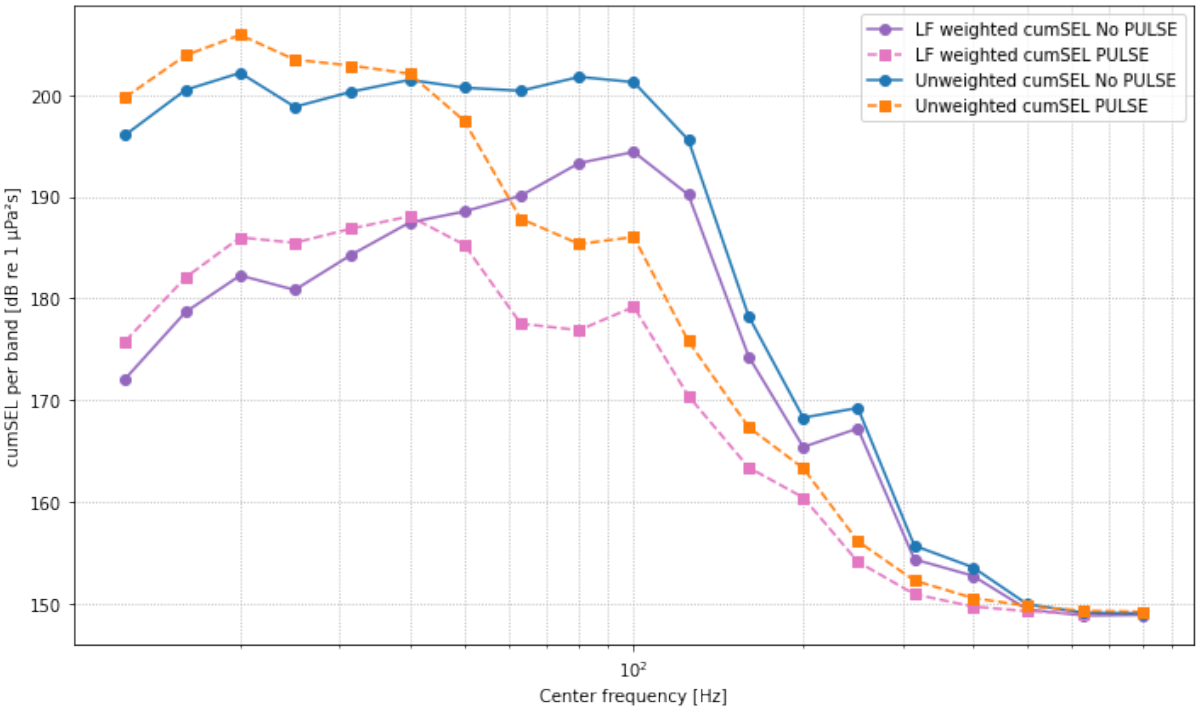

Figure D.6: Frequency-weighted cumSEL spectrum for low-frequency cetaceans comparing the scenarios with and without DBBC.[3]

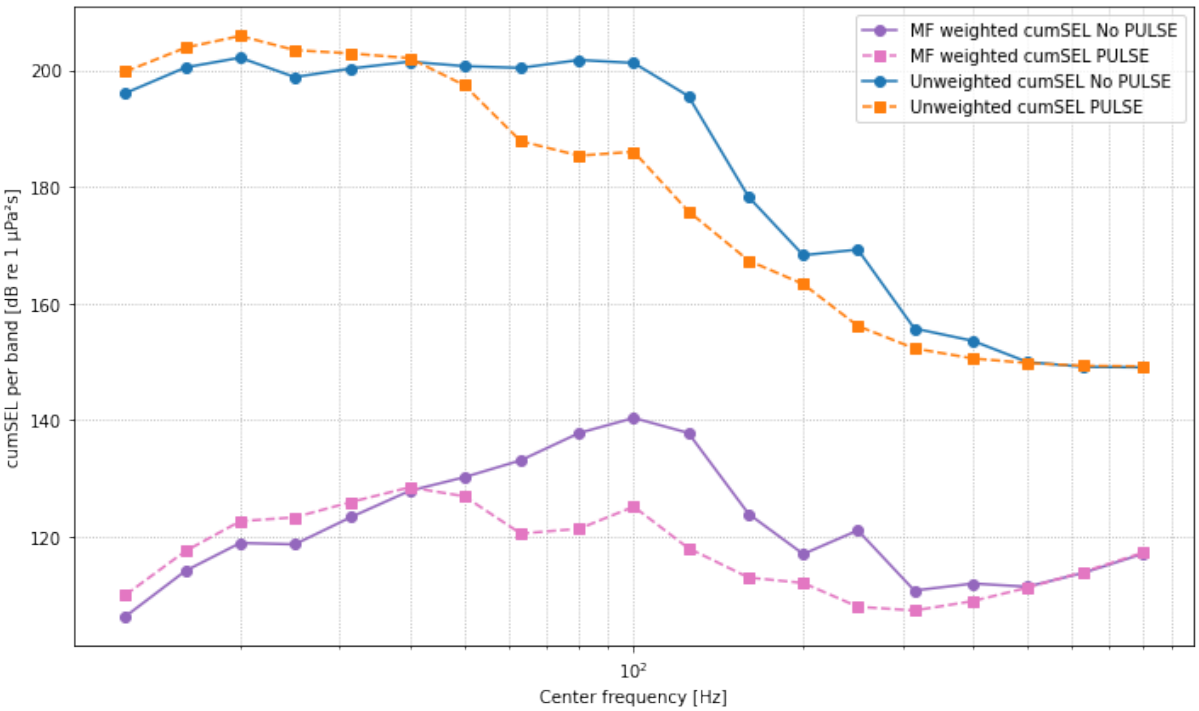

Figure D.7: Frequency-weighted cumSEL spectrum for mid-frequency cetaceans comparing the scenarios with and without DBBC.[3]

[3]Modelled at 750 m from the monopile and 2 m above the seabed.

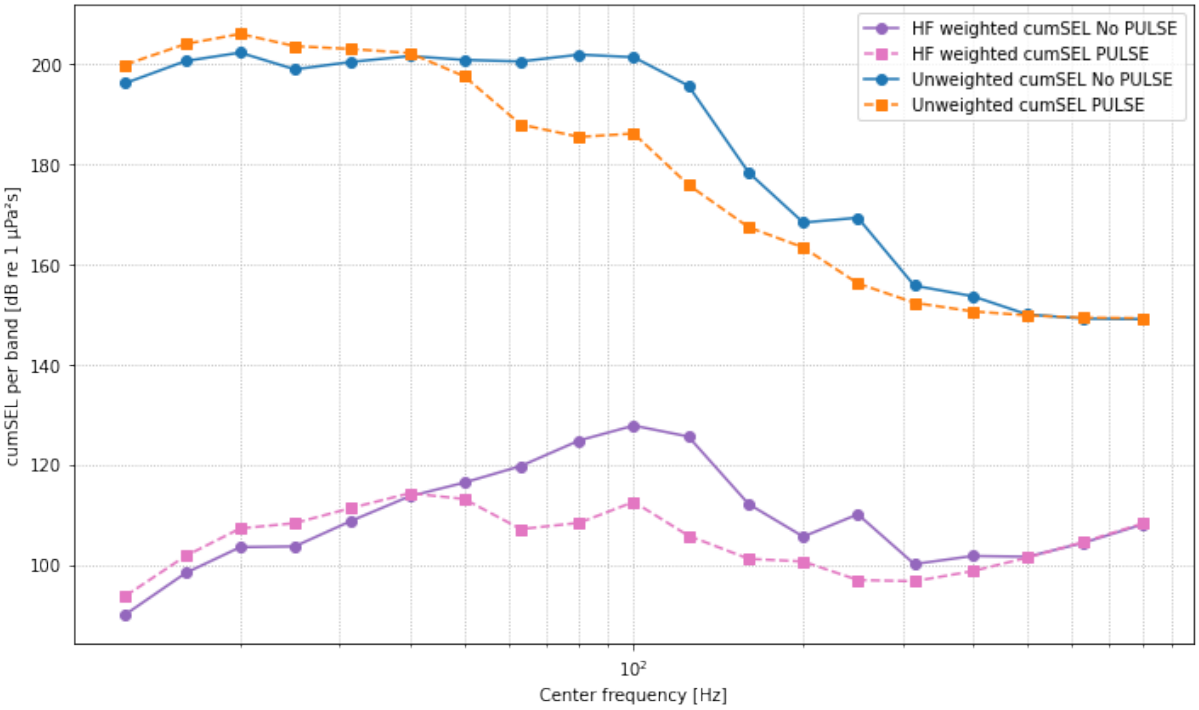

Figure D.8: Frequency-weighted cumSEL spectrum for high-frequency cetaceans comparing the scenarios with and without DBBC.[3]

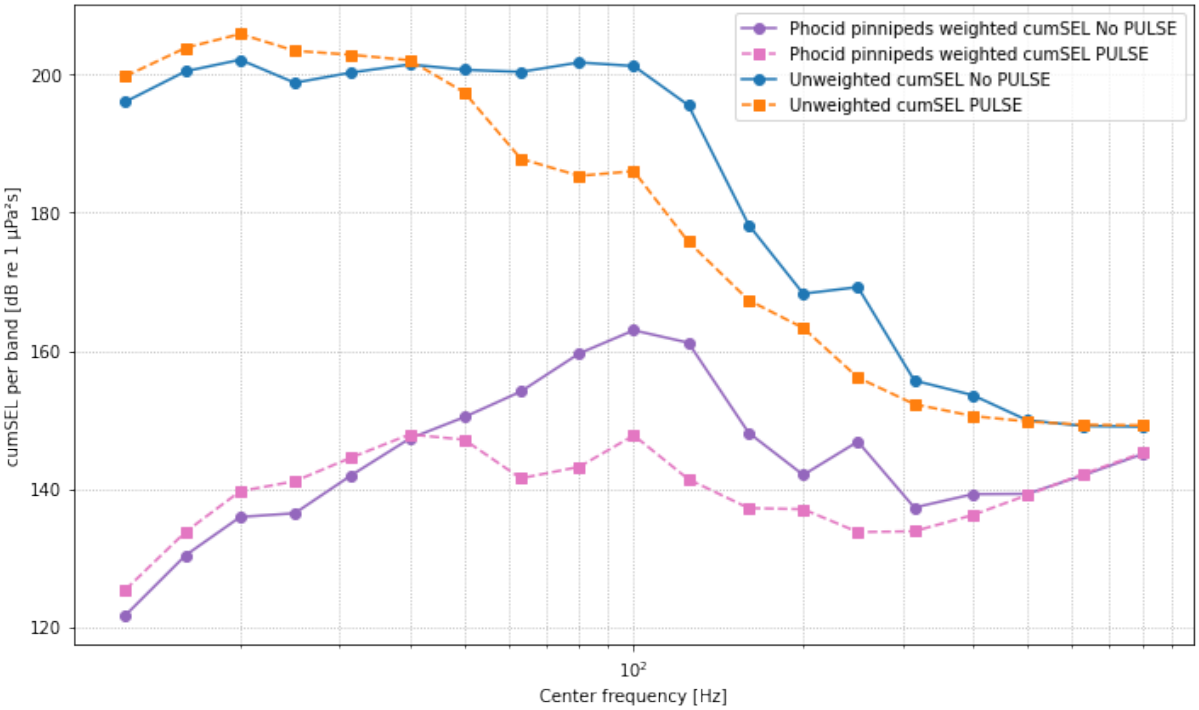

Figure D.9: Frequency-weighted cumSEL spectrum for phocid pinnipeds comparing the scenarios with and without DBBC.[3]

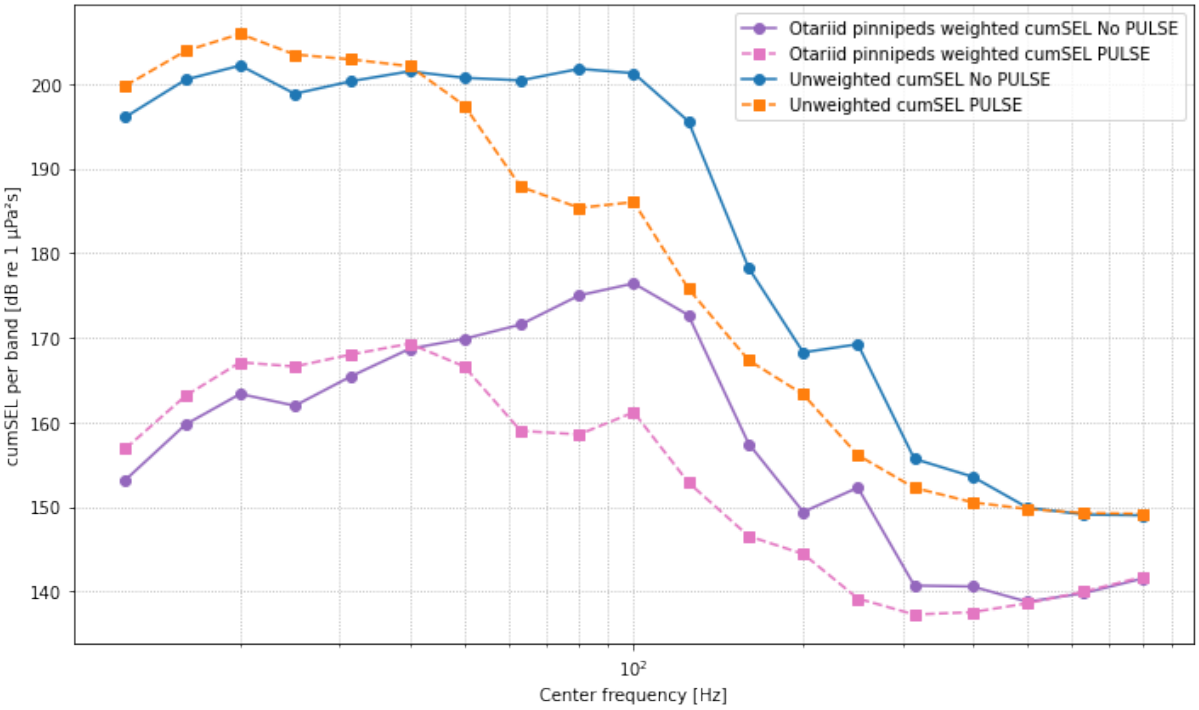

Figure D.10: Frequency-weighted cumSEL spectrum for otariid pinnipeds comparing the scenarios with and without DBBC.[3]

[3]Modelled at 750 m from the monopile and 2 m above the seabed.

E | Clay-sand case

E.1 Input parameters

Description	Parameter	Soft clay layer	Dense sand layer	Unit
Young's modulus	E	16.2	576	MPa
Poisson's ratio	ν	0.49	0.49	-
Soil density	ρ	1400	2090	kg/m^3
Damping ratio of compressional waves	α_p	4.91	1.85	%
Damping ratio of shear waves	α_s	8.89	4.63	%
Compressional wave velocity	V_p	1390	1886	m/s
Shear wave velocity	V_s	62	304	m/s

Table E.1: Parameters for soil properties and wave characteristics for soft clay layer on top of dense sand layer. Parameters are derived from Ainslie, MA [92].

E.2 Drivability results for impulse elongation

Penetration [m]	Energy [kJ]	Blows
7.995	550	84
10.99	550	180
11.01	550	183
	1100	183
13.00	1100	446
	1650	446
14.99	1650	669
	2200	669
15.01	2200	671
16.99	2200	853
17.01	2200	855
18.49	2200	1015
	2750	1015
18.51	2750	1017
20.99	2750	1285
	3300	1285
21.01	3300	1287
23.00	3300	1502
	3849	1502
24.99	3849	1709
	4400	1709
25.01	4400	1711
25.99	4400	1789
26.01	4400	1791
27.50	4400	1946
	4950	1946
Total		**1946**

(a) (A) Reference case (no PULSE)

Penetration [m]	Energy [kJ]	Blows
7.995	550	72
10.99	550	156
11.01	550	160
	1650	160
13.00	1650	407
	2200	407
14.99	2200	654
	2750	654
15.01	2750	656
16.99	2750	870
	3300	870
17.01	3300	872
18.49	3300	1038
	3849	1038
18.51	3849	1040
20.99	3849	1357
	4950	1357
21.01	4950	1359
23.00	4950	1598
	5500	1598
24.99	5500	1908
25.01	5500	1911
25.99	5500	2044
26.01	5500	2048
27.50	5500	2400
Total		**2400**

(b) (B) Medium PULSE case

Table E.2: Drivability output for the clay–sand profile: reference (A) versus 50 % PULSE (B).

E.3 Noise levels for impulse elongation

Hammer energy	No PULSE		Medium PULSE	
[kJ]	SEL [dB re 1 μPa^{2}s]	L_{peak} [dB re 1 μPa]	SEL [dB re 1 μPa^{2}s]	L_{peak} [dB re 1 μPa]
550	164.5	181.71	162.45	176.87
1100	167.16	183.44	[-]	[-]
1650	166.17	183.28	166.73	183.07
2200	167.28	183.20	165.63	182.39
2750	167.75	183.01	166.51	183.01
3300	168.83	183.45	167.82	183.34
3849	170.02	185.04	168.77	183.64
4400	170.77	185.83	[-]	[-]
4950	[-]	[-]	170.03	184.21
5500	[-]	[-]	171.77	185.60

Table E.3: SEL and L_{peak} values for PULSE without a DBBC.

E.4 Weighted cumulative noise (PULSE)

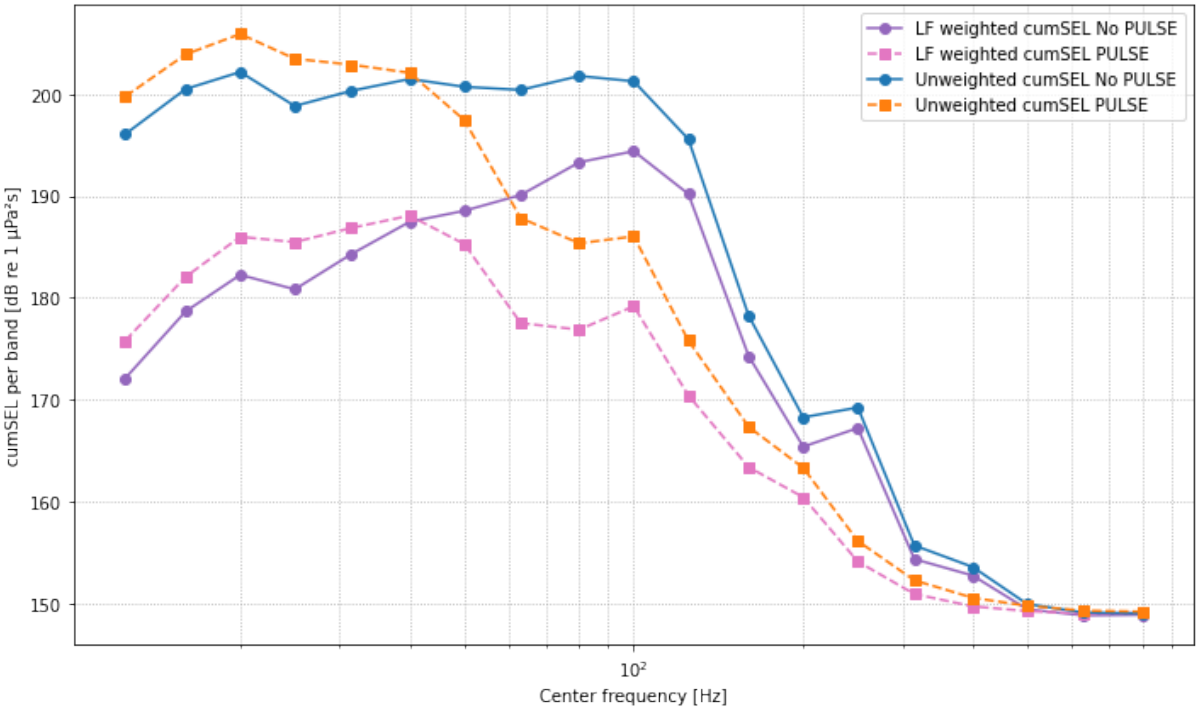

Figure E.1: Frequency-weighted cumSEL spectrum for low-frequency cetaceans comparing the scenarios with and without PULSE in a clay-sand stratigraphy.[3]

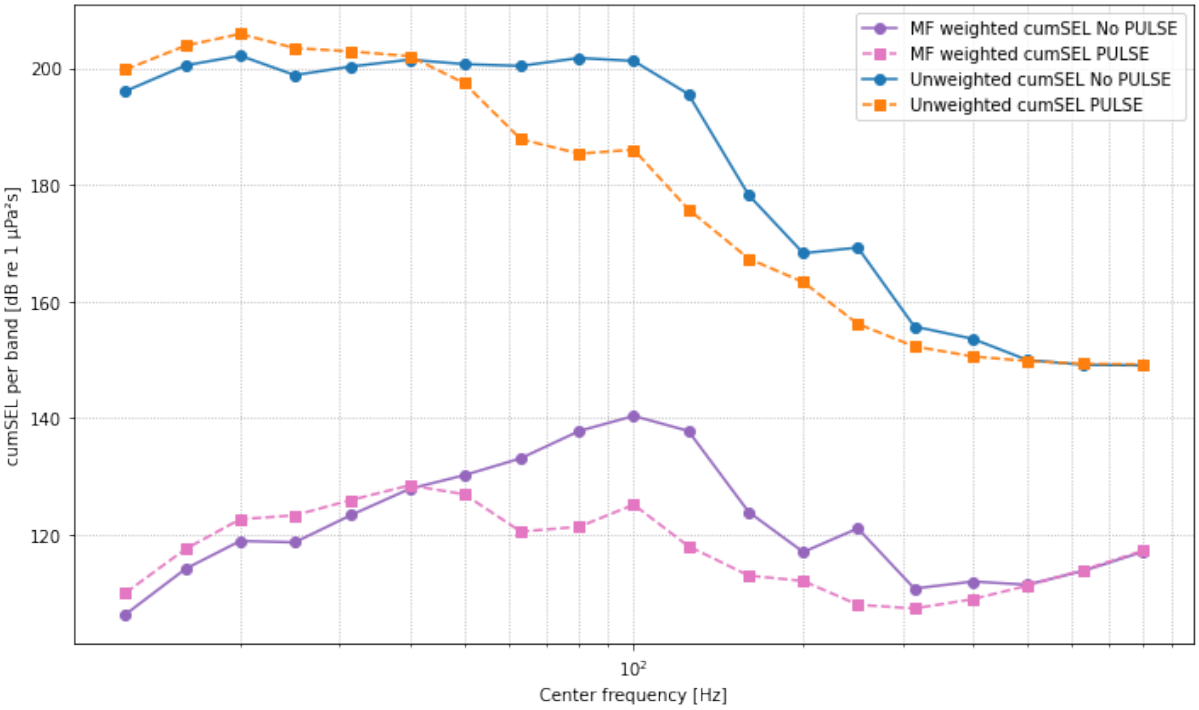

Figure E.2: Frequency-weighted cumSEL spectrum for mid-frequency cetaceans comparing the scenarios with and without PULSE in a clay-sand stratigraphy.[3]

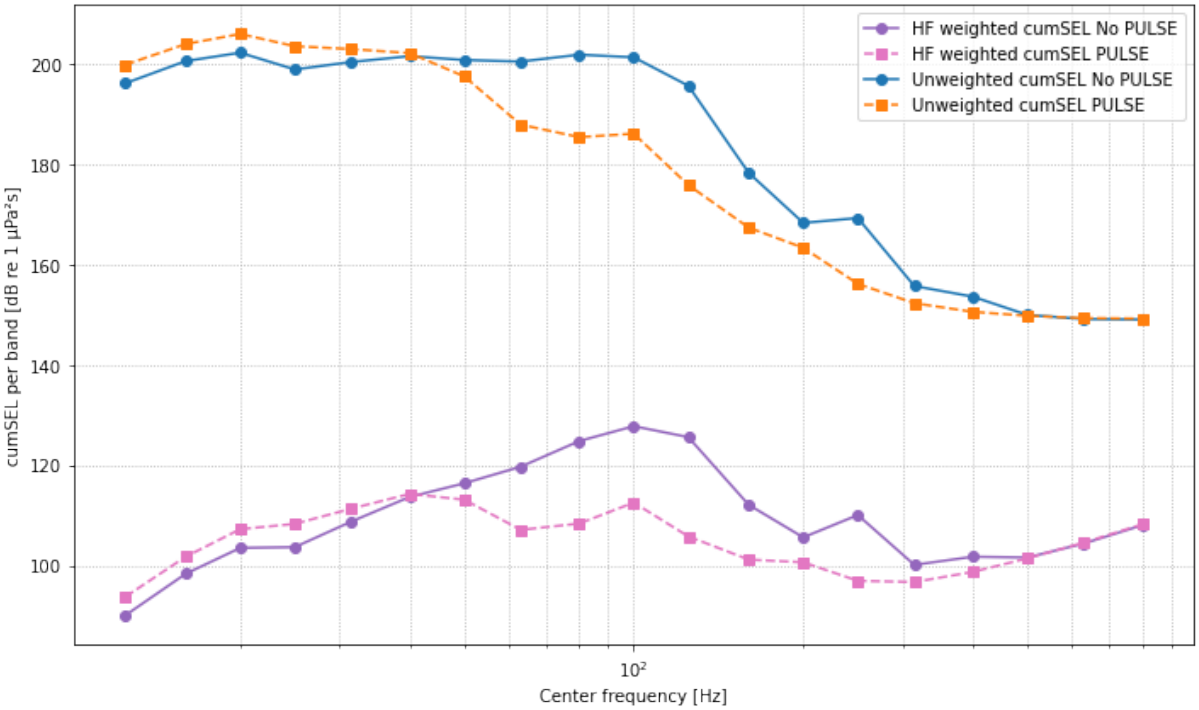

Figure E.3: Frequency-weighted cumSEL spectrum for high-frequency cetaceans comparing the scenarios with and without PULSE in a clay-sand stratigraphy.[3]

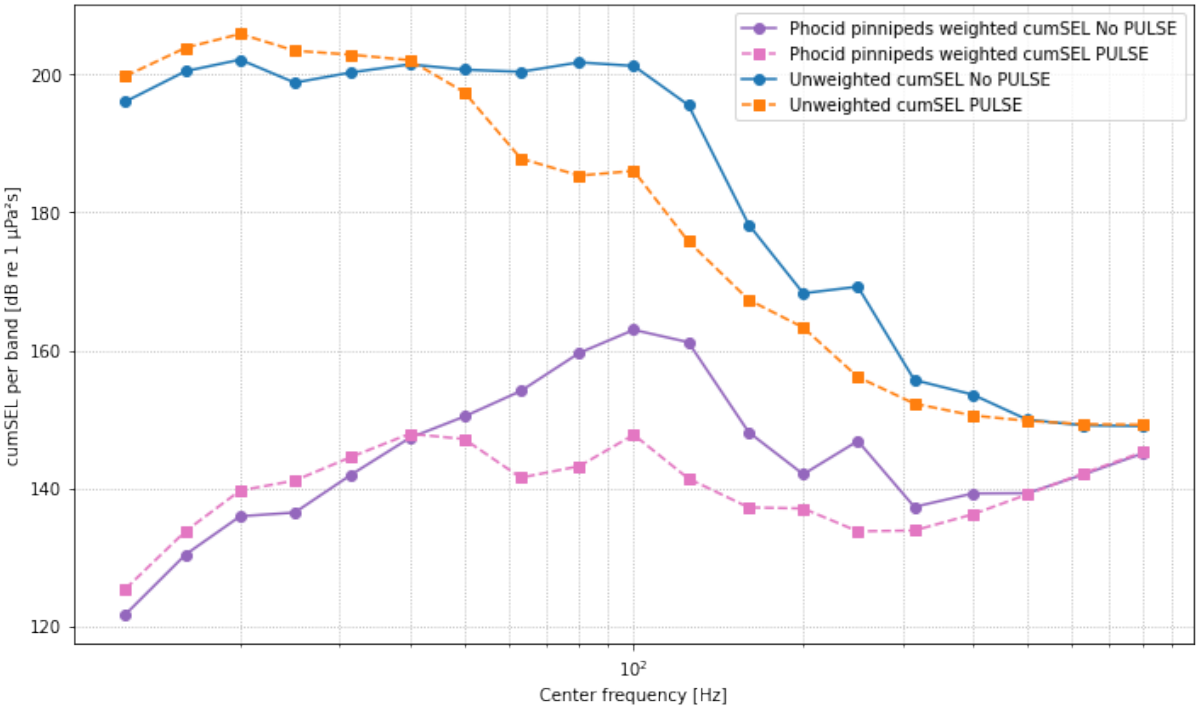

Figure E.4: Frequency-weighted cumSEL spectrum for phocid pinnipeds comparing the scenarios with and without PULSE in a clay-sand stratigraphy.[3]

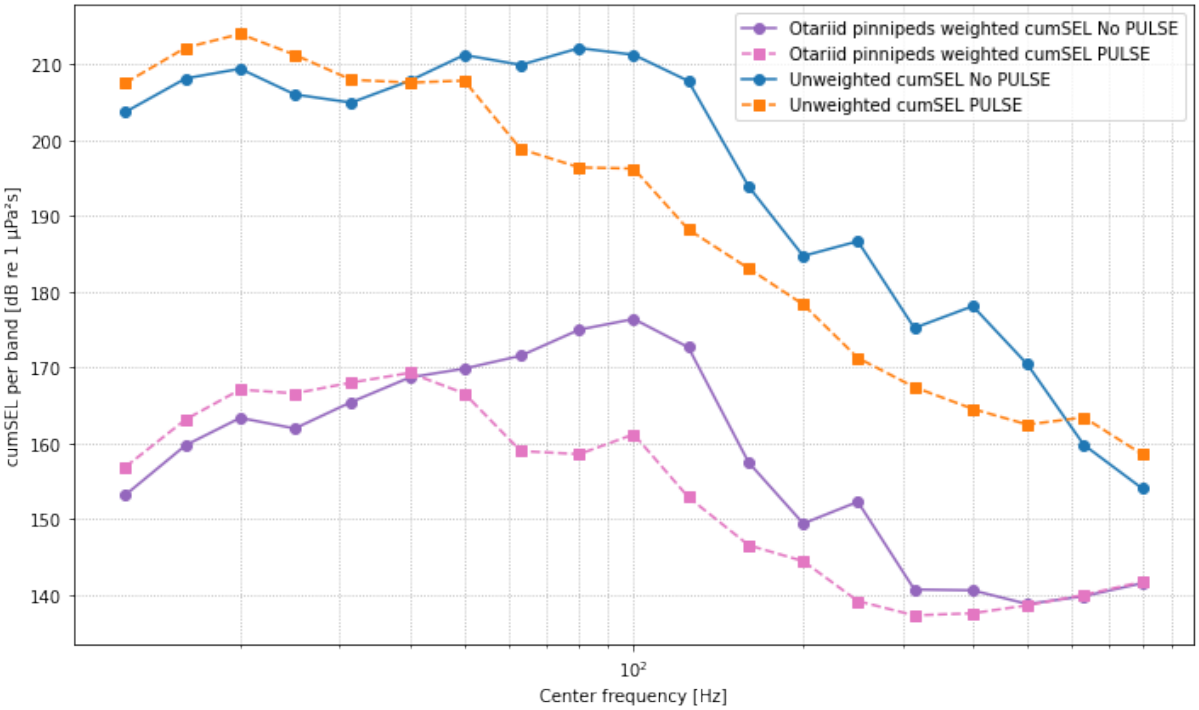

Figure E.5: Frequency-weighted cumSEL spectrum for otariid pinnipeds comparing the scenarios with and without PULSE in a clay-sand stratigraphy.[3]

[3]Modelled at 750 m from the monopile and 2 m above the seabed.